ROBERT MANNING STROZIER LIBRARY
FLORIDA STATE UNIVERSITY

The use of this thesis is subject to the usual restrictions governing the use of manuscript material. The literary rights of the author must be respected. Passages must not be copied or closely paraphrased without the previous written consent of the author. If the reader obtains any assistance from this volume, he must give proper credit in his own work.

The persons whose signatures appear below attest to their acceptance of the above restrictions. (Borrowing libraries are asked to secure the signatures of each user.)

NAME	ADDRESS	DATE

B

THE FLORIDA STATE UNIVERSITY

COLLEGE OF ARTS AND SCIENCES

A NUMERICAL MODEL STUDY OF CIRCULATION IN THE ALBORAN SEA

by

Ruth H. Preller

A Dissertation submitted to the
Department of Meteorology
in partial fulfillment of the
requirements for the degree of
Doctor of Philosophy

Approved:

James J. O'Brien
Professor Directing Dissertation

Steve A. Piacsek

Stephen

T. N. Krishnamurti

Ruby Krishnamurti

April, 1985

A NUMERICAL MODEL STUDY OF CIRCULATION IN THE ALBORAN SEA

Ruth H. Preller, Ph.D.
The Florida State University, 1985

Major Professor: James J. O'Brien, Ph.D.

Reduced gravity and two-layer numerical models have been used to study the circulation in the westernmost basin of the Mediterranean Sea, the Alboran Sea. Circulation is forced by flow through a 20 km wide port in the western boundary representing the Strait of Gibraltar.

The reduced gravity model domain is a rectangle measuring 600 km x 160 km with 10 km x 5 km grid resolution. When forced by an eastward or northeastward inflow, the model solutions evolve to a steady state which exhibits a meandering current. The first meander of the current forms the northern boundary of an anticyclonic gyre. Horizontal dimensions of the gyre are strongly dependent up on the inflow angle, vorticity associated with the incoming current, magnitude of the incoming transport and the north-south extent of the basin. The meandering current is considered a standing Rossby wave with a highly distorted vorticity trajectory due to the interaction of the current with the northern and southern boundaries. When velocity (transport) is increased, the wavelength increases approximately as $\sqrt{v}$. As a result the anticyclonic gyre shifts east as velocity increases and west as velocity decreases. These solutions show that bottom topography, winds and coastline features are not necessary mechanisms for the

formation of the gyre.

Two-layer model solutions were obtained using realistic topography, geometry and a westward moving lower layer. The addition of the lower layer flow and topography slightly distorted the circulation in the upper layer, particularly in the southern half of the basin. The basic characteristics of the gyre, however, were not changed. With topography included, the lower layer flow followed a path similar to that observed for the Mediterranean Deep Water. When topography was removed, the flow followed the path taken by the Levantine Intermediate Water.

The high variability of the horizontal dimensions and location of the gyre has been observed both experimentally and through satellite imagery. Model results show that the high variability is caused by variations in the inflow velocity.

Drifter tracks, both observational and model derived, help determine the circulation in both layers of the Alboran Sea. The close comparison between model and experimental dirfters lends credibility to the model circulation and dynamics.

Experiments using climatological wind to force the model show that a strong wind driven circulation from the Balearic Sea causes cyclonic circulation to form in the location of the Alboran gyre. This cyclonic circulation, however, is very weak and when combined with the Atlantic water inflow serves only to slightly weaken the anticyclonic gyre.

ACKNOWLEDGEMENTS

This work was supported by the Office of Naval Research, Coastal Science Program under contract N00014-81-AB-11-12. Computations were performed on the two-pipeline Texas Instruments Advanced Scientific Computor at the Naval Research Laboratory in Washington, D. C.

I wish to express my deep gratitude to Dr. James J. O'Brien as my major professor for his encouragement and patience during the course of this project. I would also like to acknowledge Drs. Ruby Krishnamurti, T. N. Krishnamurti, Steve Piacsek and Jerry Stephens for serving on my doctorial committee.

I would also like to express my appreciation to my two co-workers on the Donde Va? project, Dr. Thomas Kinder and Mr. Paul Laviolette for their many hours of stimulating conversation. I wish to thank Drs. Alan Wallcraft and George Heburn for assistance with computer oriented model problems. The assistance and support rendered to me by Dr. Dennis Conlon was greatly appreciated.

I would also like to acknowledge the assistance of Ms. Charlene Parker, Ms. Pam Posey and Ms. Gretchen Dawson in the preparation of the final copy of the dissertation.

Finally, I wish to thank my parents whose support throughout my academic career has always been appreciated and to Jeff Hawkins who was willing to work all of those long hours with me.

TABLE OF CONTENTS

LIST OF TABLES

LIST OF ILLUSTRATIONS PAGE

1. INTRODUCTION

The Alboran Sea serves as an excellent region in which to study the effects of strait flow on an adjacent sea. As the westernmost Mediterranean basin, the Alboran Sea is the first to receive the inflowing Atlantic water from the Strait of Gibraltar. This incoming jet is thought to be largely responsible for many of the circulation features observed in the Alboran, in particular a meandering current and a persistent anticyclonic gyre which dominates the circulation of the western Alboran Sea.

Mean flow through the Strait of Gibraltar is driven by sea level and density differences resulting from the evaporative loss of water in the Mediterranean. The characteristics of the incoming Atlantic water have been observed to be quite different from those of the subsurface Mediterranean water. In particular, the Atlantic water is always less dense and less saline (salinity = 36.5) than the Mediterranean water (salinity =38.5)(Gascard and Richez, 1984; Kinder and Parrilla, 1984a and 1984b; Parrilla and Kinder, 1984). The Atlantic water flows through the narrow (20 km) and shallow (300 m) Strait of Gibraltar into the Alboran Sea forming a 150 to 200 m deep upper layer. The large volume transport of inflowing Atlantic water, between 1 and 2 x 10^6 m^3/sec (Lacombe, 1971; Bethoux, 1979; Lacombe and Richez, 1982; Kinder and Parrilla, 1984a and 1984b), forms a narrow jet

approximately 30 km wide with surface speeds near the strait of 100 cm/sec (Lacombe, 1961; Peluchon and Donguy, 1962; Grousson and Faroux, 1963; Lanoix, 1974; Cheney, 1977; Petite et al., 1978; Wannamaker, 1979; Kinder, 1984 and Perkins and Saunders, 1984). The Mediterranean water, located at depths greater than 200 m, flows slowly westward at approximately 5 cm/sec, AND exits through the Strait of Gibraltar. It has been observed that this Mediterranean water can exist as two subsurface layers: an intermediate layer, the Levantine Intermediate Water, and a lower layer, the Mediterranean Deep Water. The intermediate water has been located (Gascard and Richez, 1984; Parrilla and Kinder, 1984) in the northern and central Alboran Sea while the deep water has been observed only along the Morroccan coast (Bryden and Stommel, 1982; Gascard and Richez, 1984; and Parrilla and Kinder, 1984).

The general circulation of the Alboran sea has been observed and documented by numerous authors (Ovchinnikov, 1966; Lanoix, 1974; Parrilla and Kinder, 1984). One observed pattern of the upper layer Atlantic water circulation is given by the dynamic height contours from Lanoix (1974). The Atlantic water inflow enters the basin and flows northeast to approximately $4^{o}W$, curves southward and then splits (Fig. 1). Part of the jet flows west and is incorporated into the anticyclonic gyre while the remainder flows southeast to Cape Tres Forcas and then along the African coast forming the southern periphery

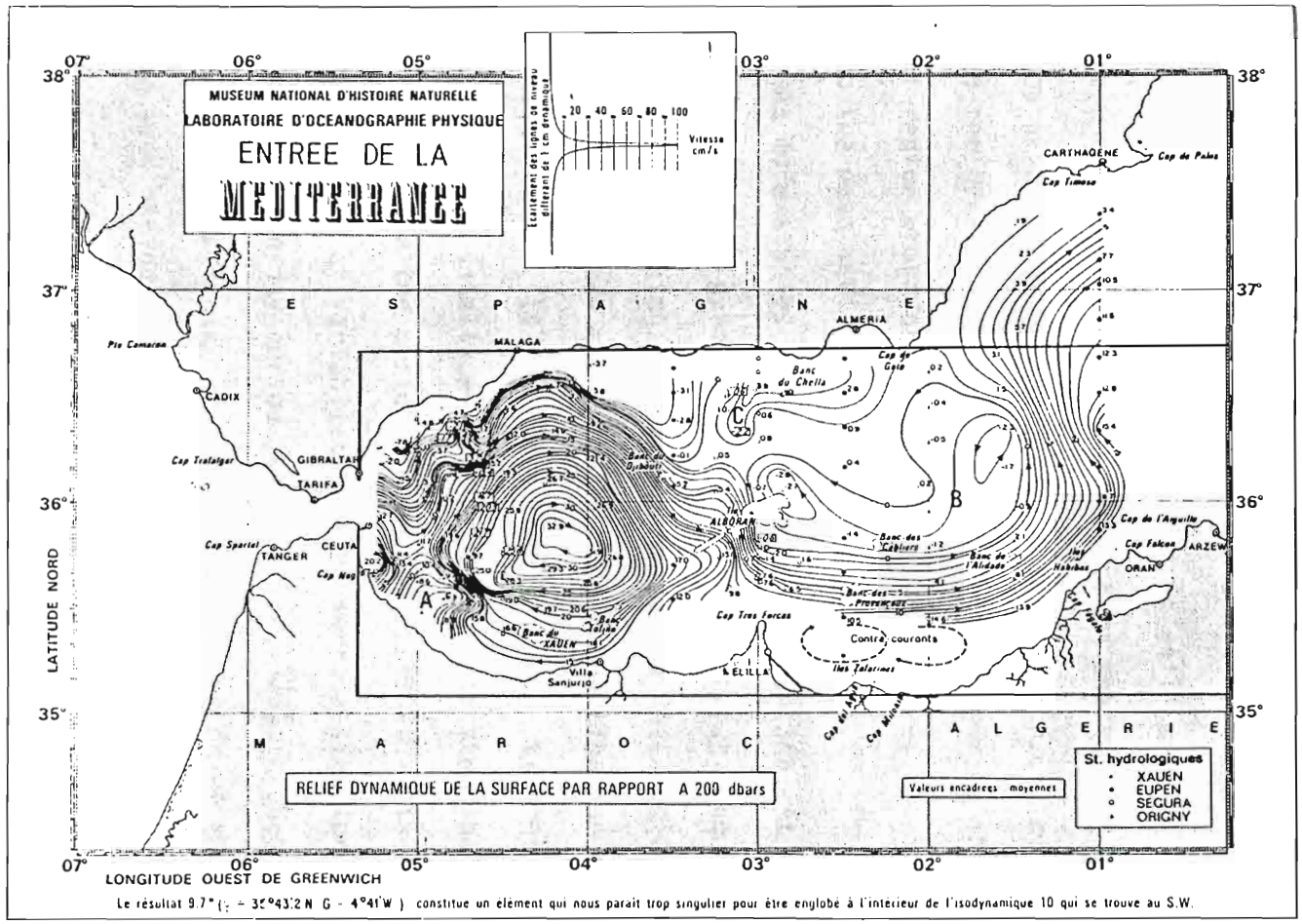

FIG. 25

Fig. 1. Dynamic topogrpahy of the surface relative to 200 dbar for July-August 1962 (Lanoix, 1974). Overlaid rectangle is the reduced gravity model geometry.

of a cyclonic circulation. Observations indicate that the anticyclonic circulation extends to at least 200 m depth. The existence of an anticyclonic gyre below 200 m depth is still a point of controversy. Drifter data (Pistek, et al., 1984) from the western Alboran Sea at depths greater then 200 m indicate that cyclonic circulation exists below the gyre. However this circulation reverses in the southern shelf region where drifters either turn towards the Strait of Gibraltar or to the east moving along the Alboran ridge.

As more studies are made of the Alboran Sea, it becomes obvious that the Alboran gyre observed by Lanoix is just one of many configurations which can exist. Satellite infrared imagery indicates that variations may exist in the shape, location and intensity of the gyre (Wannamaker, 1979). In a recent study, LaViolette has compiled a time series of satellite infrared imagery of the Alboran Sea taken twice daily for the period October 6-16, 1982. This time series shows a large amount of variability in the surface signature of the gyre during this ten day period (LaViolette, 1983). Cheney and Doblar (1982) have documented a change in the location of the front over a two week period while Bucca and Kinder (1983) have observed that the time scale of surface variations can be much shorter (1-2 days) then that of subsurface (100 m) variations (1-2 weeks). Figures 2a-f show the variability of the gyre observed using satellite infrared imagery. Figure 2a shows the gyre occupying the entire north-south extent of the

January 1

February 18

January 22

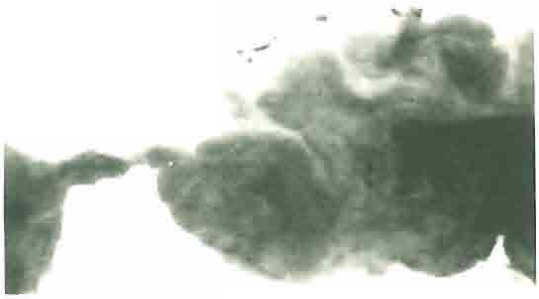

March 2

February 1

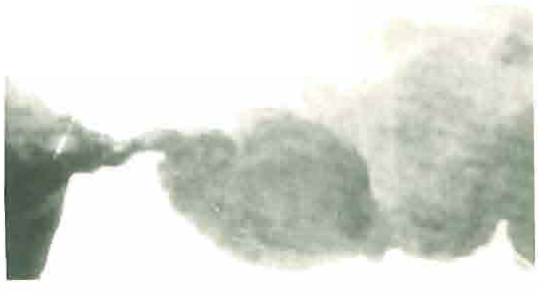

March 7

Fig. 2. Infrared satellite imagery of the Alboran Sea, 1982. Lighter shades indicate colder water.

basin while Fig. 2f shows a gyre of much smaller north-south extent. Satellite imagery indicates that the inflow may enter the basin in a due east or north of east direction. If it is assumed that the northern boundary of the gyre is defined by the Atlantic water inflow, then the angle at which the Atlantic water enters the Alboran sea should have important effects on the dimensions of the gyre. Though the gyre's size and shape may vary, both hydrographic data and satellite infrared imagery support the year round existence of the gyre (Stevenson, 1977; Cheney, 1978; Wannamaker, 1979; Burkov et al., 1973; Gallagher et al., 1981).

Several theories have been suggested to explain the existence of the anticyclonic gyre (Lanoix, 1974; Ovchinnikov et al., 1966; Nof, 1978; Miller and Whitehead, 1979; Preller and Hurlburt, 1982; and Bryden and Stommel, 1982). Ovchinnikov suggested that the gyre is formed by wind stress forcing. However, the established permanence of the gyre seems to disprove this theory (Miller and Whitehead, 1979). Nof, using an analytical model, determined that if the initial vorticity in the channel is approximately equal to the Coriolis parameter, the current will turn north, contrary to turning to the south (right), as expected in the northern hemisphere. The vorticity in this case could be determined upstream from the outlet by the length of the strait and topographic effects within the strait.

Miller and Whitehead (1979) found that an anticyclonic gyre,

similar to the Alboran gyre, formed in rotating tank experiments. In these experiments, a density driven current enters into the basin, turns right and hugs the southern wall. For particular values of the Rossby radius, the jet separates from the wall. The resulting gyre as well as the jet are initially a Rossby radius in size. The gyre continues to grow, accumulating fluid from the jet. Without some limiting effect the gyre would grow without bound. Miller and Whitehead have suggested that a coastal feature, Cape Tres Forcas, acts as a barrier to the gyre growth. Preller and Hurlburt (1982) discuss the importance of the relationship of the geometry of the Strait of Gibraltar to the Alboran sea. Inflow could be forced, geometrically, into the Alboran sea in a northeasterly direction. Bryden and Stommel (1982), using a Bernoulli argument, suggested that the Mediterranean water exiting the strait could provide a source of anticyclonic vorticity to the Atlantic water inflow.

The purpose of this study is to simulate the observed surface and subsurface circulation patterns of the Alboran Sea, in particular the path of the incoming jet and the anticyclonic gyre, and to understand the dynamics of the system. Two types of layered hydrodynamic numerical models are used in this study: the reduced gravity and two-layer models. The reduced gravity model is the simplest model capable of simulating the major circulation features of the upper 200 m. The two-layer model is then used to investigate the subsurface circulation

and the possibility of baroclinic instability and the effects of bottom topography.

The model formulation and parameters are discussed in section 2. A review of the early reduced gravity results as well as new reduced gravity results are presented in section 3. Section 4 describes the two-layer results while section 5 presents a summary and conclusions. Appendix A is included to discuss the effects of wind stress forcing.

2. THE ALBORAN SEA MODELS

Two types of numerical models are used in this study: a reduced gravity model and a two-layer model. Both models are nonlinear and have been adapted from the Hurlburt and Thompson (1980) Gulf of Mexico model to the Alboran Sea. The reduced gravity model is regarded as a two layer model in which the lower layer is infinitely deep and at rest. Thus the interface between the two layers may deform with virtually no resulting motion in the lower layer. An appropriate value for the gravitational acceleration is chosen to demonstrate the behavior of the first internal mode. The infinitely deep lower layer of the reduced gravity model precludes the existence of bottom topography and baroclinic instability. The two "active" layer model contains the minimum number of layers which allow baroclinic instability and the inclusion of topography and the pycnocline.

Both models are stably stratified with a fixed density contrast between two immiscible layers. All other thermodynamic effects are excluded. The models also make use of the hydrostatic and Boussinesq assumptions and retain a free surface in a rotating right-handed coordinate system. The primitive equations on a β-plane define both models and the vertically integrated equations appear in transport form

as

$$\frac{\partial \vec{V}_i}{\partial t} + (\nabla \cdot \vec{V}_i + \vec{V}_i \cdot \nabla)\vec{v}_i + \hat{k} \times f\vec{V}_i$$

$$= -h_i \vec{\nabla} P_i + (\vec{\tau}_i - \vec{\tau}_{i+1})/\rho + A\nabla^2 \vec{V}_i$$

$$\frac{\partial h_i}{\partial t} + \nabla \cdot \vec{V}_i = 0$$

where i = 1,2 for the two-layer model, i = 1 for the reduced gravity model and

$$\nabla = \frac{\partial}{\partial x}\hat{i} + \frac{\partial}{\partial y}\hat{j}$$

$$\vec{P}_1 = g\eta_1$$

$$\vec{P}_2 = \vec{P}_1 - g'h_1$$

$$\vec{V}_i = h_i\vec{v}_i = h_i(u_i\hat{i} + v_i\hat{j})$$

$$g' = g(\rho_2 - \rho_1)/\rho$$

$$f = f_o + \beta(y - y_o)$$

$$\vec{\tau}_i = \tau_i^x \hat{i} + \tau_i^y \hat{j}$$

and x and y are tangent-plane Cartesian coordinates with x directed eastward and y northward, u_i and v_i are the eastward and northward velocity components in each layer, h_i is the layer thickness, t is time, g is the acceleration due to gravity, ρ_i is the density of seawater in layer i, f_o and y_o are the values of the Coriolis parameter and the y-coordinate at the southern boundary, $\vec{\tau}_1$ is the wind stress,

and $\vec{\tau}_2$ is the interfacial stress. The remaining parameters are defined in Table 1.

The model equations 1-3 are solved on a numerically staggered grid represented, in it simplest form Fig. 3, by the "C" stencil of Messinger and Arakawa (1976).

The time differencing used in this model is leap-frog, with an Euler difference used for start and restart to prevent the possibility of time splitting associated with the leap-frog scheme. Advective terms use scheme "C" from Grammeltvedt (1969). The Coriolis force is treated by using the Holland and Lin (1975) scheme. Horizontal friction is lagged in time to maintain computational stability. (See Appendix A; Hurlburt and Thompson, 1982; for more detailed explanations of the finite differencing of the equations and boundary conditions).

Two types of model geometry were used in this study; a rectangular representation and a realistic coastline. Figure 1 shows the rectangular representation of the Alboran Sea, used in many of the reduced gravity experiments, superimposed on the Lanoix map of dynamic heights. This domain is 600 km X 160 km with 10 km X 5 km grid resolution for each dependent variable. Forcing in these experiments is due to the prescribed inflow velocity across the 3 grid point, 15 km wide, western port representing the Strait of Gibraltar. The inflow is exactly compensated by outflow through the open eastern boundary

TABLE 1

Model parameters for the pivotal experiment

Parameter	Definition	Value
A	eddy viscosity	$100\ m^2 sec^{-1}$
β	(df/dy)	$2 \times 10^{-11}\ m^{-1}\ sec^{-1}$
f	Coriolis parameter	$8 \times 10^{-5}\ sec^{-1}$
g'	reduced gravity due to stratification	$.02\ m\ sec^{-2}$
g	acceleration of gravity	$9.8\ m\ sec^{-2}$
H_1	undisturbed upper layer depth	200 m
H_2	undisturbed lower layer depth (two layer) (reduced gravity)	 2400 m ∞
$L_x \times L_y$	horizontal dimensions of the domain (rectangular box) (irregular geometry)	 600 km X 160 km 420 km X 230 km
$\Delta x \times \Delta y$	horizontal grid spacing for each dependent variable	10 km X 5 km
Δt	time step (semi-implicit) (explicit)	 2700 sec 900 sec
$\vec{v}1in$	upper layer inflow velocity	30 cm/sec
$\vec{v}2in$	lower layer inflow velocity	.2 cm/sec
α	angle of inflow	21^o north of east
τ	wind stress	$\simeq .5\ dynes/cm^2$
ts	inflow spinup time	30 days

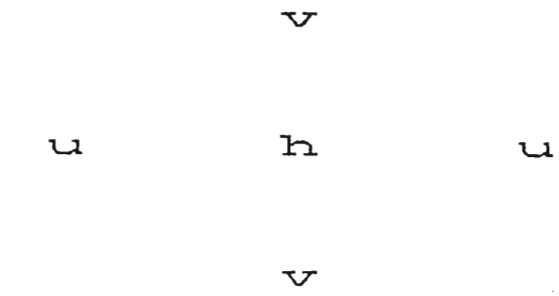

Fig. 3. The staggered grid, "C" stencil of Messinger and Arakawa, 1976.

(Hurlburt and Thompson, 1980). Except at the inflow and outflow ports, the boundaries are rigid and a no-slip boundary condition is prescribed for the tangential flow.

The results of two different types of models will appear in this study. The first is the semi-implicit model, the second is a two-layer model (Hurlburt and Thompson, 1980). Boundary conditions at the open ports state that the tangential component is set to zero one-half grid distance outside the physical domain. In the initial semi-implicit reduced gravity cases (Preller and Hurlburt, 1982), a viscous boundary layer using linear interfacial stress was applied at the eastern boundary to damp oscillations which could appear due to the integral constraint on outflow. The maximum value used for the drag coefficient was 10^{-3}. The viscous damping decreased exponentially over a distance of 50 km from the eastern boundary. Except for this viscous boundary, the interfacial stress between the upper layer and the lower layer was zero.

Figures 4a and 4b depict the two different bottom topographies and the irregular geometry used in the two-layer experiments. These irregular boundaries and bottom topographies were obtained from the Synthetic Bathymetric Profiling system (SYNBAPS)(Vanwyckhouse, 1973; and Vanwyckhouse, 1979) data set of topography. Values were interpolated using a nine point scheme from the 10 minute resolution of the data set to the 10 km x 5 km resolution of the model. The coastline

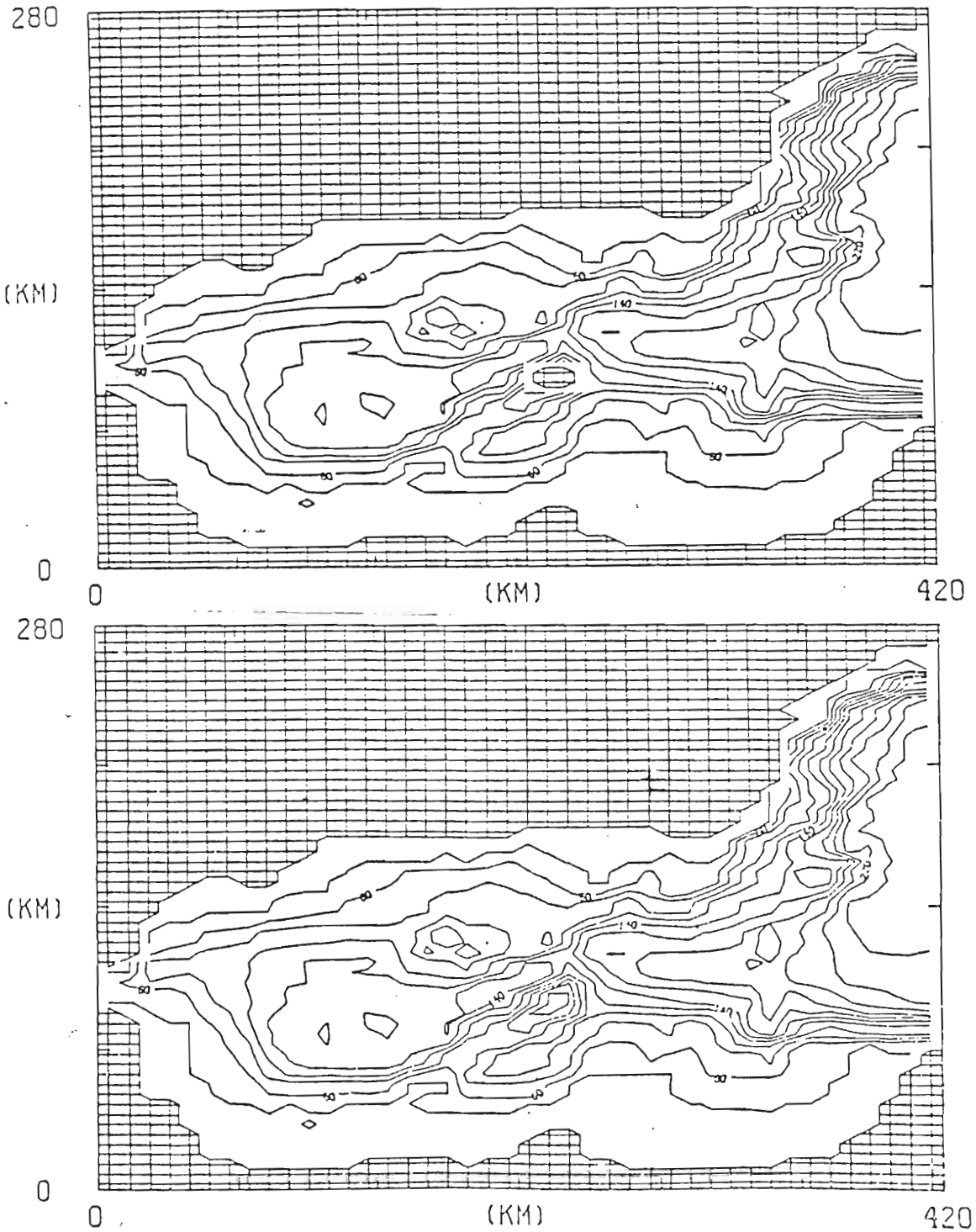

Fig. 4. Alboran Sea bottom topography interpolated from the Synthetic Bathymetric Profiling System (SYNBAPS) data. a)Topography with idealized Alboran Island and b) topogrpahy with ridge only. Values are in meters x 10^{-1} with a contour interval of 20.

was then drawn using a cutoff depth of 20 m to eliminate errors existing on the boundary of the data set. One restriction of the existing formulation of the layered models is that when the topography intersects the interface between layers, the solutions become unstable. Thus allowing for the 200 m deep upper layer and vertical displacement of the interface, the bottom topography of the Alboran Sea was restricted to a minimum depth of 400 m. Using this "cutoff" depth of 400 m creates a somewhat broad shelf and a flattened Alboran ridge, Fig. 4b ("seuill d'Alboran", Giermann et al, 1968). To include the shallow topography associated with the Alboran Island, a four grid point island is included on the ridge, Fig 4a. The actual surface area of this small volcanic island is 600 m x 250 m. A four point island 20 km x 10 km, however is smallest island allowed by the numerical design of the model. A detailed description of the topography of the Alboran sea is found in Parrilla and Kinder (1984).

Parameters for each of the model standard cases are given in Table 1. The only dissipation in the model, other then the viscous boundary layer, is due to horizontal friction. The value for the coefficient of eddy viscosity was chosen to keep the grid interval Reynolds number

$$Re = \frac{v\Delta x}{A} > 10$$

thus keeping friction from having an unrealistically strong damping

effect on important features of the solutions. This cutoff value was determined by examining the results of a large number of numerical model experiments. The value chosen for reduced gravity due to stratification was appropriate for observed density differences in the Alboran Sea (Gascard and Richez, 1984; Bryden and Stommel, 1982 and Parilla and Kinder, 1984). In the two layer model, the value of g' is multiplied by $(H_1 + H_2)/H_2$ to yield the same internal values for gravity wave speed, radius of deformation and Rossby wave speed as in the reduced gravity model. The undisturbed upper layer thickness is based on many observations of the Alboran Sea which show a sharp density-salinity gradient at 150-200 m depth.

Horizontal grid spacing was chosen to allow the resolution of the mesoscale features being studied in the Alboran Sea. A minimum of 8-10 grid points, in both horizontal dimensions, is necessary to properly resolve a feature. The Alboran gyre is defined with an average diameter of 100 km. Thus the model has an average of 10 grid points with which to define the gyre.

For cases using the irregular geometry, the western inflow port is 20 km wide and the eastern outflow port is 200 km wide. Initial reduced gravity model experiments (Preller and Hurlburt, 1982) used a 15 km wide port. Later reduced gravity experiments used a 20 km wide port to agree with the size of the port obtained from the SYNBAPS topographic data set. The change was based on the variation of the

width of the strait with respect to depth. At the 100 m contour, the midpoint of the 200 m deep upper layer, the width of the strait measures 18 km. In the later experiments, 20 km was chosen as a closer estimate of the average strait width. In the lower layer, the eastern boundary serves as the inflow port while the Strait of Gibraltar becomes the outflow boundary. A simple schematic of the inflow-outflow design for the reduced gravity and two-layer models is depicted in Fig. 5. Specification of the model forcing is accomplished using one of two methods: 1) by prescribing velocity, ($\vec{v}1in$), or 2) by prescribing transport, ($\vec{V}1in$), and allowing the model to determine the velocities.

Using a standard inflow velocity of 30 cm/sec through a 20 km wide 200 m deep port determines an inflow transport of 1.2×10^6 m^3/sec^{-1} or (10^6 $m^3/sec^{-1} = 1$ sv) 1.2 sverdrups. For cases using the standard inflow angle, the 30 cm/sec eastward component was given an additional 12 cm/sec northward component. Thus the total velocity in these cases was 33 cm/sec and total mass transport 1.3 sv. This values agrees with observations of Strait of Gibraltar inflow (Lacombe and Richez, 1982; Kinder and Parrilla, 1984a and 1984b. A standard inflow value of .2 cm/sec was chosen for the lower layer to agree with observation. Transport out of the Mediterranean is known to be less than incoming transport due to the effect of evaporation being greater than precipitation and river runoff. An inflow of .2 cm/sec, through a

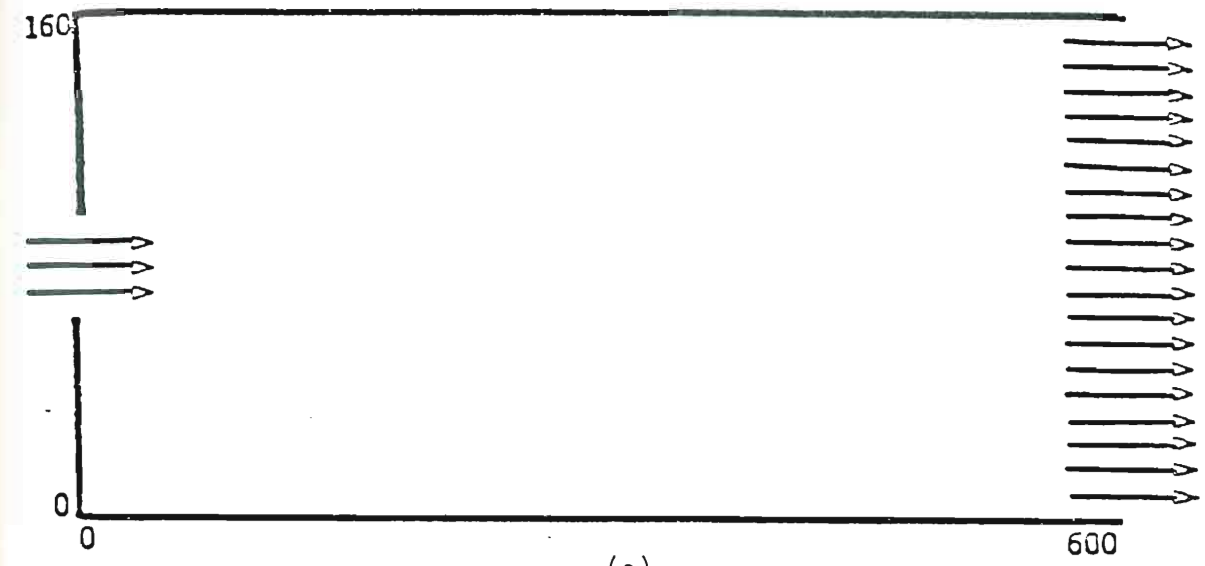

(a)

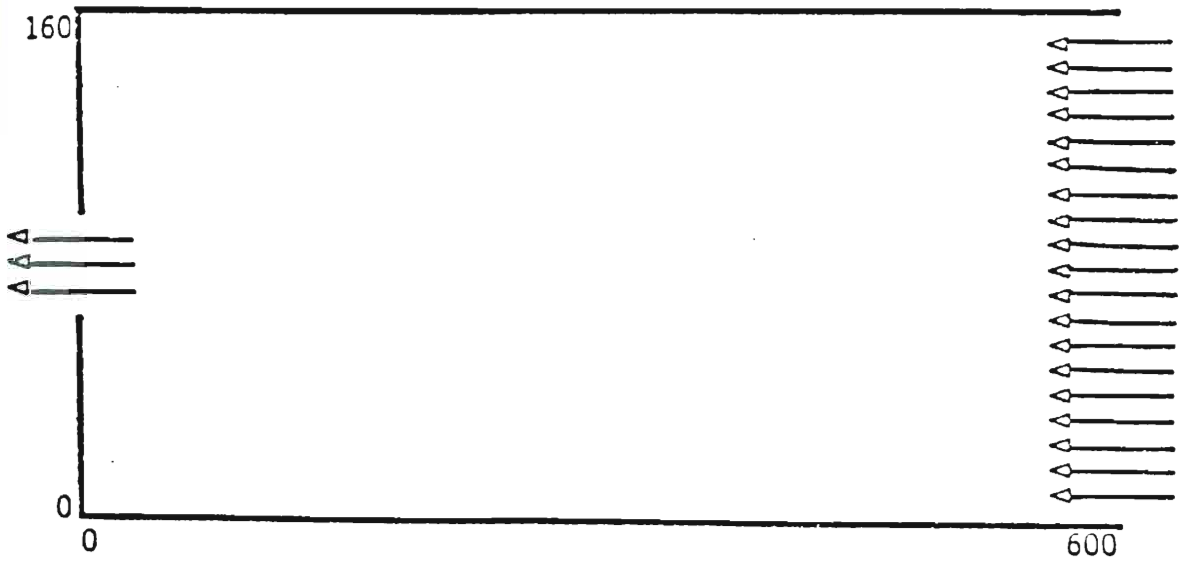

(b)

Fig. 5. Inflow and outflow boundaries for a) the upper layer and b) the lower layer.

200 km wide boundary which is a maximum of 2400 m deep, creates a mass transport of 1.0 sv. It also creates velocities along the southern shelf near the Strait of Gibraltar of 10 cm/sec agreeing with the observations of Gascard and Richez (1984) and Bryden and Stommel (1982). Inflow is gradually increased from zero to its maximum value over a finite period of time. The inflow velocities increase as

$$e^{-(T_s^2/t^2)}$$

where T is the "spin up" time and t is the actual time. This method is used to minimize the excitation of high frequency waves. The standard angle of inflow was chosen to be 21^{o} north of east based on the geometric orientation of the Strait of Gibraltar with respect to the Alboran Sea. This angle was varied based on direct observations (Lacombe, 1961; Lacombe and Richez, 1982) and inferences from satellite imagery.

3. MODEL EXPERIMENTS - The semi-implicit reduced gravity cases

The first goal of this study was to simulate the circulation of the Alboran Sea in accordance with observations and to gain an understanding of the dynamics from these simulations. The reduced gravity model, the simplest model able to simulate the major features of the circulation above the pycnocline, is used to study the anticyclonic circulation of the upper layer (200 m) and the Atlantic water inflow. This model has demonstrated substantial skill in simulating the circulation and dynamics of the Gulf of Mexico (Hurlburt and Thompson, 1980) and the Caribbean (Heburn et al, 1982).

Over fifty numerical experiments were performed using this model. The early results of these experiments are discussed in Preller and Hurlburt (1982). A uniform velocity profile was used to force inflow through the 15 km wide Strait of Gibraltar into the basin. An inflow velocity of 90 cm/sec was chosen to agree with observations of surface flow (Lacombe and Richez, 1982; Perkins and Saunders, 1984 and Parrilla and Kinder, 1984).

Flow was allowed to exit (or enter) the eastern boundary through the viscous boundary layer. The most striking feature existing in all of the solutions was a meandering eastward current. The first meander of the current forms the northern boundary of an anticyclonic circulation while the second meander bounded the southern side of a

cyclonic circulation.

Tests were performed to assure that in these reduced gravity cases, the use of a viscous boundary layer at the open eastern boundary did not distort the interior solutions. Figure 6 shows two solutions which differ only in the east-west extent of the basin. Model solutions are presented in terms of pycnocline anomaly, PA. The anomaly represents the deviation of the interface between the upper and lower layers from its initial position. Downward deviations, a thickening of the layer, are defined by solid contours while upward deviations, a thinning of the layer, are define by dashed contours. The two solutions agree out to the first 400 km. The only disagreement appears between 400-500 km, the location of the viscous boundary layer. The viscous boundary has the effect of spreading the pycnocline anomaly contours and diminishing the jet structure to a more uniform flow across the boundary.

Initial attempts were made to duplicate the Lanoix configuration of the gyre. This gyre fills the entire north-south extent of the basin and extends approximately 180 km in the east-west direction. Preller and Hurlburt (1982) have shown that a gyre of similar dimensions existed as a steady state solution when inflow was forced in a northeastward direction, Fig. 7a. A weak cyclonic circulation exists in the eastern half of the Alboran Sea with the inflowing Atlantic water hugging the southern boundary. When inflow was not angled but

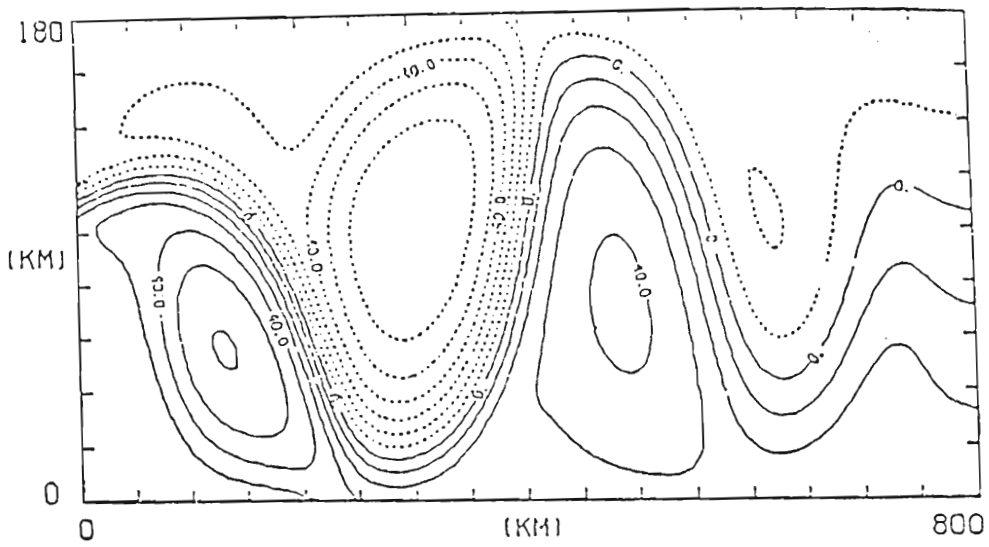

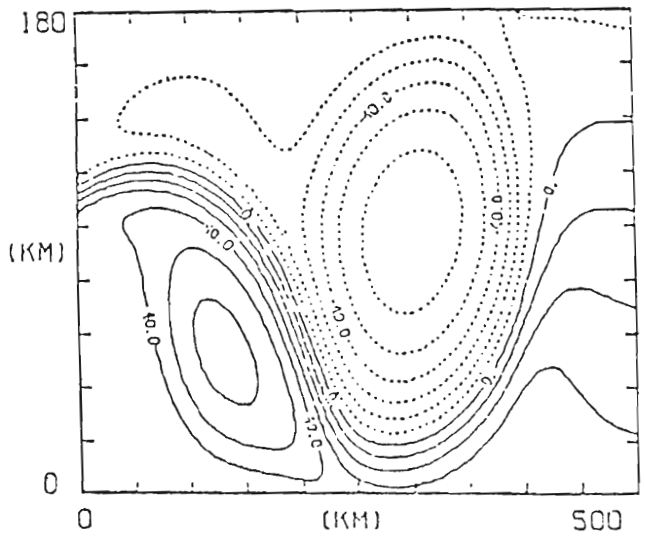

Fig. 6. Pycnocline anomaly of angled inflow reduced gravity cases. Cases are identical except for the length of the basin a) 180 x 800 km basin; b) 180 x 500 km basin. Scale factor for these figures is x/y, 1/2.5. Contour interval is 10 m.

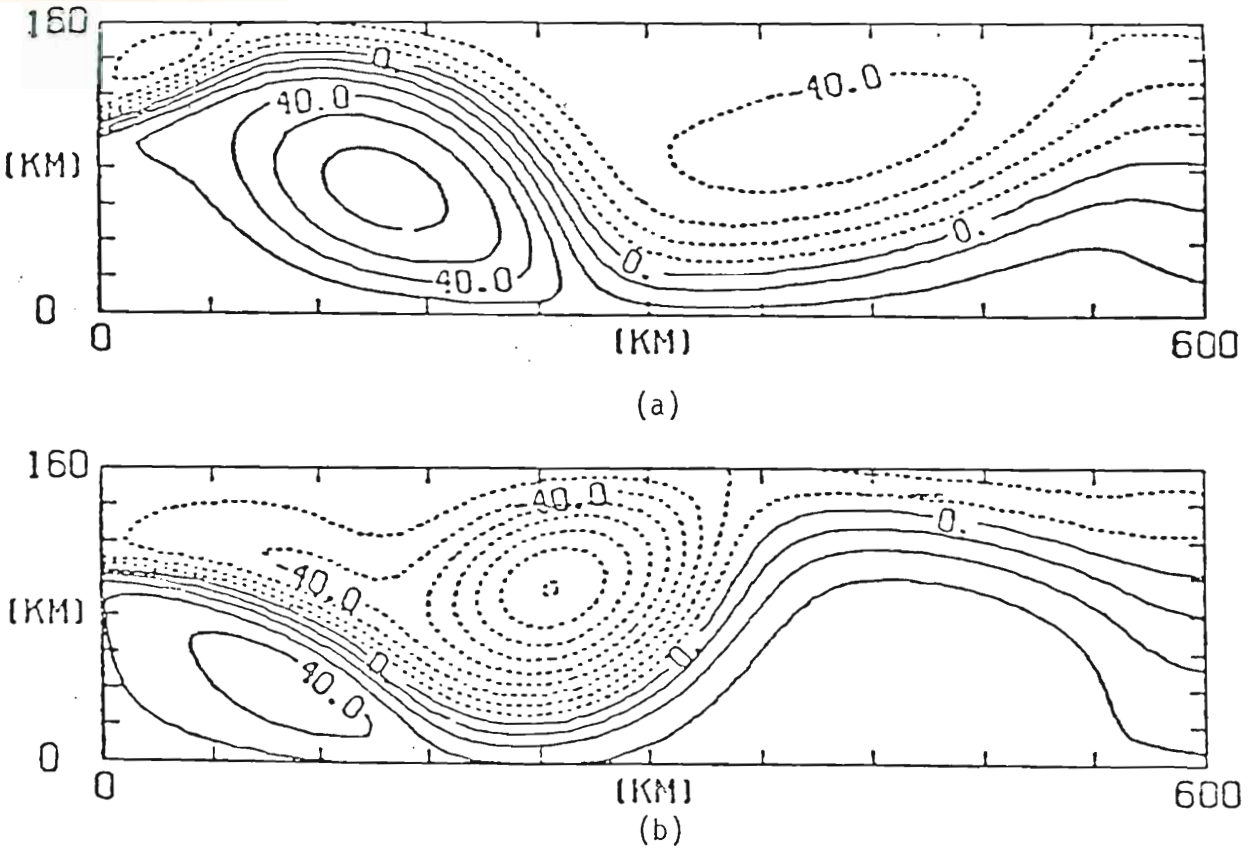

Fig. 7. Steady state reduced gravity model solutions for a) 90 cm/sec 21^{o} angled inflow and b) 90 cm/sec due east inflow. Contour interval is 10 m.

forced in due east, the jet quickly turned to the south forming a weaker anticyclonic gyre of smaller dimensions with a stronger cyclonic gyre to the east (Fig. 7b). These steady state solutions indicate that if the inflow is forced northward, geometrically, the gyre forms with a larger north-south extent.

The east-west extent of the model gyre of Fig. 7a is approximately 250 km, somewhat large when compared to the Lanoix configuration. Using a 90 cm/sec eastward inflow with a 15 km wide port in a 200 m deep layer results in an inflow mass transport of 2.7 sv. In cases where the inflow was angled, a 36 cm/sec northward component was added creating a v = 97 cm/sec and a transport of 3.0 sv. This value borders on the upper limits of the observed mass transport. The inflow velocity, 90 cm/sec, was chosen to agree with surface observations. However, the model being used is a layer averaged model and the prescribed inflow velocity is the velocity of the entire 200 m deep layer. In a recent experiment (Kinder and Parrilla, 1984) transport was measured and calculated in the Strait of Gibraltar to be 1.3 sv. To agree with the observed mass transport and with the geometry of the port as obtained by the SYNBAPS data, the port was widened to 20 km and the inflow velocity reduced to 30 cm/sec resulting in a 1.2 sv inflow.

The results of an experiment using the new inflow velocity 30 cm/sec angled 21^{o} north of east and an identical case using 90 cm/sec

angled 21^{o} north of east are shown in Figs. 8a and b. In this case and the remaining reduced gravity experiments, the port width was expanded to 20 km. As a result, in the angled inflow cases of v = 97 cm/sec and v = 33 cm/sec creating mass transports of 3.9 sv and 1.3 sv respectively. Reducing the transport decreased the amplitude of the meander, reducing the east-west dimension of the gyre to 180 km in agreement with the Lanoix gyre. Decreasing the transport by one third decreases the gyre intensity to one third of its previous value from a maximum PA of 75 m to a maximum PA of 25 m. The center of the gyres shift from 200 km to 100 km while the gyre's east-west extent decreases from 260 km to 180 km. The remaining solutions will use 30 cm/sec as the standard inflow velocity.

These steady state solutions raise some very important points. It has been suggested (Porter, 1976) that the dimensions of the gyre are directly related to the bottom topography with the Alboran Island limiting its east-west extent. However, the reduced gravity model, which does not incorporate bottom topography, results in a gyre of the proper dimensions. Miller and Whitehead (1979) found in rotating tank experiments that without a coastline feature, Cape Tres Forcas, their gyre grew without bound. These reduced gravity cases included no such coastline features. It will be shown that the dimensions of the gyre determined by the reduced gravity model depend upon the magnitude of the mass transport, the conservation of potential vorticity of the jet

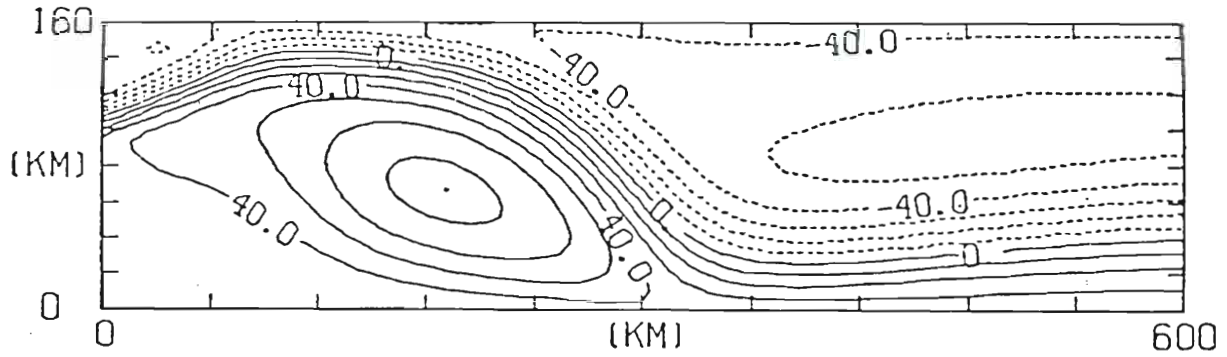

(a)

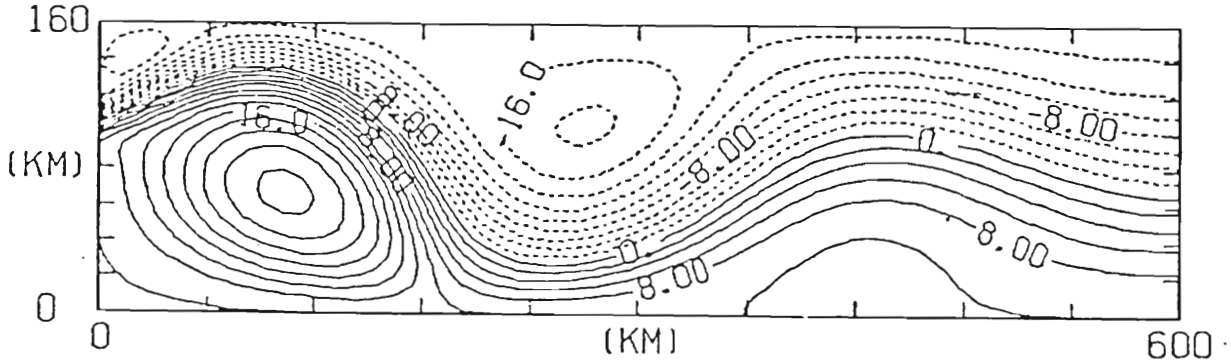

(b)

Fig. 8. Steady state reduced gravity solutions for a model wih a 20 km wide port and 21° angled inflow of a) 90 cm/sec (Contour interval is 10 m) and b) 30 cm/sec (Contour interval is 2 m).

and the effects of side wall boundaries.

a. The effects of rotation on the incoming Atlantic water

To examine the effects of rotation, a number of reduced gravity model tests were performed using a centered four grid point port with constant cross-port inflow velocity of 30 cm/sec due east and a 50 m deep upper layer. This depth was chosen to make the Rossby radius compatable with the of third the Miller and Whitehead rotating tank experiments. In their experiment, the incoming jet enters the tank, turns immediately right and clings to the side wall, forming no gyre. This configuration appears to be due to the fact that the Rossby radius is less then the channel width (7.3 cm versus 10.2 cm). In cases where the Rossby radius is larger then channel width, Miller and Whitehead's experiments show that the jet separates from the wall. The model test cases have a Rossby radius to channel width ratio of 13 km/20 km. This test was performed to determine if under these conditions, the model jet would also cling to the boundary forming no gyre. In the model test cases the only parameter varied was the Coriolis parameter from the standard value of $f = 8 \times 10^{-5} sec^{-1}$, to f=-f to f=0 to f=2f. Figures 9a-d and 10a-d show early spin up solutions at day 30 and later solutions at day 50 for the four cases studied. The solution show in Figs. 9a and 10a resembles the Miller and Whitehead results. The flow turns right and remains close to the

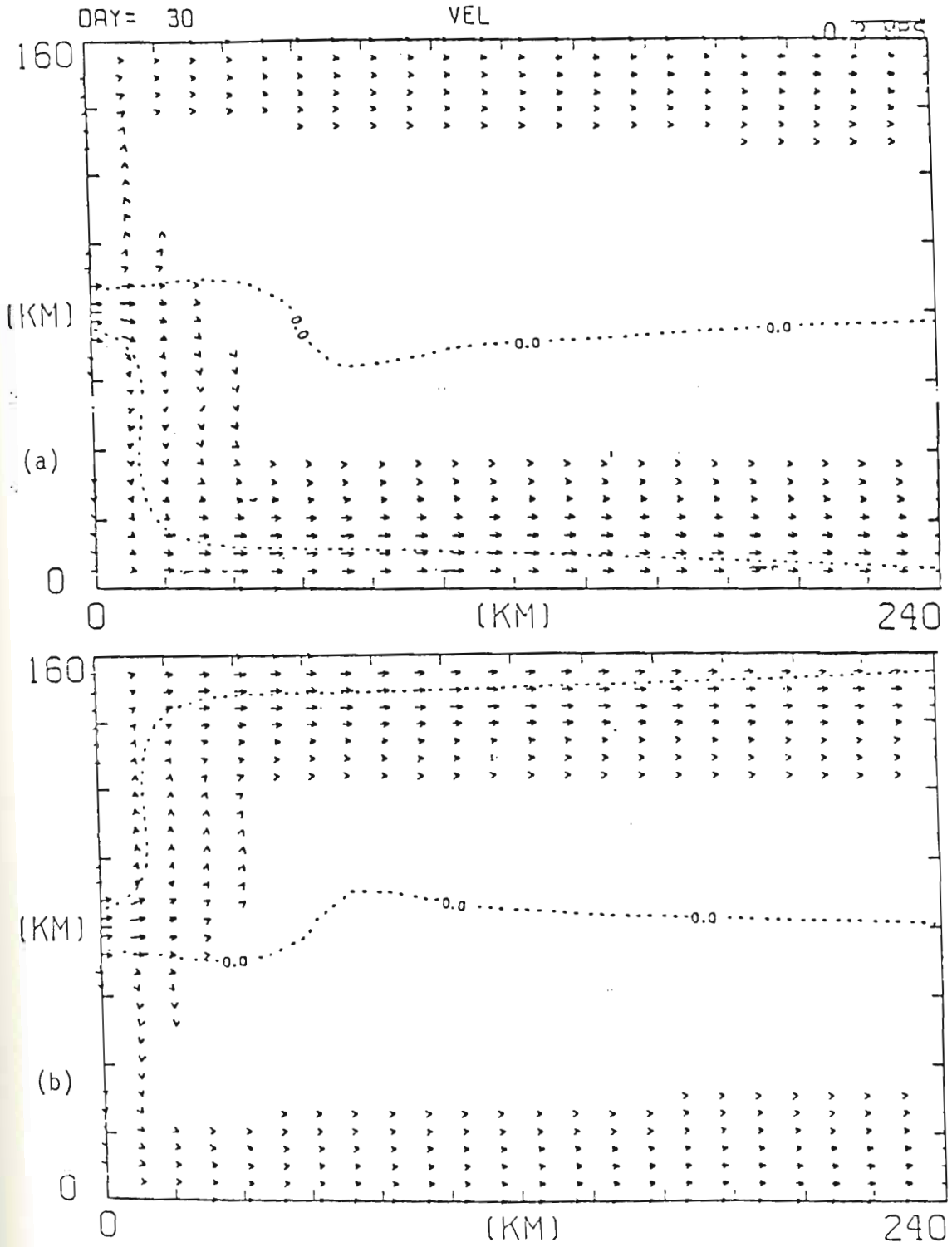

Fig. 9. Solutions in terms of velocity for reduced gravity cases at day 30 for a)$f = 8 \times 10^{-5}$ sec^{-1}, b) f= -f. Maximum velocity vector is 30 cm/sec.

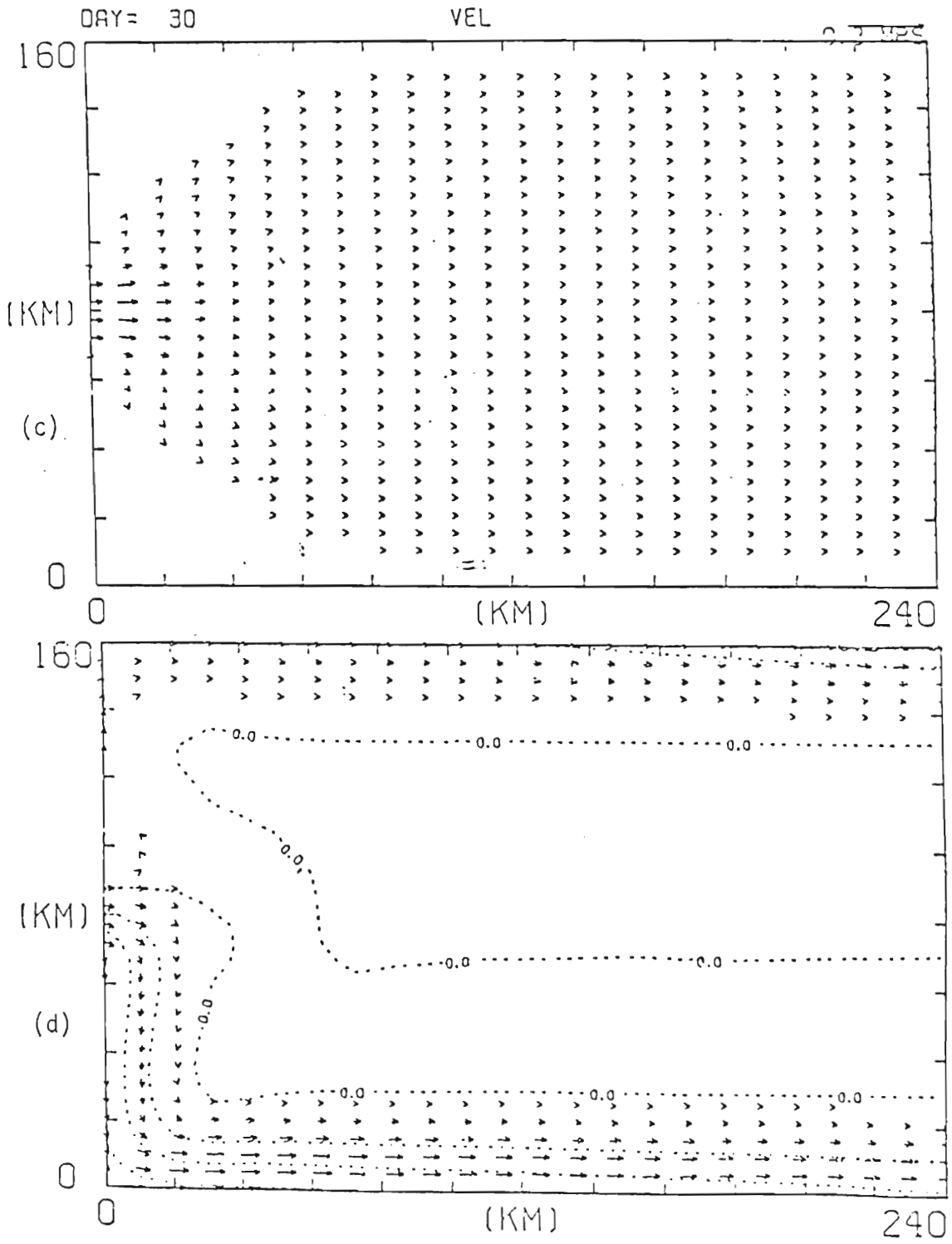

Fig. 9. Solutions in terms of velocity for reduced gravity cases at day 30 for c) f = 0, d) f = 2f. Maximum velocity is 30 cm/sec.

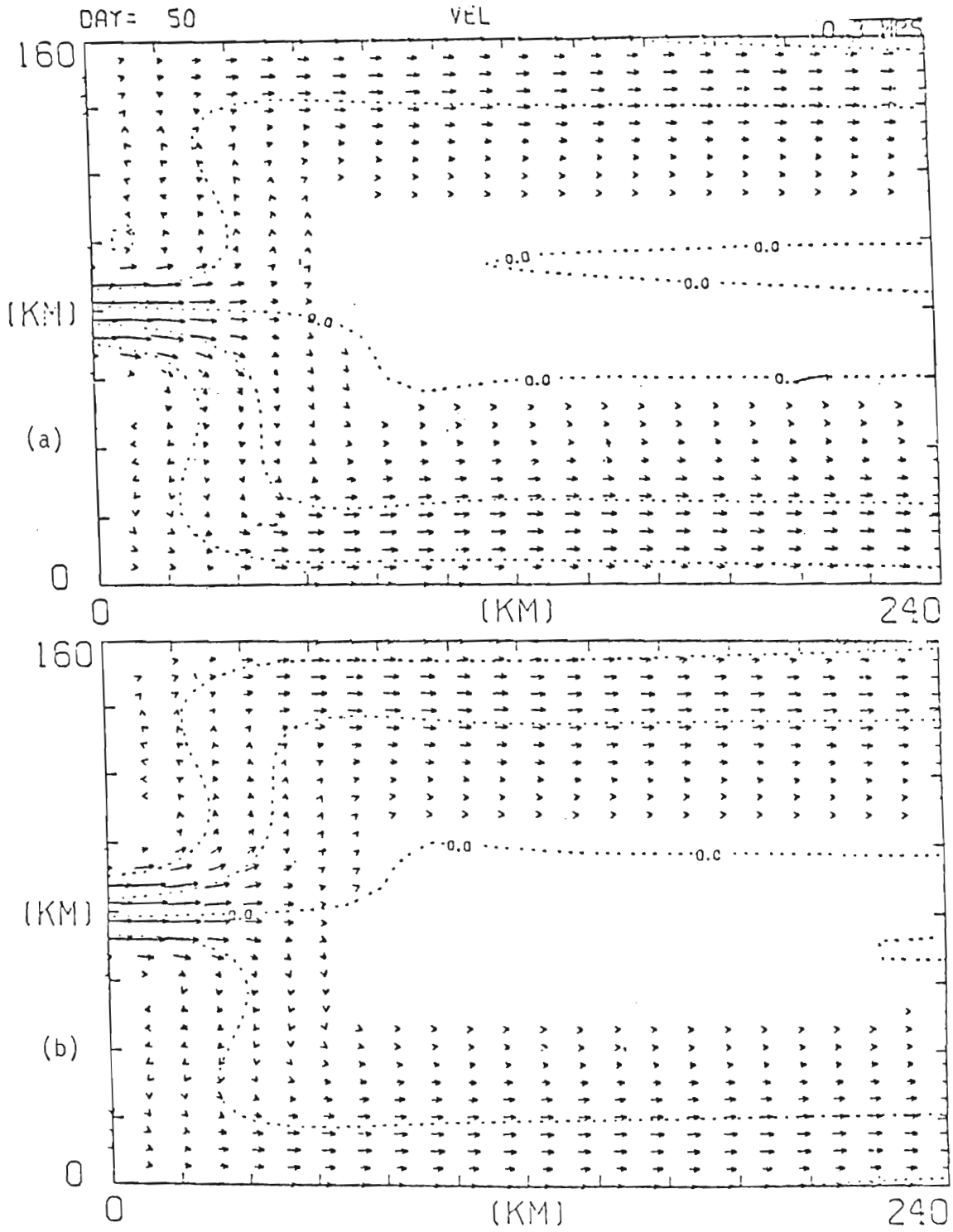

Fig. 10. Solutions in terms of velocity for reduced gravity cases at day 50 for a) $f = 8 \times 10^{-5}$ sec^{-1}, b) $f = -f$. Maximum velocity vector is 30 cm/sec.

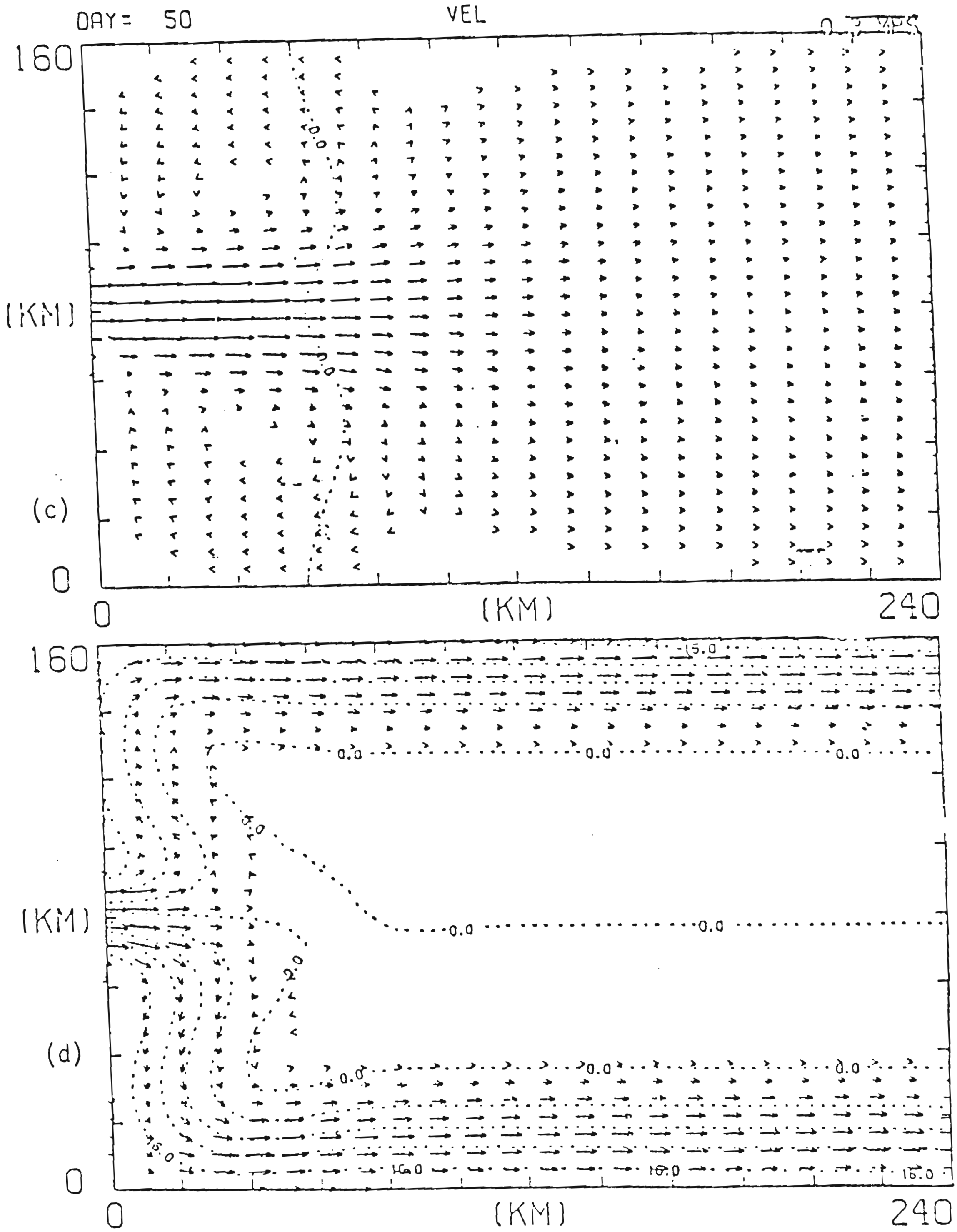

Fig. 10. Solutions in terms of velocity for reduced gravity cases at day 50 for c) f = 0, d) f = 2f. Maximum velocity is 30 cm/sec.

boundary. By day 50, the solutions show a different type of circulation from that seen by Miller and Whitehead. As the jet now penetrates farther into the basin, so does the southward turning flow. The growth of an anticyclonic circulation away from the wall appears to be an effect of the eastward extension of the jet, not the cause. As the jet extends farther east and south in time, the circulation within the anticyclonic gyre grows more intense and the dimensions of the gyre increase. This growth is finally limited when the jet impinges on the southern boundary. Reversing the sign of f, Figs. 9b and 10b, turns the inflow to the north. When f is zero, Figs. 9c and 10c, the flow spreads symmetrically about a line through the center of the basin. Doubling the Coriolis parameter, Figs. 9d and 10d, turns the flow more sharply towards the south. Thus as the fluid enters into the basin, two forces have a major effect on it; rotation and, to a lesser extent, viscosity. The viscosity of the fluid causes the spin-off of counter circulating gyres on both sides of the inflowing water. These gyres are symmetric about the jet in the case of f=0. These results show the same dynamic characteristics as a case of uniform flow in a pipe as it enters a region with larger surface area. However, the Coriolis force has the additional effect of turning the incoming jet to the right in the northern hemisphere. These results are not unexpected for a jet moving into a motionless viscous fluid in a rotating system.

b. The effects of upstream induced shear

These results do not answer an important question raised by satellite imagery and hydrographic data. If Coriolis effects turn the inflow towards the south, why is the inflow most often observed to be turned towards the north?

The experiments presented in Figs. 7 and 8 show that angling the inflow, based on the geometric orientation of the strait, results in an inflow which enters the Alboran Sea in a northeastward direction forming a large anticyclonic gyre. It was also suggested by Nof (1978) that shear, established in the flow upstream from the outlet, may cause this northward deflection. Figure 11 shows the results of two reduced gravity experiments with shear imposed at the inflow boundary. The first case Fig. 11a, used an imposed shear creating negative relative vorticity of 1.8×10^{-5}. This value is of the order of the Coriolis parameter. As a result, the steady state solutions turns northward in agreement with Nof. In the second case, Fig. 11b, the relative vorticity is equal but opposite in sign and the inflow turns southward as it enters the basin. Additional experiments were performed which show that if the negative relative vorticity is reduced enough ($< .5 \times 10^{-5}$), the flow no longer turns north.

Thus both the geometric orientation and shear induced upstream in the strait can turn the incoming jet north. For simplicity, the remaining cases will address only the angled inflow situation.

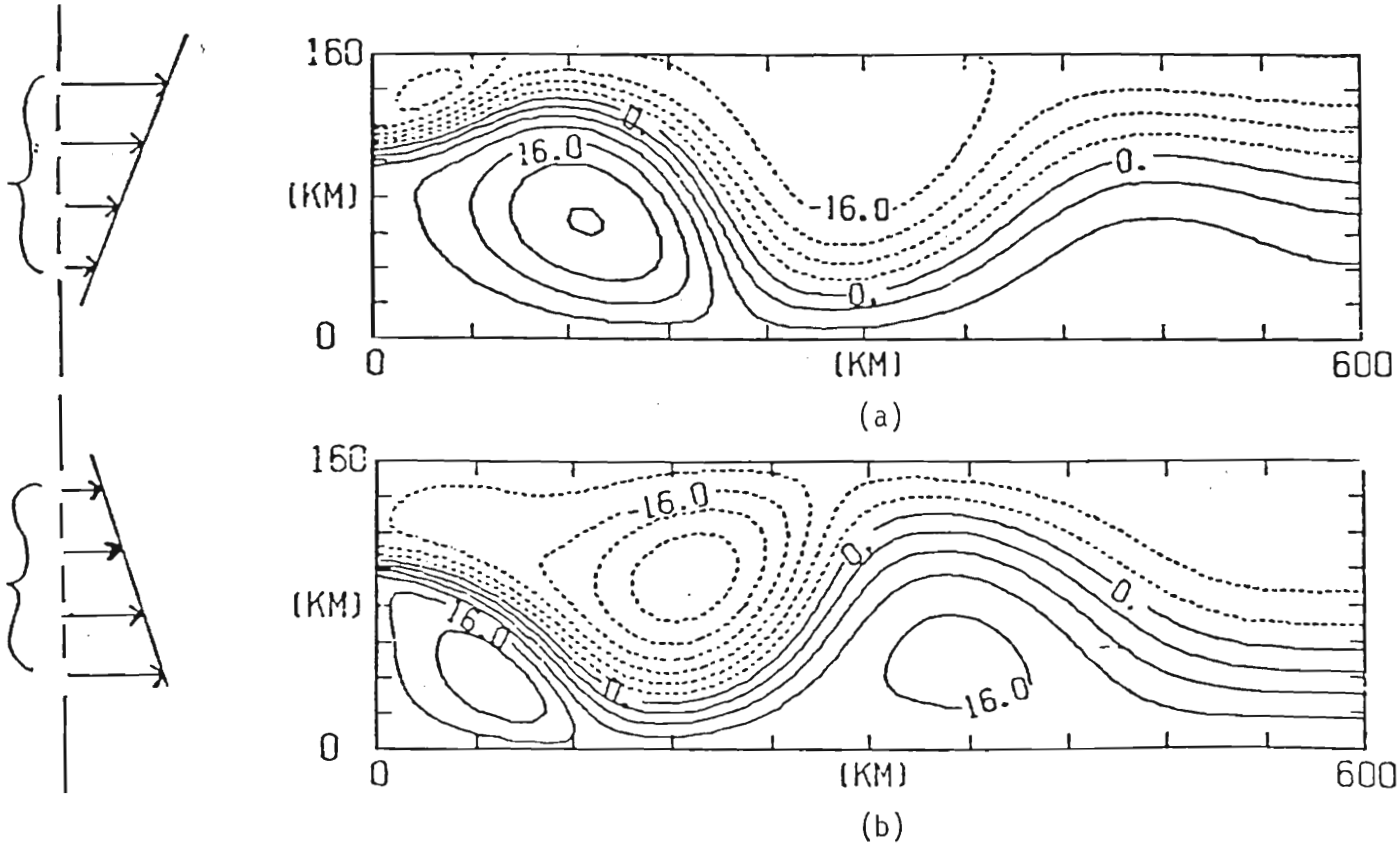

Fig. 11. Steady state solutions of a) negative vorticity at inflow and b) positive vorticity at inflow. Contour interval is 4 m. Average velocity is 30 cm/sec. Side figure indicates the velocity profile at the inflow port.

c. Boundary effects

In the case of the angled inflow and shear inflow, where the velocity has a northward component, the Coriolis force would act as a restoring force and turn the flow southward. The restoring force in a β-plane would be expected to produce north-south oscillations about eastward moving current axis. This type of wave motion is described by Rossby wave theory (Rossby, 1939). In the steady state reduced gravity solutions presented here the "wave" is stationary. If the Alboran gyre was strictly formed as a result of a stationary Rossby wave, which maintains a constant absolute vorticity trajectory, its wavelength should be given by (Haltiner and Martin, 1957)

$$L_x = 2\pi(U/\beta)^{\frac{1}{2}}$$

For the Alboran gyre case, this would result in a wavelength an approximately one and one half times larger than observed. Thus, the restoring effects of the Coriolis force only partly determine the path taken by the inflow as it enters the Alboran sea. When the flow enters the basin in a northeastward direction, the additional effect of the northern boundary becomes important.

A number of reduced gravity experiments were performed to look at the interaction between the jet and the north-south boundaries. In the following three cases, the inflow was a constant 90 cm/sec across a 20

km wide port and angled 21^{o} north of east. All parameters in the three cases were the same, the only difference being the port location. Case one uses the standard Alboran Sea port north of the center of the basin. The port of case two is located exactly in the center of the basin, while the port of case three is one point south of the center of the basin. Figure 12 shows the three quite different steady state solutions of these cases. The most dramatic difference occurs between the centered port solution and the south of center port solution. The role played by the northern boundary is best seen by observing model solutions in their "spin up" stage. In case three, Figs. 13 and 14, the jet enters the basin in a northeastward direction. The northward movement of the current places it in a region of increasing f. In order to conserve potential vorticity, a negative relative vorticity (anticyclonic movement) is needed. Vorticity conservation causes it to curve back toward the south and an anticyclonic gyre forms south of the incoming jet. North of the jet lies a less intense, somewhat wide spread cyclonic circulation. The situation of case two, Figs. 15 and 16, is quite different. As the solution is "spun up" and the jet travels farther north, it begins to encounter the frictional effect of the northern boundary. The boundary affects the shear of the flow which is developing near the northern boundary, inducing large negative relative vorticity. Attempting to conserve potential vorticity, the flow moves farther northward. This, in turn, creates a stronger shear

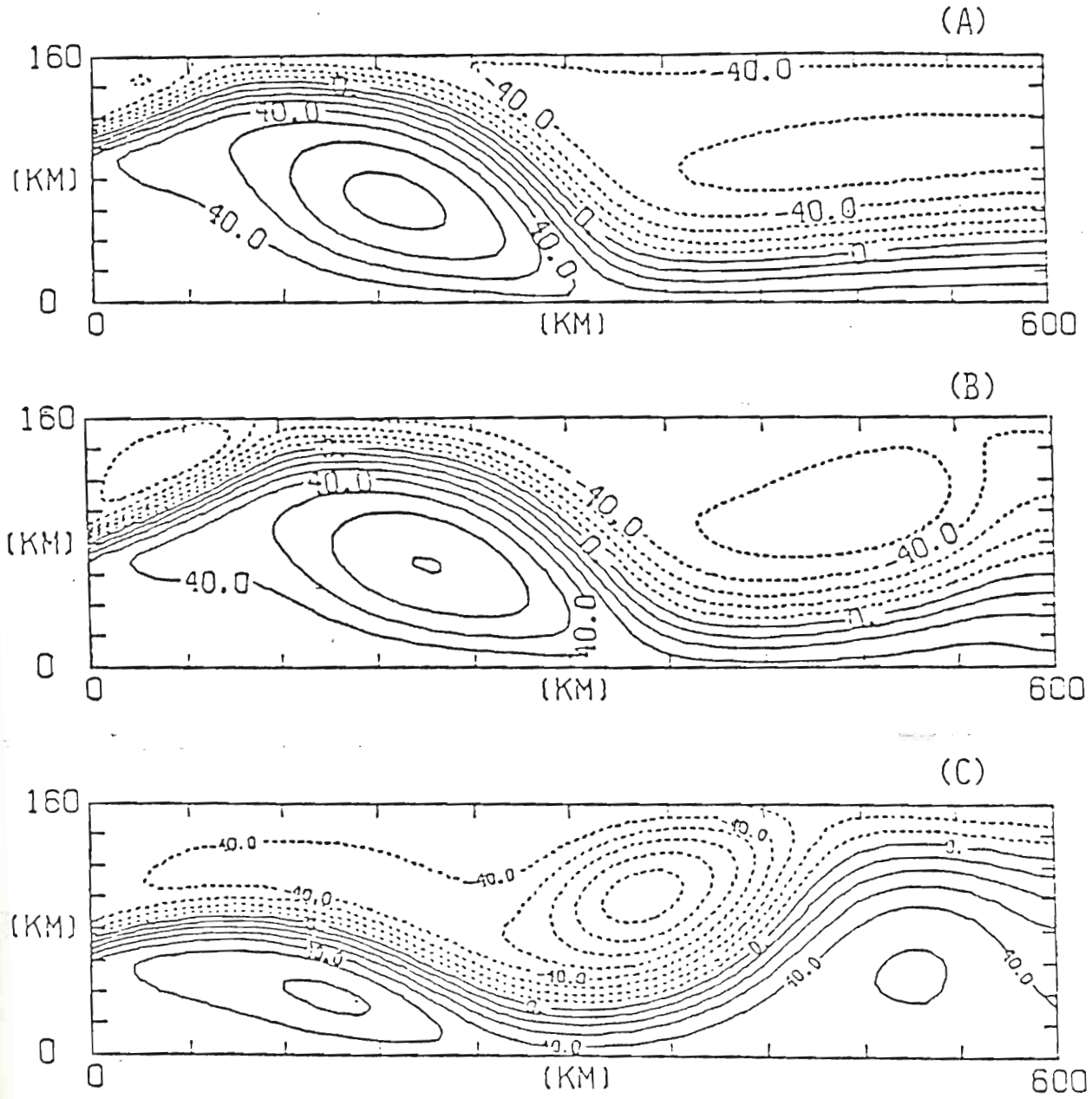

Fig. 12. Solutions of three reduced gravity cases with 90 cm/sec velocity angled 21° at day 600 for a) port north of the center, b) port exactly centered, and c) port one point south of the center. Contour interval is 10 m.

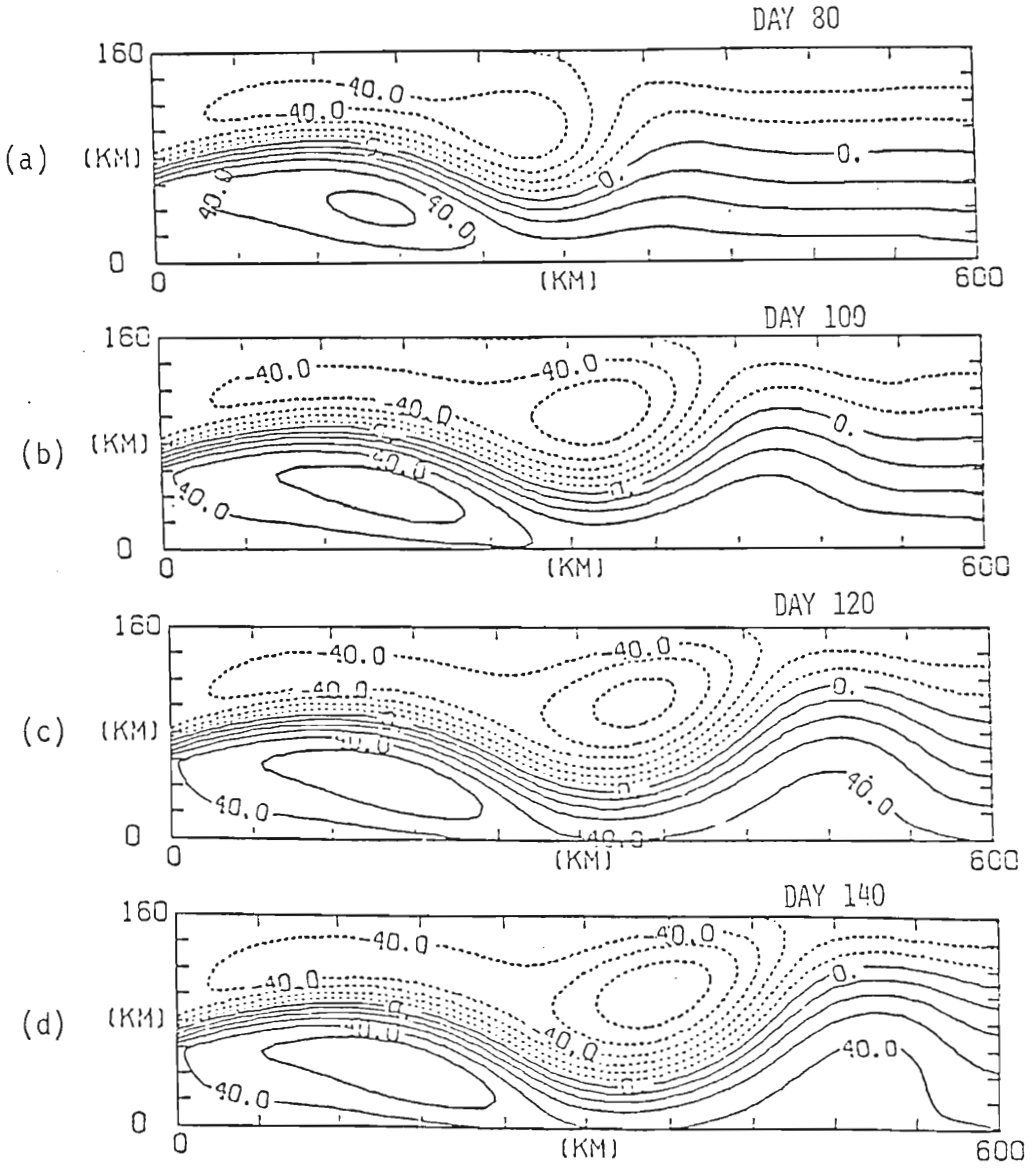

Fig. 13. Spin up solutions of the one point south of center port case at a) day 80, b) day 100, c) day 120 and d) day 140. Contour interval is 10 m.

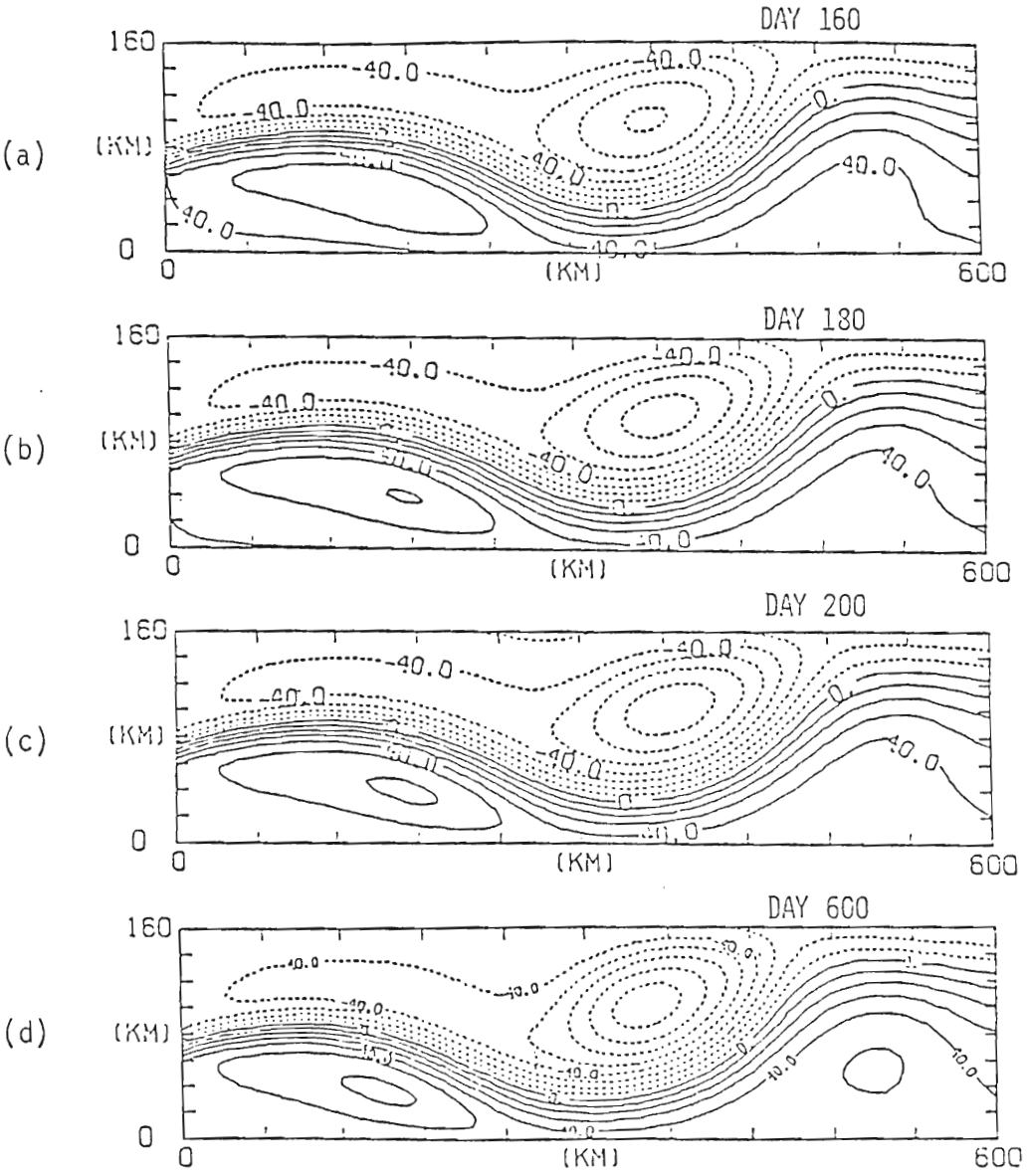

Fig. 14. Spin up solutions of the case presented in Fig. 13 at a) day 160, b) day 180, c) day 200 and d) day 600. Contour interval is 10 m.

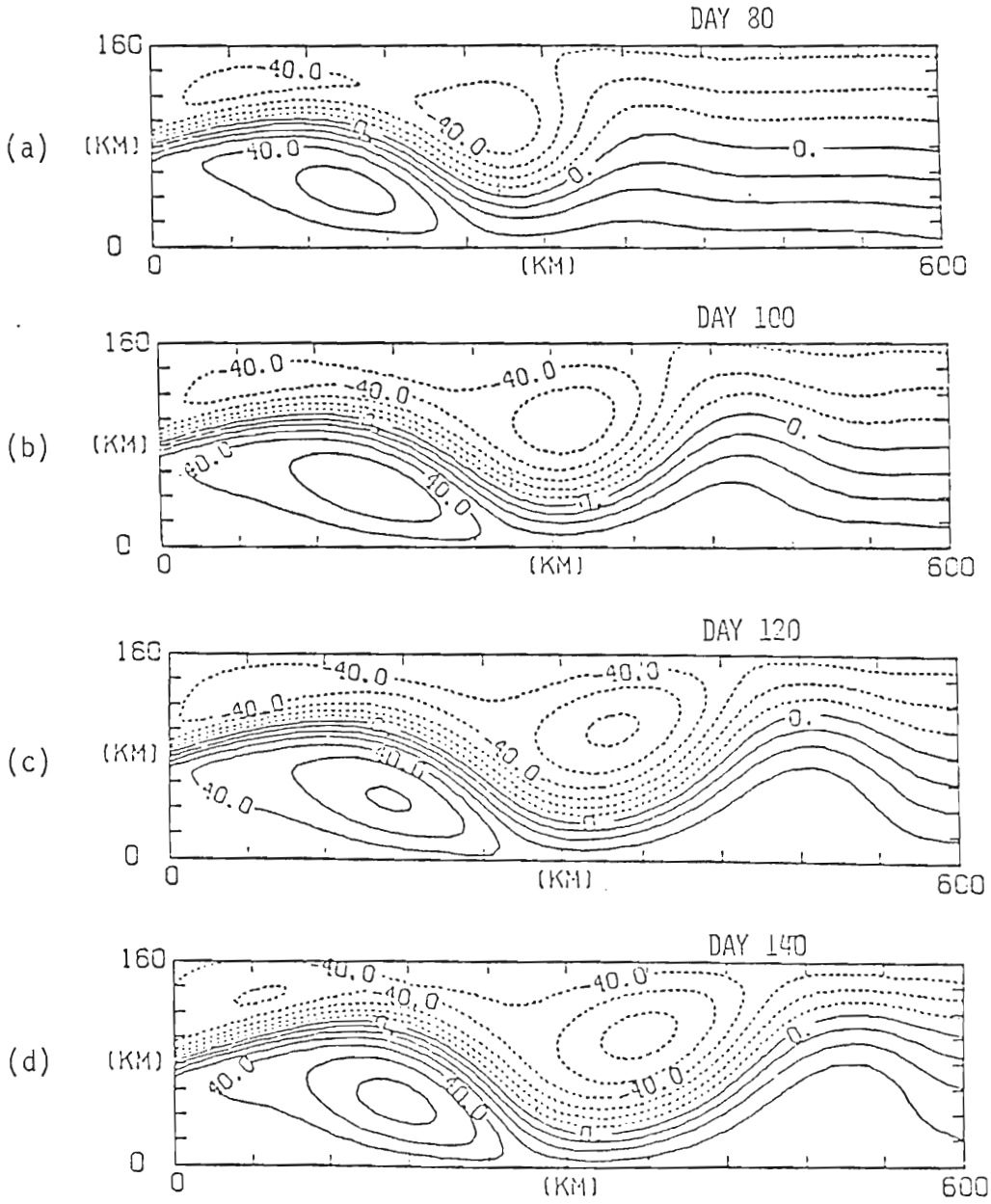

Fig. 15. Spin up solutions of the centered port case at a) day 80, b) day 100, c) day 120 and d) day 140. Contour interval is 10 m.

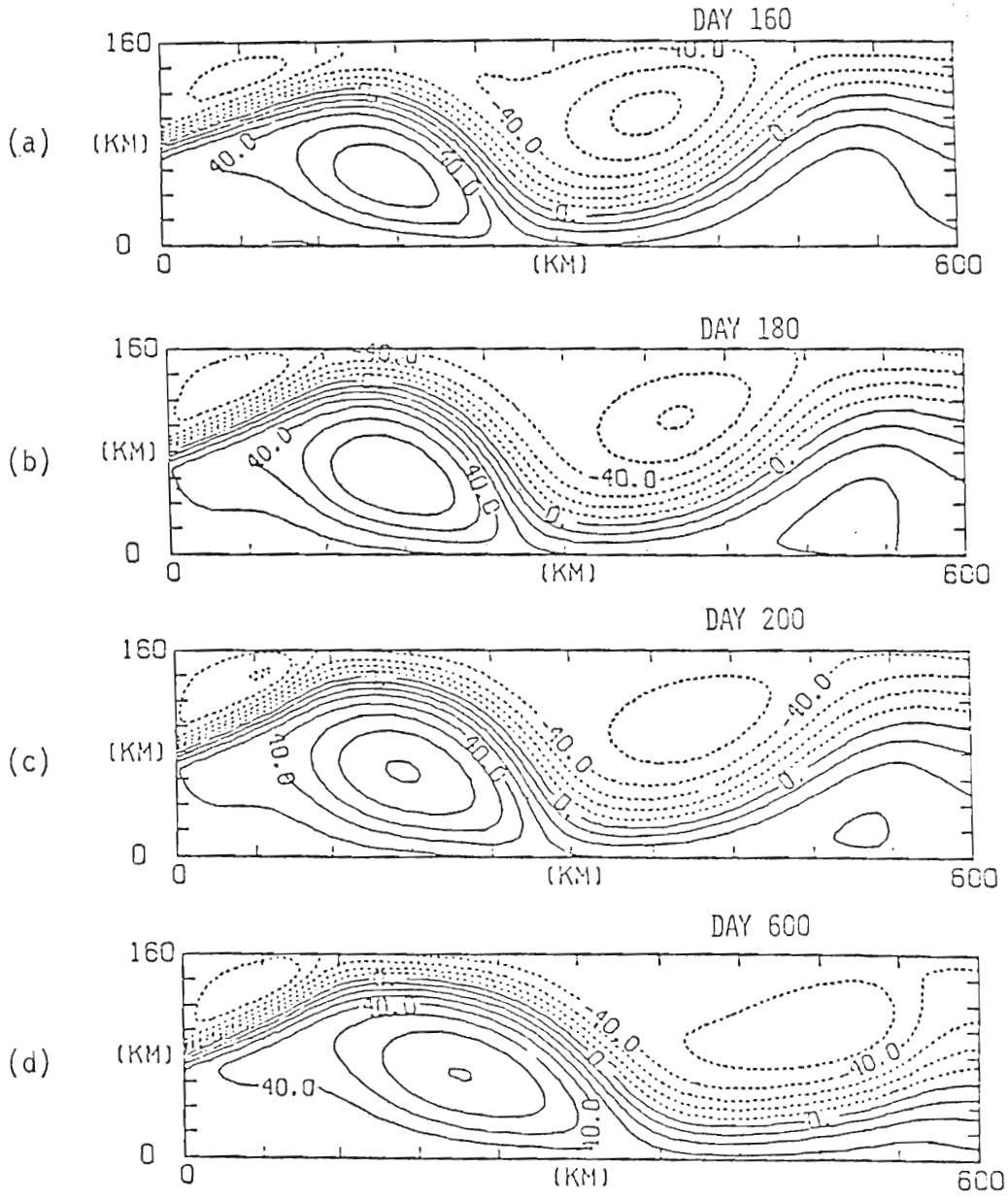

Fig. 16. Spin up solutions of the case presented in Fig. 15 at a) day 160, b) day 180, c) day 200 and d) day 600. Contour interval is 10 m.

at the boundary causing larger negative relative vorticity, forcing the flow still farther northward. This continues until the jet is far enough north that the cyclonic circulation to its north is separated into two cyclonic gyres one to the east and one to the west of the inflow. The jet then intersects the boundary and is deflected to the south.

In the case of the realistic Alboran Sea port a similar argument exists except that the jet strikes the northern boundary farther west than in the centered port case. As a result, the cyclonic gyre west of the inflow is confined to a smaller region and the center of the anticyclonic gyre is located farther west than in the centered port case.

Potential vorticity contours for the centered and south port cases, Figs. 17a-e and 18a-e, show how the northern boundary alters the vorticity in the centered port case. In particular, the east-west gradient of potential vorticity, Fig. 17e, is no longer constant near the northern boundary as in the south port case, Fig. 18e. Large values of potential vorticity now exist in the northwestern corner of the basin over the cyclonic gyre. Figures 19a-c shows the steady state contours of potential vorticity for all three different port locations. Contours of potential vorticity for the north port case are similar to those of the centered port case with slightly larger magnitudes in the northwest corner.

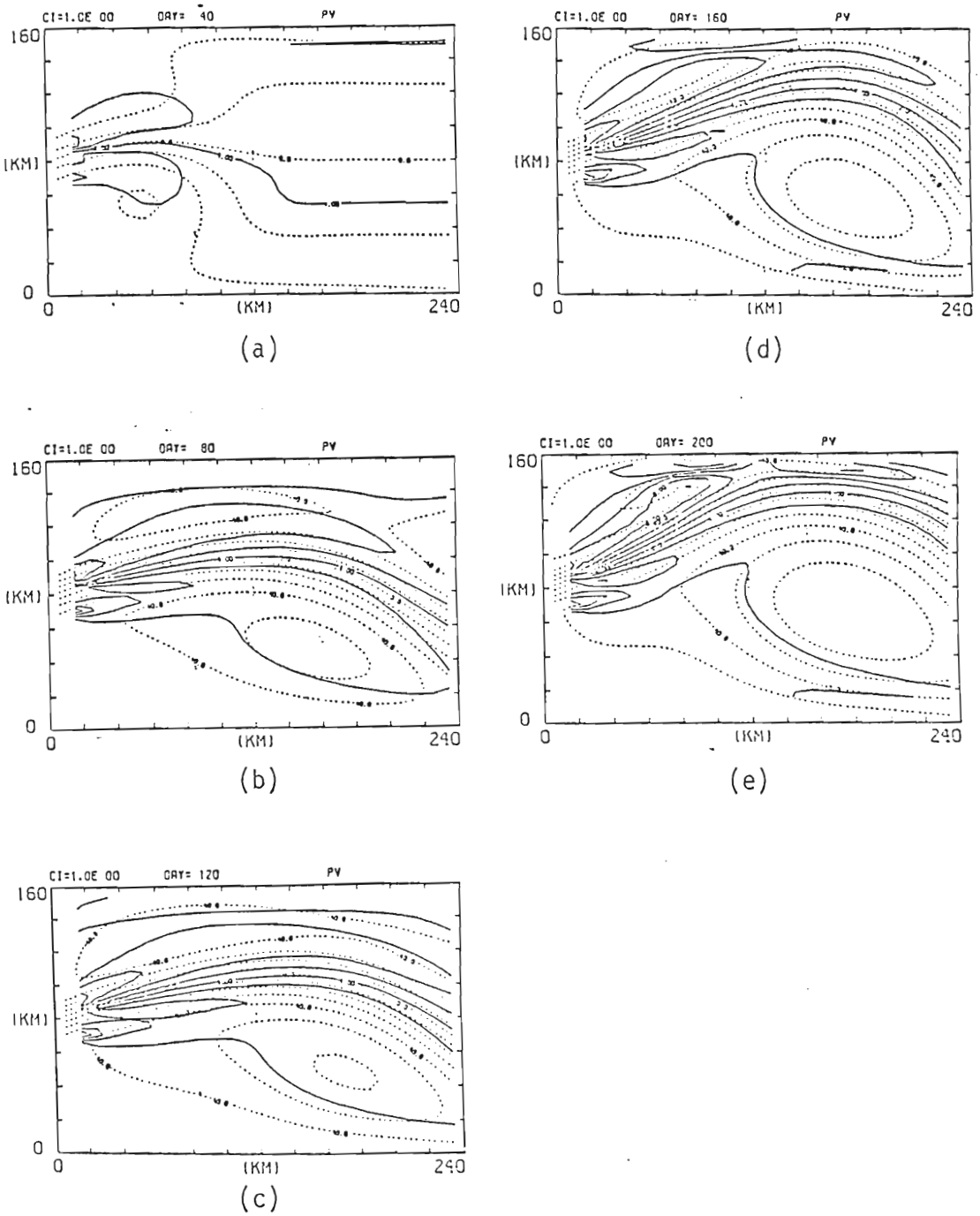

Fig. 17. Potential vorticity contours superimposed over PA contours for the centered port at a) day 40, b) day 80, c) day 120, d) day 160, and e) day 200. PA contour interval is 10 m. Potential vorticity contours have been multiplied by a factor of 10^7, contour interval is 1.

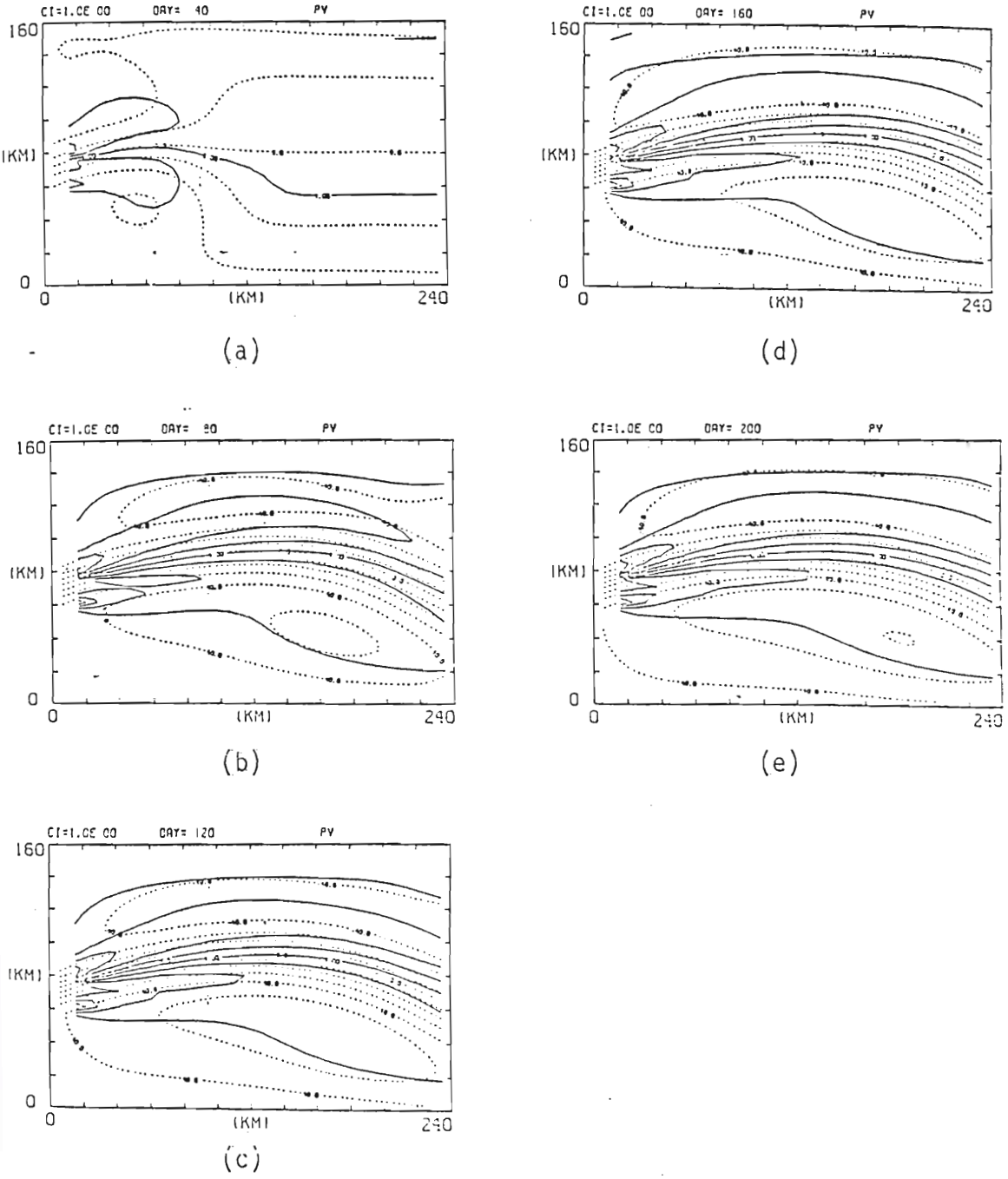

Fig. 18. Potential vorticity at the south of center port case for a) day 40, b) day 80, c) day 120, d) day 160 and e) day 200. PA contour interval is 10 m. Potential vorticity contour is 1. Values of potential vorticity increase north of the jet.

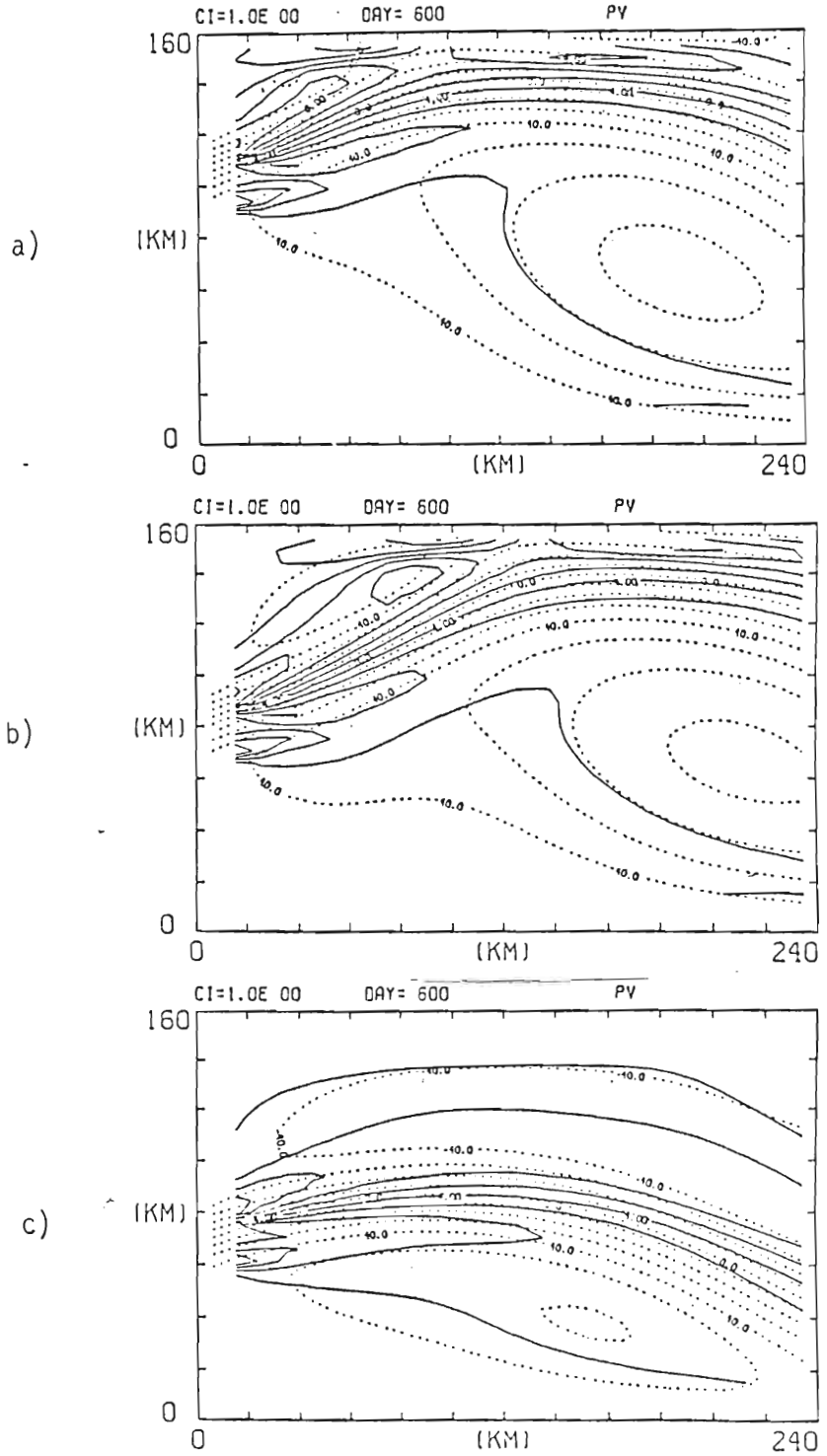

Fig. 19. Potential vorticity contours at day 600 for a)north port, b)centered port and c) south port.

Solutions were also obtained for cases with 30 cm/sec angled inflow. The steady state solutions for the centered, Fig. 20a, and south of center, Fig. 20b, indicate that when the initial shears set up by the inflow entering the motionless basin are small, that the effect of the induced shear from the northern boundary becomes more critical. In the Alboran Sea port case (north port), previously shown in Fig. 8b, the jet strikes the northern boundary quickly, resulting in a gyre whose center is located west of of those in the previous two cases.

In all of these cases, once the jet is deflected southward by the northern boundary, its path is then limited by the width of the basin (i.e. southern boundary). Figure 21 shows a case where the north-south extent of the basin is doubled. The northern boundary is far enough from the port that the curvature of the inflow is similar to the south port case, Fig. 12c. The jet continues south until it is deflected by the southern boundary. When the dimensions of the basin were extended in the east-west direction, Fig. 6a, the current would continue to meander downstream, the amplitude of the meanders being limited by the width of the channel.

These reduced gravity results show that in a one-layer basin, the approximate dimensions of the Alboran Sea, an anticyclonic gyre lies to the south of the incoming Atlantic water and a cyclonic gyre to its north. This two gyre system is similiar to jet flow in a rotating viscous fluid (Batchelor, 1970). The anticyclonic gyre, however,

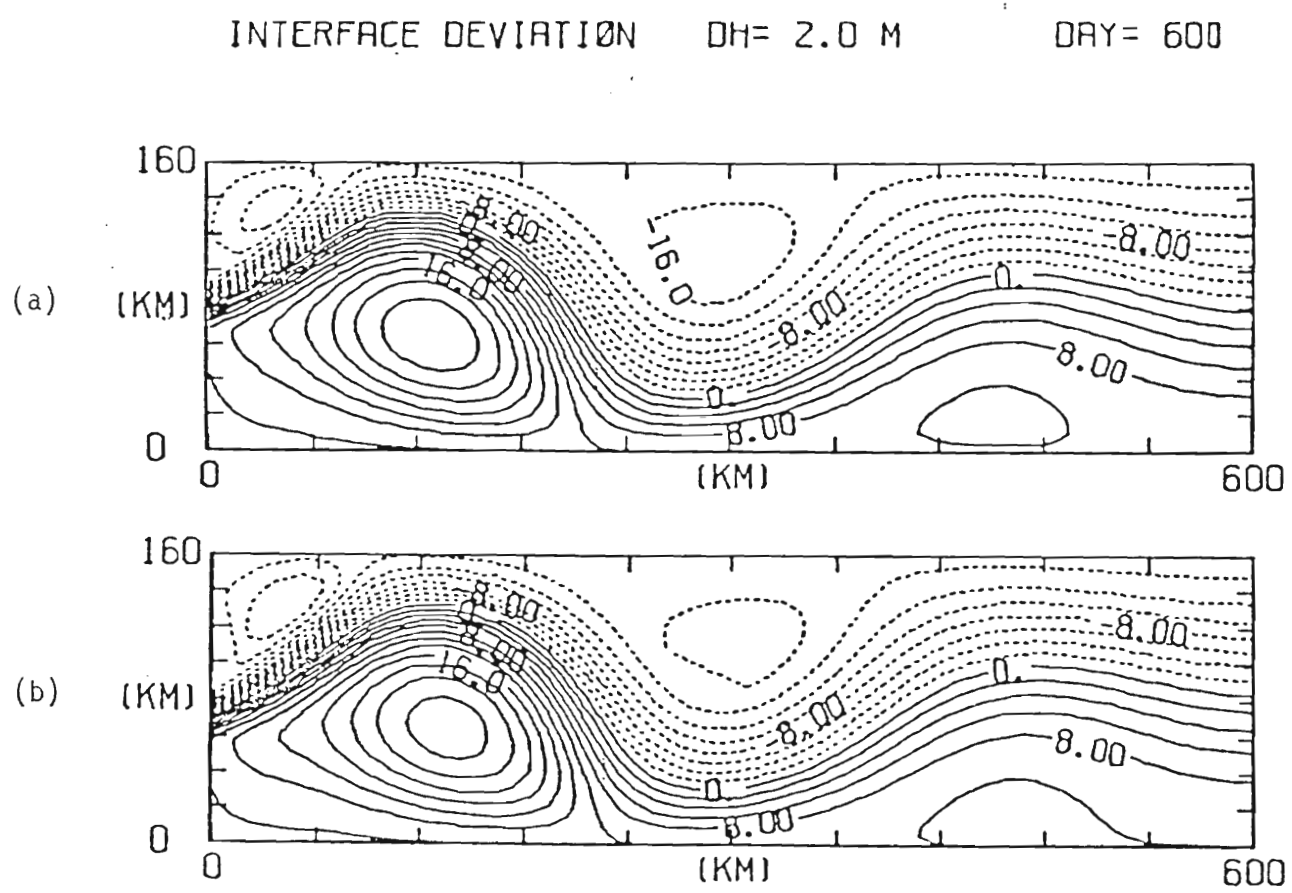

Fig. 20. Steady state soltuions using 21° angled 30 cm/sec inflow for a) centered port, b) north port. Contour interval is 2 m.

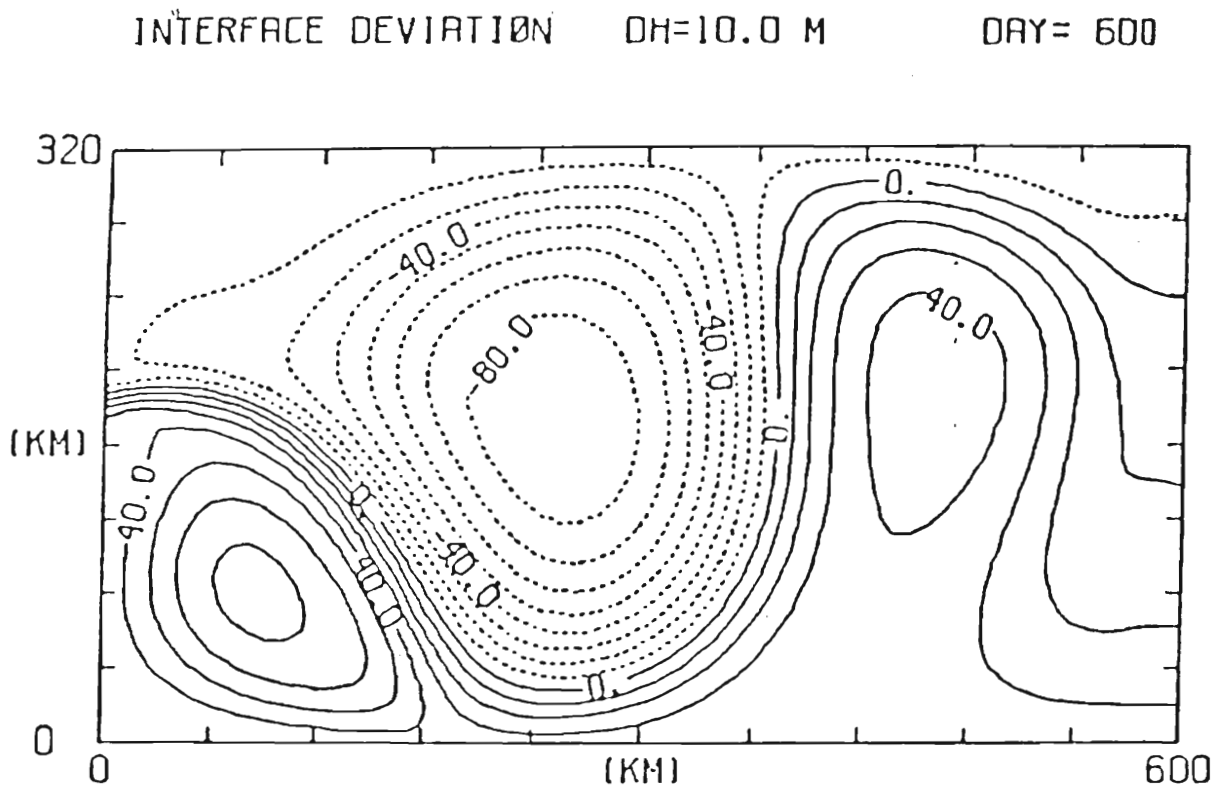

Fig. 21. Solution for a reduced gravity model iwth the north-south extent of the basin doubled. Inflow is 90 cm/sec angled 21°. Contour interval is 10 m.

dominates the circulation closest to the strait. This is due to the location of the strait in the northern half of the basin thus allowing a larger area south of the inflow over which the gyre can form. The largest north-south dimensions of this anticyclonic gyre are also dependent on the inflow's northward movement as it enters the basin. The northward component of the inflow can be a result of the geometry of the Alboran Sea-Strait of Gibraltar system or it can by caused by shear induced into the current upstream in the strait. The interaction of the northern and southern boundary with the jet alters the simple path of curvature determined by Rossby wave theory, reducing the wavelength of the oscillating flow.

4. THE TWO-LAYER CASES

Although the dynamics of the one active layer model explain a large part of the formation of the Alboran gyre, a westward moving lower layer must be included to examine the circulation of the Alboran Sea completely. The effect of the lower layer flow as well as the effect of the complicated bottom topography was examined using a two-layer model. This model can also be useful in determining the importance of baroclinic instability. If results of the two-layer and reduced gravity models are similiar, it eliminates baroclinic instability as a major part of the dynamics. Figure 22 shows a cross section of the two-layer model. Velocity components as well as layer thickness are calculated. Topographic variations are included in the lower layer thickness term.

a. Comparison tests between two-layer and reduced gravity models

The first tests using a two-layer model were designed to be comparable with the reduced gravity tests. These tests used either 90 cm/sec or 30 cm/sec inflow in the upper layer. Standard lower layer inflow was .2 cm/sec. The Alboran Sea topography minus the idealized Alboran Island was used in these first tests. Figures 23a and b shows the solution of a 90 cm/sec, due east inflow case for a) the reduced gravity model and b) the two-layer with topography (Fig. 4b) model.

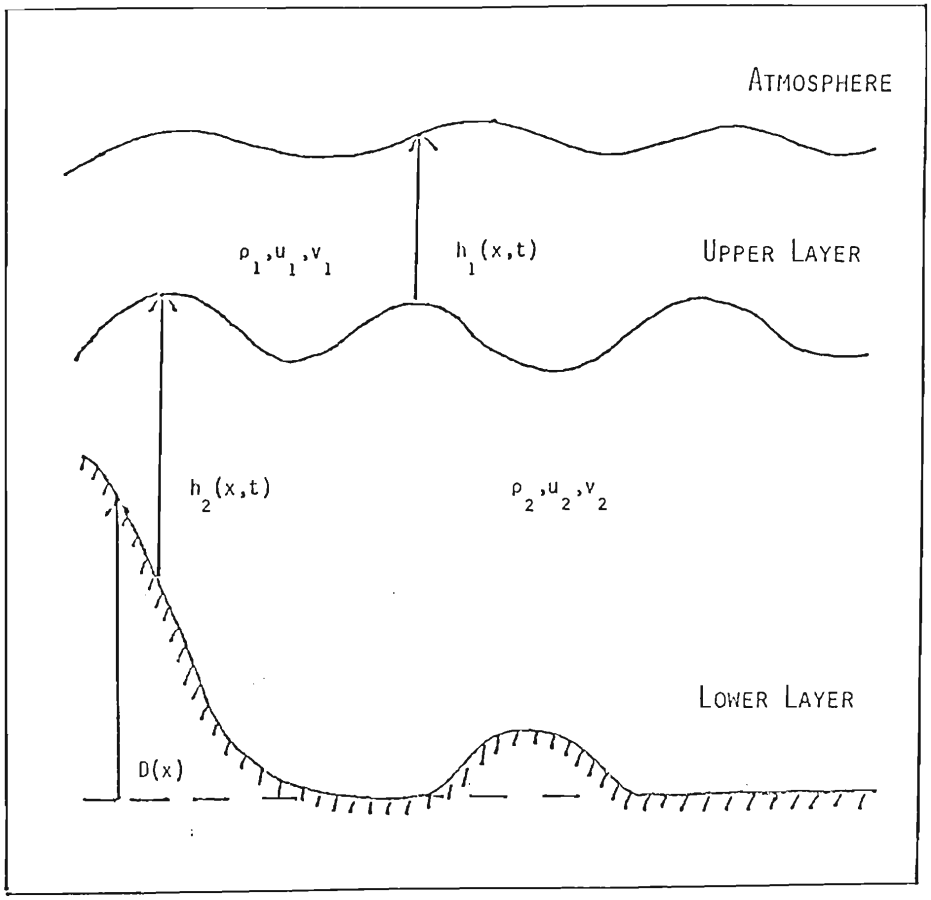

Fig. 22. A vertical cross section of the two-layer model. D(x) represents the height of the bottom topography above a reference level (2600 m).

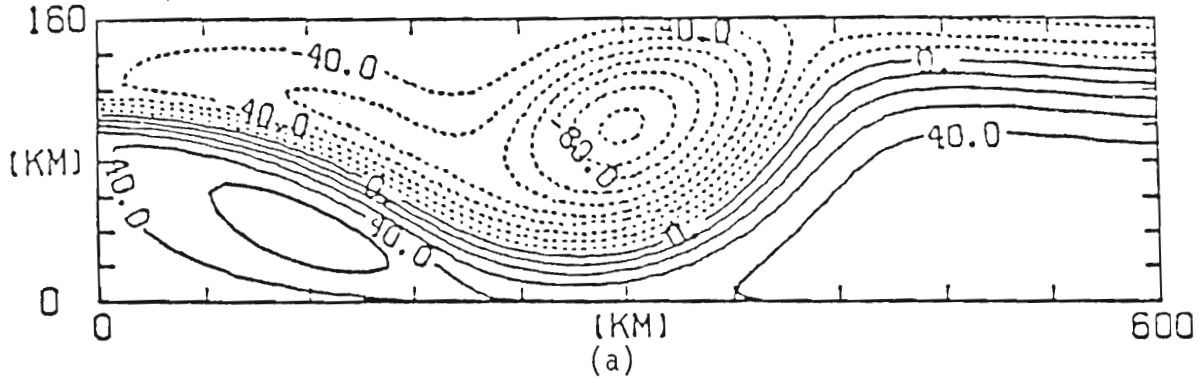

(a)

INTERFACE DEVIATION
DH=10.0 M

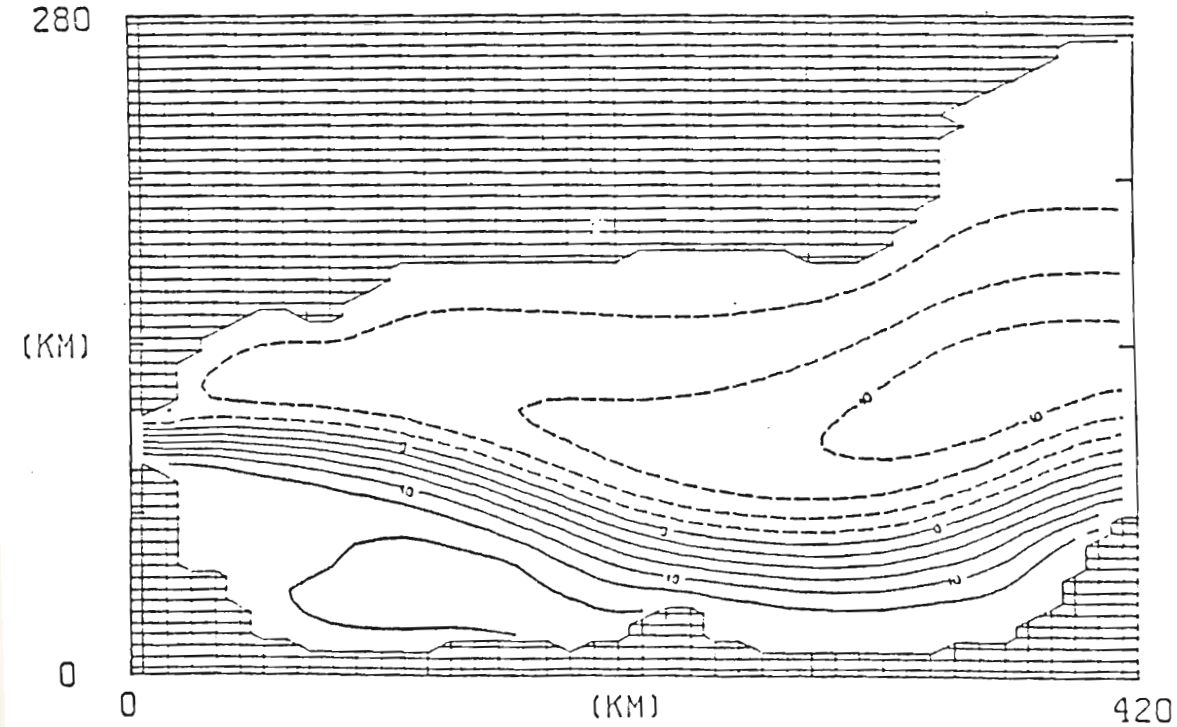

(b)

Fig. 23. Steady state solutions using 90 cm/sec due east inflow in a a) reduced gravity model and b) a two-layer model with topography shown in Fig. 4b and .2 cm/sec lower layer inflow.

These solutions look quite similar in the western half of the Alboran Sea. In the 90 cm/sec case, both contain a small anticyclonic gyre similar to that often seen in observations, Fig. 24. However, they differ quite dramatically in the eastern half of the basin. In the case with topography, the inflow is deflected from striking the southern boundary sharply by Cape Tres Forcas. Since the inflow does not strike this boundary at as large an angle, it does not deflect as sharply to the north. As a result, the small intense cyclonic gyre which appears to the east of the Alboran gyre in the reduced gravity case does not form in the two-layer case.

Two tests were also performed angling the inflow by the standard 21^{o} north of east using 30 cm/sec, Figs. 25a and b and 90 cm/sec, Fig. 26. The resulting circulation of the first test shows the Alboran gyre confined west of the Alboran Island. This gyre is approximately 200 km in its east-west extent and has a maximum PA of 20 m. These solutions closely resemble the reduced gravity solutions of Fig. 10b with the gyre of the two-layer case being slightly wider and less intense. Since the inclusion of a moving lower layer with topography results in only minor differences between these solutions and those of the reduced gravity case, it is concluded that the flow in the upper 200 m is the most critical in defining the anticyclonic gyre. Results of the second experiment, Fig. 26b, using the 90 cm/sec, 3.9 sv inflow are similar to results shown in Fig. 8a. The use of real geometry, shows more

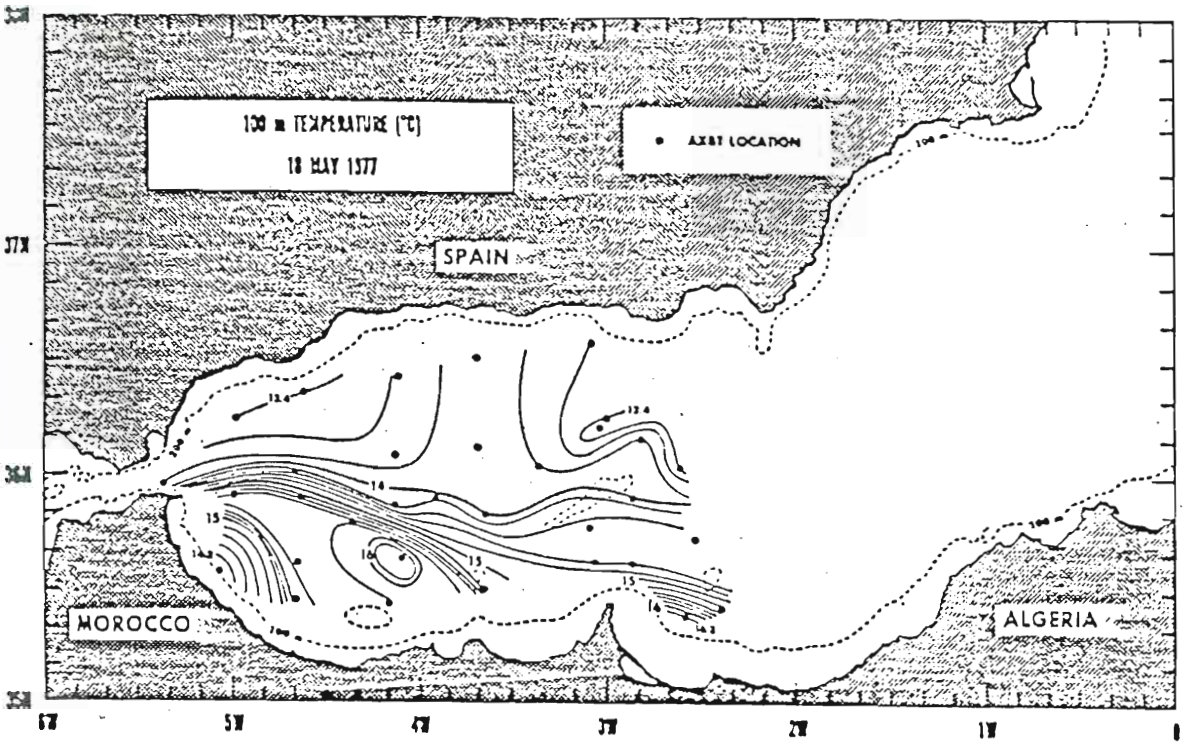

Fig. 24. Contours of temperature in ^{o}C at 100 m for the Alboran Sea, May 18, 1977. (From Cheney and Doblar, 1982).

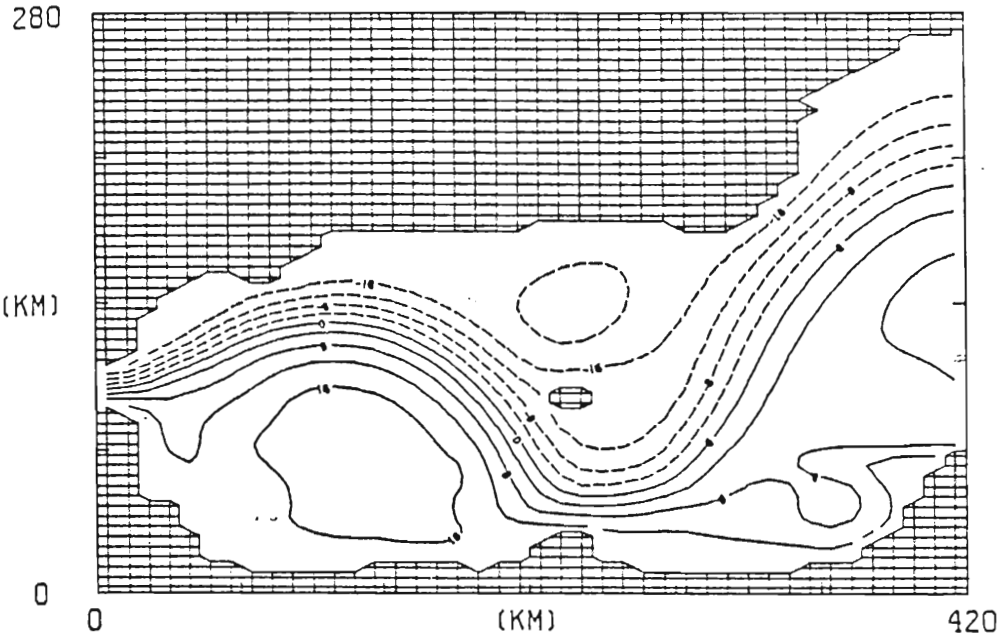

(a)

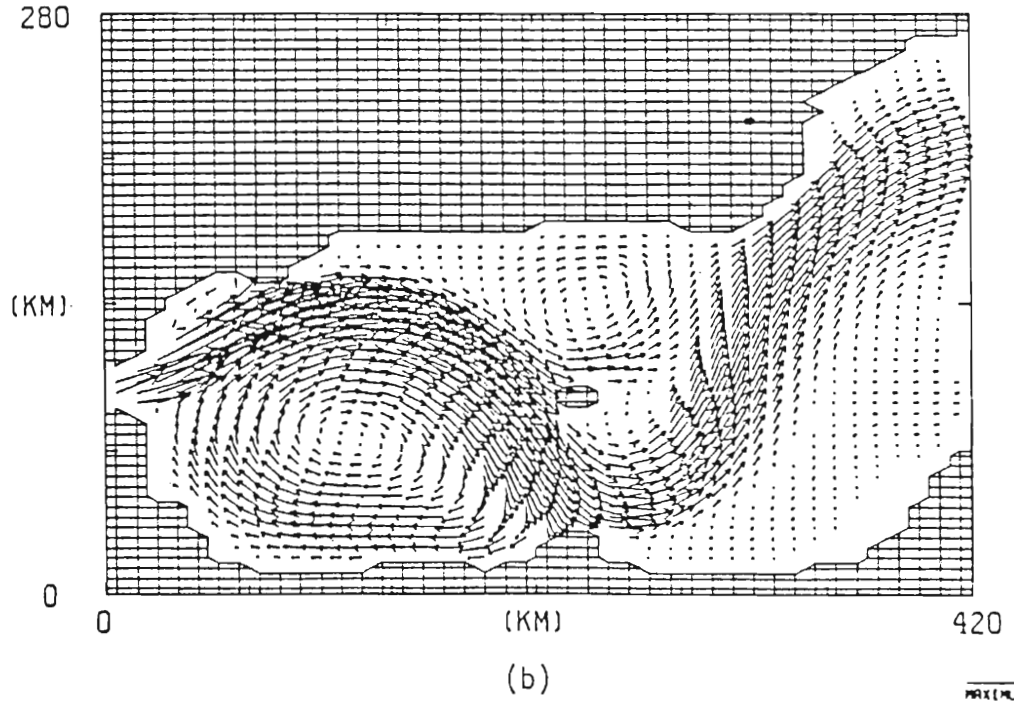

(b)

Fig. 25. Solutions for a "standard" inflow, 30 cm/sec 21^{o} angled inflow in the upper layer and .2 cm/sec in the lower layer, with topography at day 360. a)PA contour interval is 4 m, b) Velocities with a maximum velocity vector of 50 cm/sec.

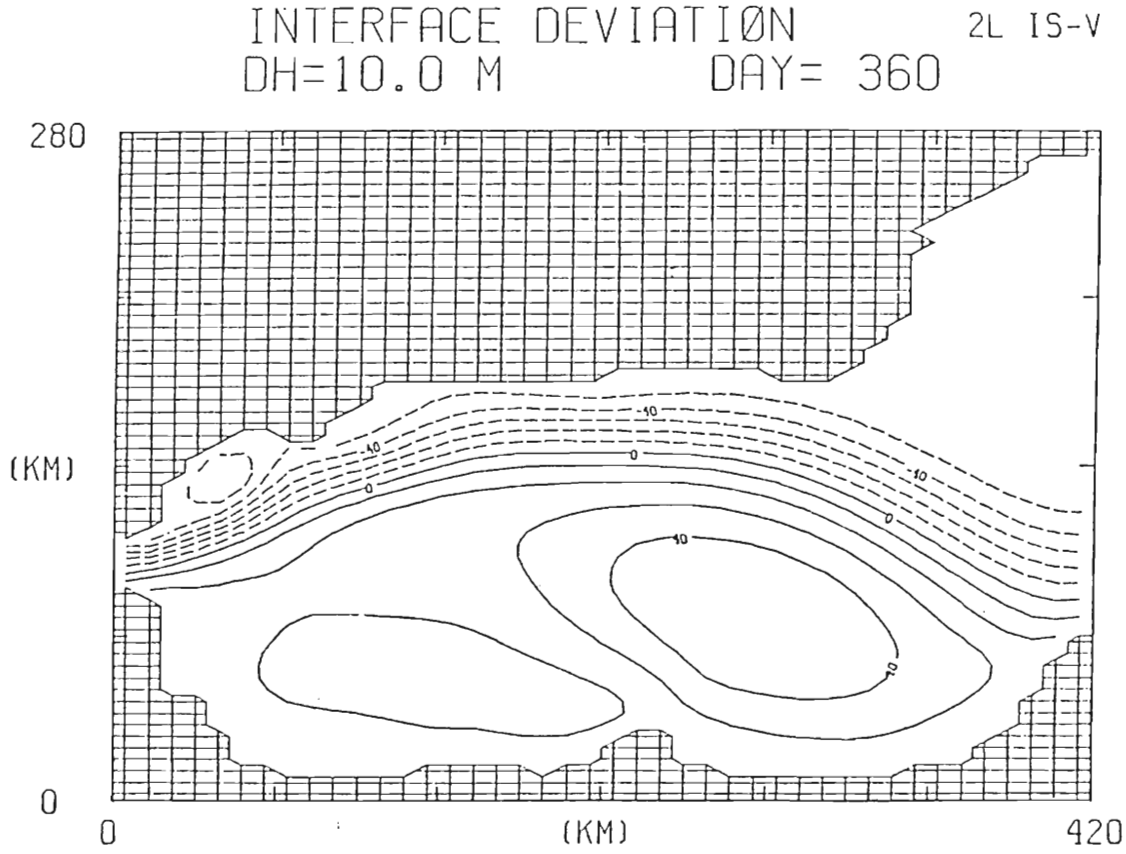

Fig. 26. Solutions for a 90 cm/sec angled 21° north of east inflow and .2 cm/sec lower layer inflow, two-layer case with topography at day 360. Contour interval is 10 m.

dramatically, how important the Atlantic water inflow transport values are in determining the configuration of the gyre. Large transport shifts the center of the gyre eastward, in this case east of the island forming an unrealistic Alboran Sea circulation.

These results show that if the inflow is given a northward component, and large enough mass transport, the jet is confined north of the ridge and the anticyclonic gyre is shifted to the east. A number of tests oscillating the inflow angle from due east to 21^{o} north of east over periods of 90-360 days, were performed. These solutions gave similar results to those seen in Fig. 26. Once the inflow was directed far enough north, the jet maintains a position north of the ridge. Changing the boundary conditions at the inflow port back to due east was not sufficient to return the jet south of the island. A test was also performed in which the velocity from a steady state 30 cm/sec angled inflow case was increased to 90 cm/sec and then reduced to 30 cm/sec over a period of 180 days (Preller, 1983). When the velocity (transport) was increased, the gyre shifted eastward by approximately 100 km. Reducing the angled velocity (transport) to 30 cm/sec (1.3 sv), however, was sufficient to return the gyre to a position where it is confined west of the Alboran Island.

If the gyre is formed by a standing Rossby wave whose trajectory is distorted by the north-south boundaries, (as suggested in section 3c), then the wavelength should be approximately proportional to the

square root of the velocity. The simple reduced gravity cases of Fig. 8 show a wavelength of ≃600 km for the 97 cm/sec case and a wavelength of ≃400 km for the 33 cm/sec case. The ratio of the square roots of the velocities, 1.7, versus the ratio of the wavelengths, 1.5, show the Rossby wave approximation to be close but not exact. The wavelength does increase with velocity but not to the extent predicted by theory due to the limiting effect of the northern boundary. The distortion by the northern boundary is larger the greater the velocity. Thus as the inflow increases, the gyre shifts east a slightly smaller distance then predicted by Rossby wave theory. As the velocity decreases, the wavelength decreases and the gyre shifts westward. Similar results were obtained when the value of beta was decreased. The wavelength varied approximately as the square root of the reciprocal of beta.

Results similar to these were obtained in a one and one half layer, quasi-geostrophic model investigating the bimodality of the Kuroshio (Chao, 1982). There are two typical paths observed to be taken by the Kuroshio in the region between Kyushu and the Izu Ridge; flow either follows the 1000 m continental slope or leaves the coast upstream of the Izu Ridge near Shikoku and traverses around the ridge. Model results show that as the Kuroshio transport increases so does the wavelength of the meander forcing it around the ridge. These results as well as those obtained in the Alboran Sea model may be viewed as

multiple equilibrium states. Though this configuration can exist as an equilibrium for the Alboran Sea model, realistically such large transports (3.9 sv) are not observed in the Alboran Sea and as a result neither is a gyre shifted this far east, Fig. 26. What has been observed is the sporadic shifting of a substantial amount of the inflow north of the island (Lanoix, 1974 and Parilla and Kinder, 1984). Model results indicate that this type of change in the circulation can be caused by the sporadic increasing of the northward directed transport.

b. Topographic effects- the Alboran island-ridge system

It has been suggested (Porter, 1976) that the Alboran island-ridge system is an important if not necessary factor in determining the eastern boundary of the gyre. The reduced gravity solutions have shown that no such barrier is needed to confine the gyre to its observed dimensions. However, the island-ridge system is a very severe topographic feature and deserves further inspection. The results of four experiments using variations of the island-ridge topography are presented. The first two experiments showing the effects of the topography plus island versus the topography with ridge only are presented in Fig. 27. Unless specifically stated, the remaining two-layer experiments will use the standard 30 cm/sec angled inflow in the upper layer and .2 cm/sec inflow in the lower layer. All parameters in these two cases are identical, with only the topography varying. The

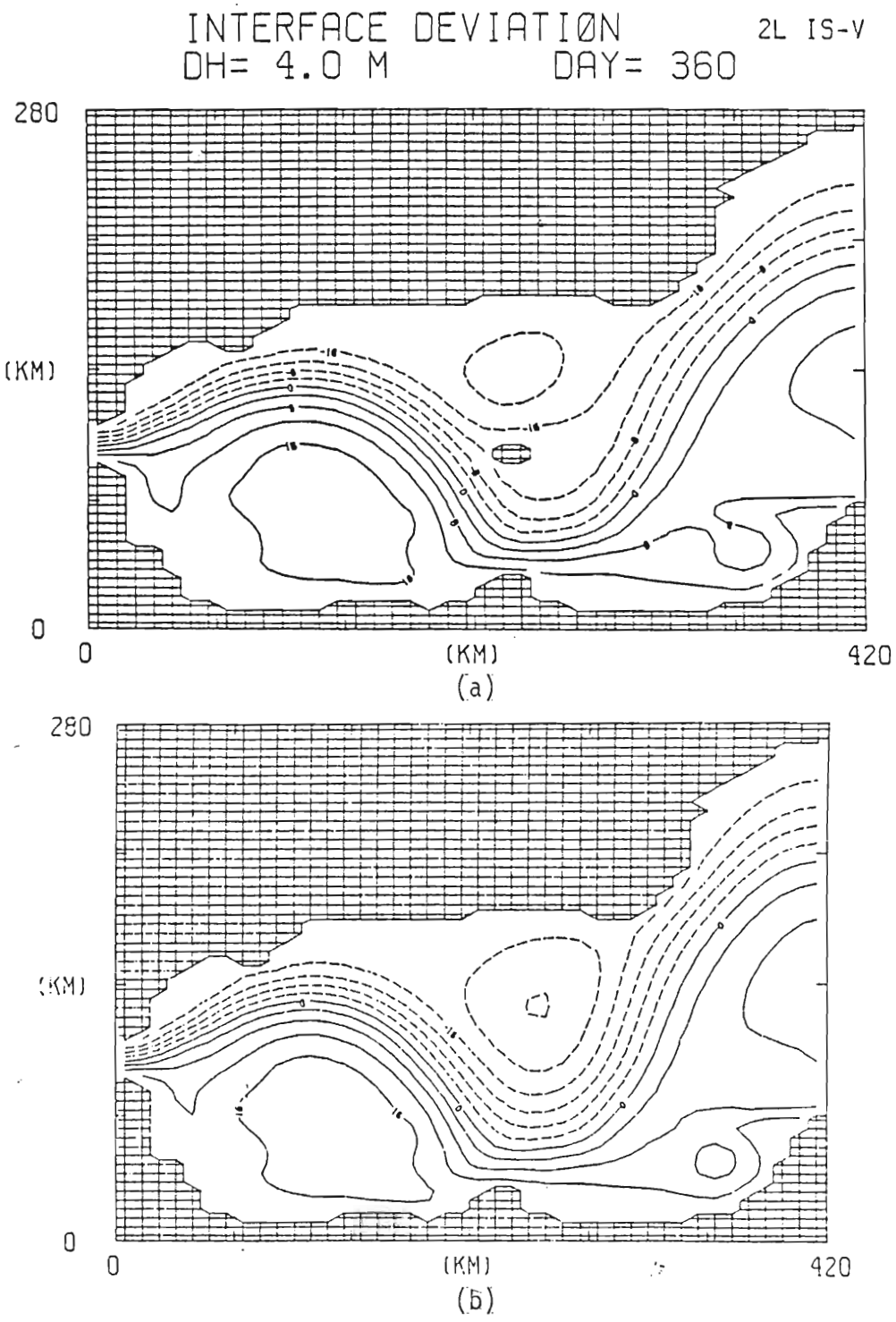

Fig. 27. Solutions for a two-layer case with standard inflow at day 360 for a) topography with island, Fig. 4a; and b) topography with no island, Fig. 4b.

main effect of the island, Fig. 27a, is to separate the incoming Atlantic flow in two such that part of the jet is deflected farther north then in the ridge only case. As a result, the cyclonic circulation north of the ridge, Fig. 27b, is slightly weaker in the island case.

Another general feature of the circulation of these two-layer cases is the sharp turning of the inflow towards the north in the region east of Cape Tres Forcas. The turning angle is sharper in cases which include the island. This is due to most of the inflow being funneled between the steepest part of the ridge (the island) and the cape. Observations, (Parrilla and Kinder, 1984), show this type of funneling of the inflow to be the dominant configuration. A portion of this inflow splits off and turns west at the cape becoming part of the anticyclonic gyre. The remainder is deflected by the cape and turned northward. This differs from the Lanoix configuration but agrees closely with the infrared satellite imagery obtained during the Donde Va experiment (Laviolette, 1983). This satellite imagery shows surface flow for the period October 6-16, 1982. During this period, the cold water which bounds the gyre extended eastward and was deflected to the north by the cape.

The next two experiments were performed with no ridge or an exaggerated ridge topography and standard inflow forcing. In the first case, Fig. 28a, the topography is similar to that of Fig. 4b but with

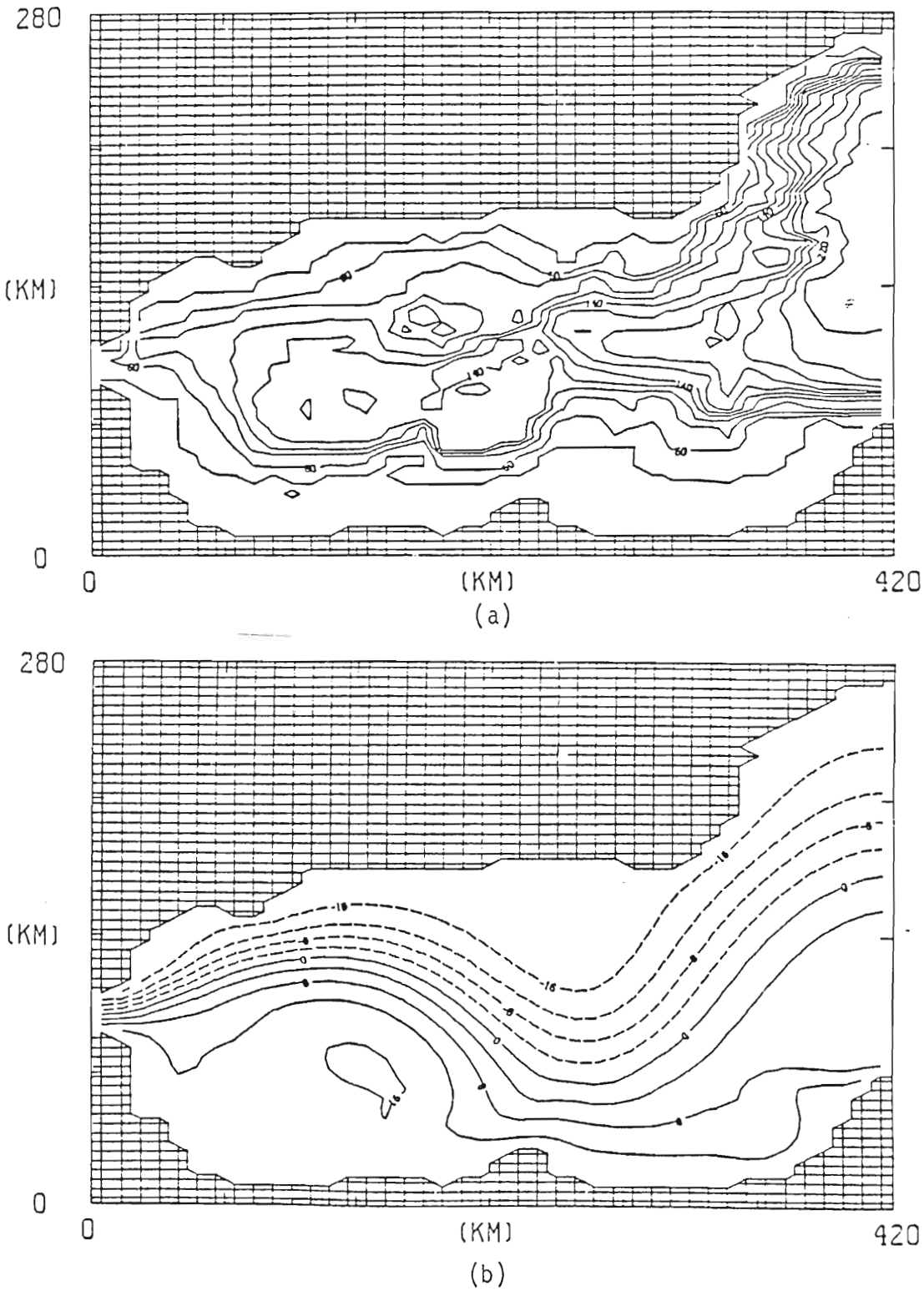

Fig. 28. Solutions of a two-layer topography case with "standard" inflow and a flattened (1200 m) ridge. a) Topography with a 200 m contour interval, b) PA contours at 4 m intervals.

the entire ridge flattened to 1200 m. When comparing these results to a case with the ridge, Fig. 27b, only small differences are seen in the PA contours. The ridge, located at depths of 400 m or greater, did not have a major effect on the upper layer circulation which is mainly responsible for defining the gyre. The lower layer circulation also differs very little since its path is determined by the topographic contours east of the ridge. If, however, the 400 m contour was extended through the upper layer, Fig. 29a and b, the PA contours change dramatically. This "large" island creates a barrier to the inflow as it turns south. As a result the majority of the inflowing jet is deflected north of this barrier. Using a 400 m contour to create an island exaggerates the effect of the ridge on the upper layer. Using a 100-200 m contour to define the effects of the ridge would be more realistic however, the east-west grid spacing of this model does not allow for the resolution of the 100-200 m contour. For this particular model the ridge only or ridge plus small island topographies, Figs. 4a and 4b, can simulate the most realistic effect of the island ridge system.

c. Topographic effects- lower layer flow with and without topography

The model results have shown that by including topography and a slowly moving westward lower layer that the general circulation patterns developed in the reduced gravity cases still exist. To

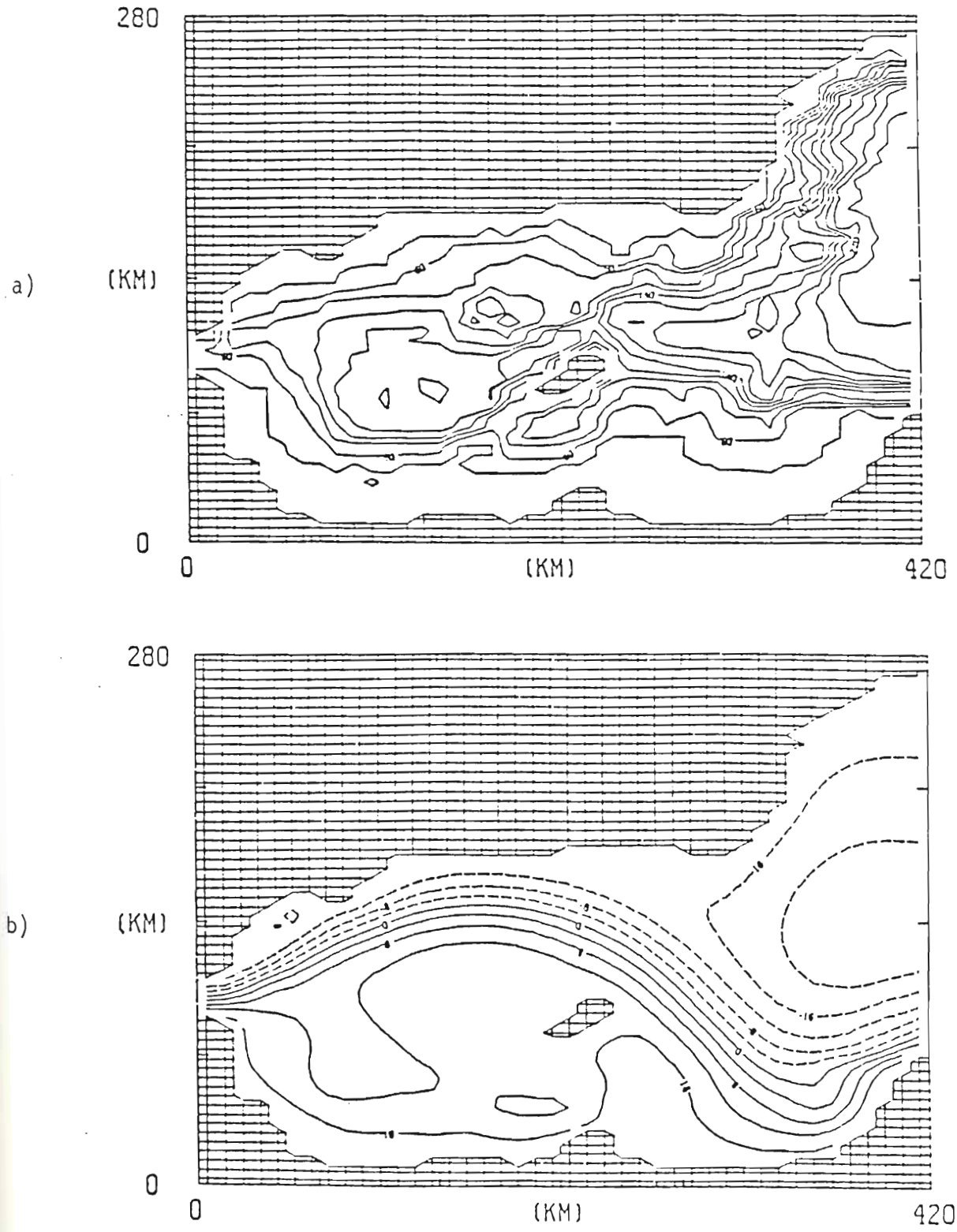

Fig. 29. Solutions of a two-layer topography case with "standard" inflow and the 400 m contour extending through the upper layer. a) Topography with a 200 m contour interval, b) PA contours at 4 m intervals.

examine, in more detail, the effects of topography on the two-layer system, a flat bottom case with geometry and the full geometry and topography case are compared. Figs. 30 a and b show two identical cases where all parameters are the same except for the bottom topography. The most obvious difference in solutions is the smooth appearance of the contours in the flat bottom case. These contours compare closely to the reduced gravity contours (Fig. 8b) since neither case included the effects of topography. Figures 26 a and b differ most markedly in the southern half of the basin. The inclusion of topography alters the smooth line of the contours in the region.

The reason for this difference becomes apparent when looking at the lower layer flow for both of these cases. In the flat bottom case, Fig. 31a, the incoming westward velocity maintains values of approximately 1-3 cm/sec throughout the basin. Flow entering through the eastern boundary is turned north by the Coriolis effect until it is deflected slightly south by the solid wall boundary. Most of the flow is channeled between the island and the basin's northern boundary. The flow then curves back again and exits through the Strait of Gibraltar. This circulation pattern is quite close to that observed in the Alboran Sea for the Levantine Intermediate water (Gascard and Richez, 1984 Parrilla and Kinder, 1984). When topography is added to the two-layer model, Fig. 31b, the path of the lower layer flow is dramatically changed. Though the prescribed inflow is also .2 cm/sec due west at

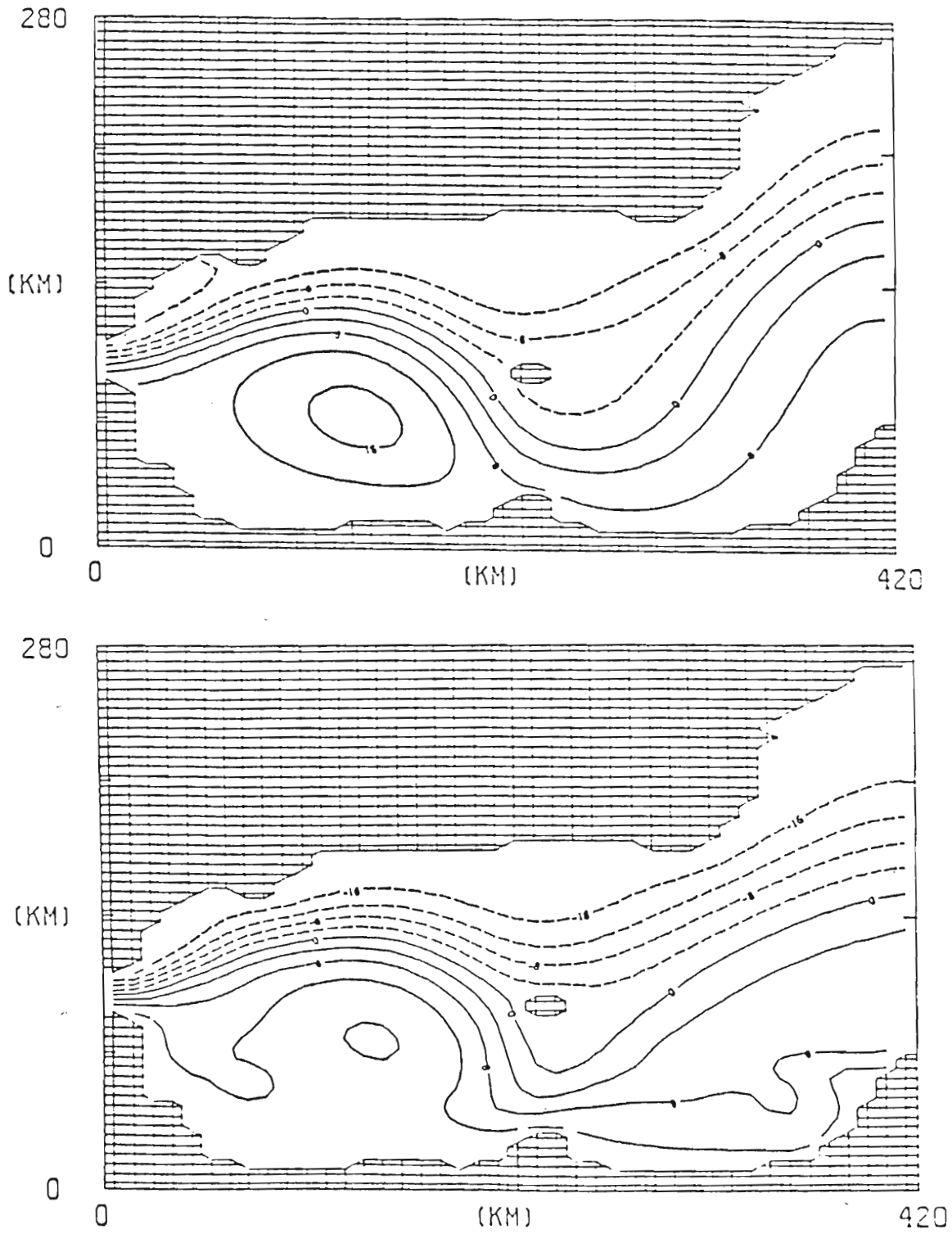

Fig. 30. PA of the two-layer "standard" cases a) with a flat bottom plus the island and b) topography plus the island. Solutions are at day 360. Contour interval is 4 m.

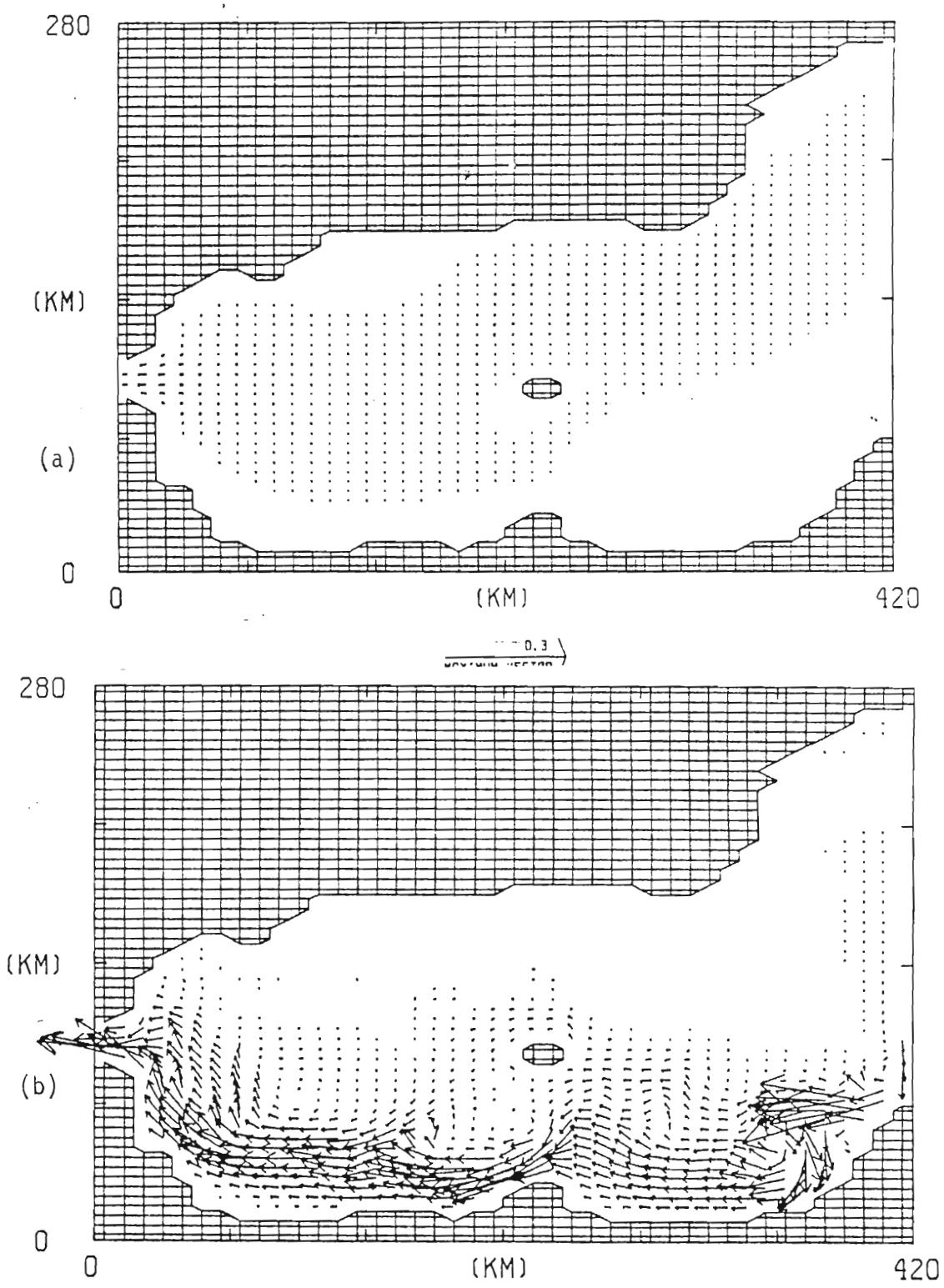

Fig. 31. Lower layer velocities for the cases shown in Fig. 30 a) flat bottom and b) topography. Maximum velocity vector is 30 cm/sec. Day is 360.

every point of the eastern inflow boundary, its westward flow is drastically halted by the steep topographic gradients in the northern half of the eastern boundary. Rather than flow up over the steep topography, the flow is turned south to a region of weaker east-west gradients. This flow reaches the southern boundary and turns west, where a portion of the flow is confined to the shelf and the remainder of the flow follows the deeper topographic contours. As a result, the majority of the inflow is confined to the southern half of the Alboran Sea. The Alboran island-ridge system deflects some of this flow north of the island and back down the northwestern side of the ridge. The majority of the flow continues westward, is forced north by the southwestern boundary of the basin and exits at the Strait of Gibraltar. A small anticyclonic recirculation is formed between the Strait of Gibraltar and the Alboran Island below the anticyclonic upper layer gyre.

The path taken by this slowly moving lower layer conserves potential vorticity. Using a scale analysis of the terms in the potential vorticity equation, it is found that

$$\frac{du}{dy} \quad \frac{dv}{dx} = \frac{.01 \text{ m}}{10 \text{ km}} = 10^{-6}$$

while f is of order 10^{-4}. Thus, the lower layer flow attempts to follow a path of constant f/h. The type of circulation found in the

lower layer of the case with topography closely follows the observed path taken by the Mediterranean Deep Water (Gascard and Richez, 1984 and Kinder and Parrilla, 1984a and Bryden and Stommel, 1982). One might expect that the Intermediate Water does not feel the effects of topography as does the Deep Water. These model results suggest that the path taken by the Deep water is topographically induced while the path taken by the Intermediate water, residing above the deep water, is only weakly influenced by the topography.

It is in the region of strong lower layer flow that an observable difference appears in the PA contours of these two cases. The southern half of the anticyclonic gyre takes on a jagged irregular shape. The incoming jet curves farther south and westward in the region just south of the Alboran ridge. These contours also indicate that more of the inflow passes north of the Alboran Island in the topography case. The curved contours in the southeastern part of the basin represent development of a weak anticyclonic circulation due to the strong curving flow below.

The interaction between upper and lower layer is clearly represented by the interface deviation. Pressure contours tend to show the separate effects of the upper and lower layers. Figure 32a shows pressure contours in the upper layer. This pattern of contours, in particular the symmetric anticyclonic gyre, closely resembles the pycnocline anomaly contours of the flat bottom case and reduced gravity

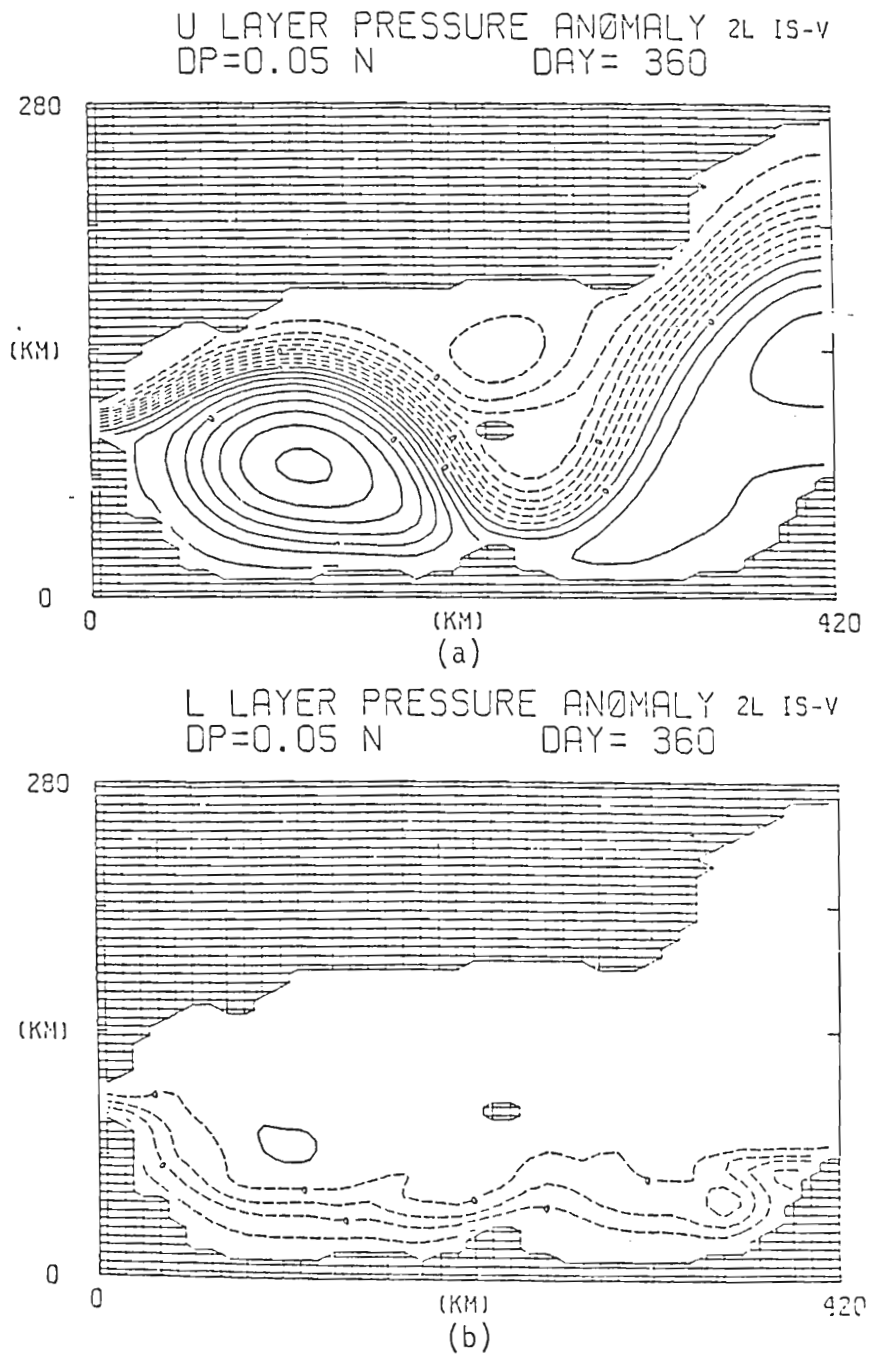

Fig. 32. Pressure anomaly contours for the solution presented in Fig. 30; a)upper layer and b)lower layer. Contour interval is .05 nt m^{-2}.

cases. Figure 32b, shows that the largest pressure gradients in the lower layer exist at the southern boundary and correspond to the region of the strong topographically steered velocity.

An additional experiment was performed in which the upper layer was quiescent while the lower layer was forced with the standard .2 cm/sec, Fig. 33. These results indicate that the addition of lower layer flow and topography has the effect of tilting the interface slightly upwards in the northern half of the basin. As a result, in the two-layer case with topography, the interface is deeper along the shelf and shallower below the gyre then in the flat bottom case. This tendency to tilt the interface upward in the north adds slightly to the negative relative vorticity near the strait. If the transport remains steady in the inflow region, the tilted interface would cause an increased velocity in the northern part of the jet, thus increasing the negative relative vorticity. If the initial shear in the inflow region was small enough such that the inflow did not turn northward, the additional shear induced by the lower layer could be enough to cause the flow to turn northward. In quantative terms, a layer depth of 200 m and a velocity of 33 cm/sec would be affected by the tilted interface resulting in an additional negative relative vorticity of

$$\frac{.003 \text{ m sec}^{-1}}{5 \times 10^{3} \text{ m}} = 6 \times 10^{-7} \text{sec}^{-1}$$

Note that this value is small when compared to the Coriolis parameter

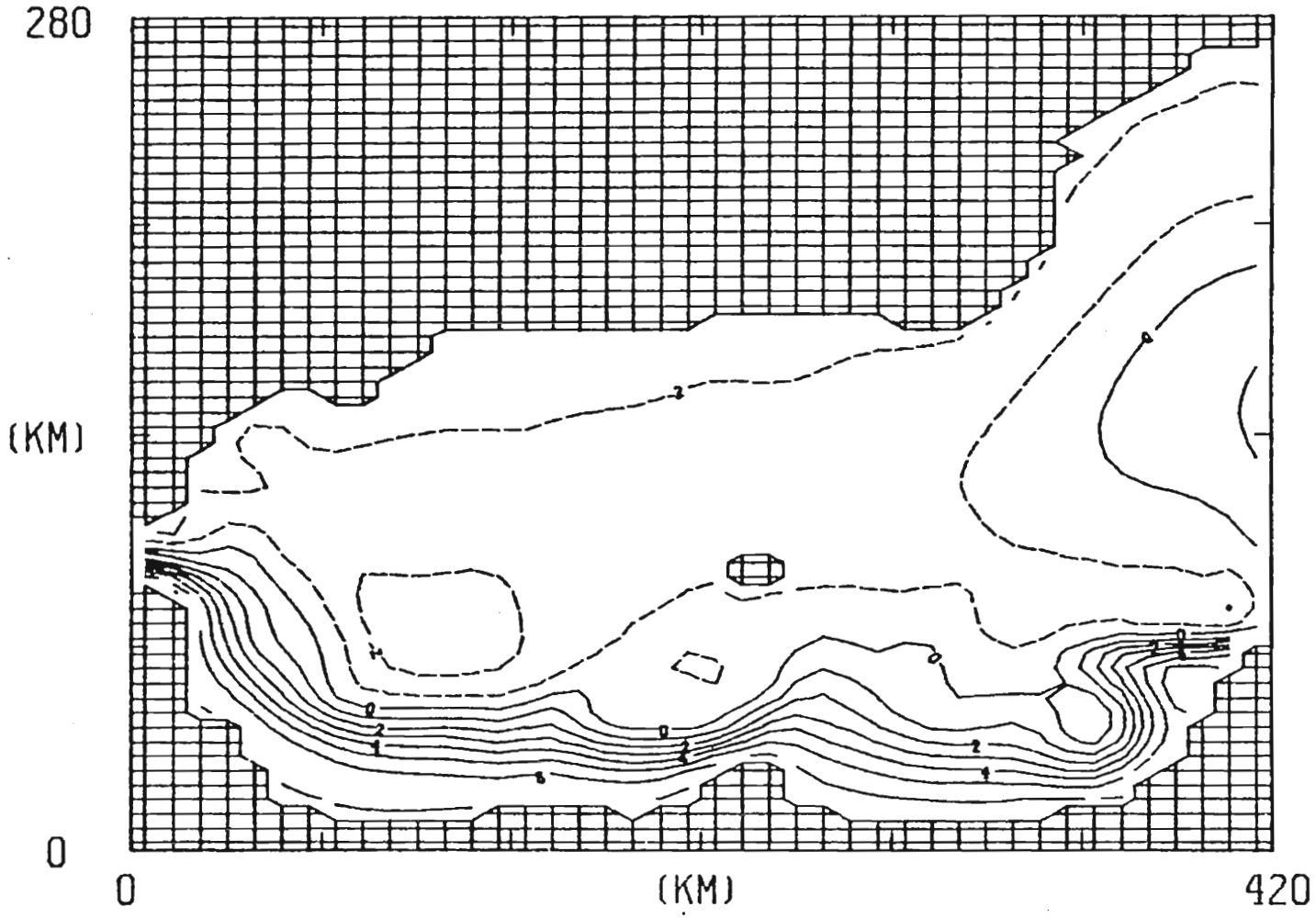

Fig. 33. Solution at day 360 of the two-layer topography case with a quiescent upper layer and standard lower layer flow. Contour interval is 1 m.

and when compared to the relative vorticity imposed at inflow in section 3c. Thus the vorticity imposed by the lower layer flow will add a small amount of anticyclonic vorticity to the upper layer, most often not enough to turn the incoming jet northward.

d. The effect of geometry on the two layer case

A comparison was also made between a flat bottom, no geometry case and a full geometry plus topography case. Figures 34 a and b show the results of two identical cases of 30 cm/sec angled inflow with and without topography plus geometry. The dashed line across Fig. 34b indicates where the wall boundary of the reduced gravity model would be or the average location of the northern boundary of the Alboran Sea. Without the northern boundary, the inflow does not turn as far north as in the case with geometry. As a result, the center of the gyre lies farther west. The cyclonic gyre which lies downstream of the anticyclonic gyre now has more room to form and expands to the north and east. This enlarged cyclonic flow, now limits the northward extension of the jet. In addition the fact that there is no longer a cape to deflect the flow northward causes the jet to exit in the southern half of the basin.

e. The circulation of the Alboran Sea as determined by drifter movement: observations and model results

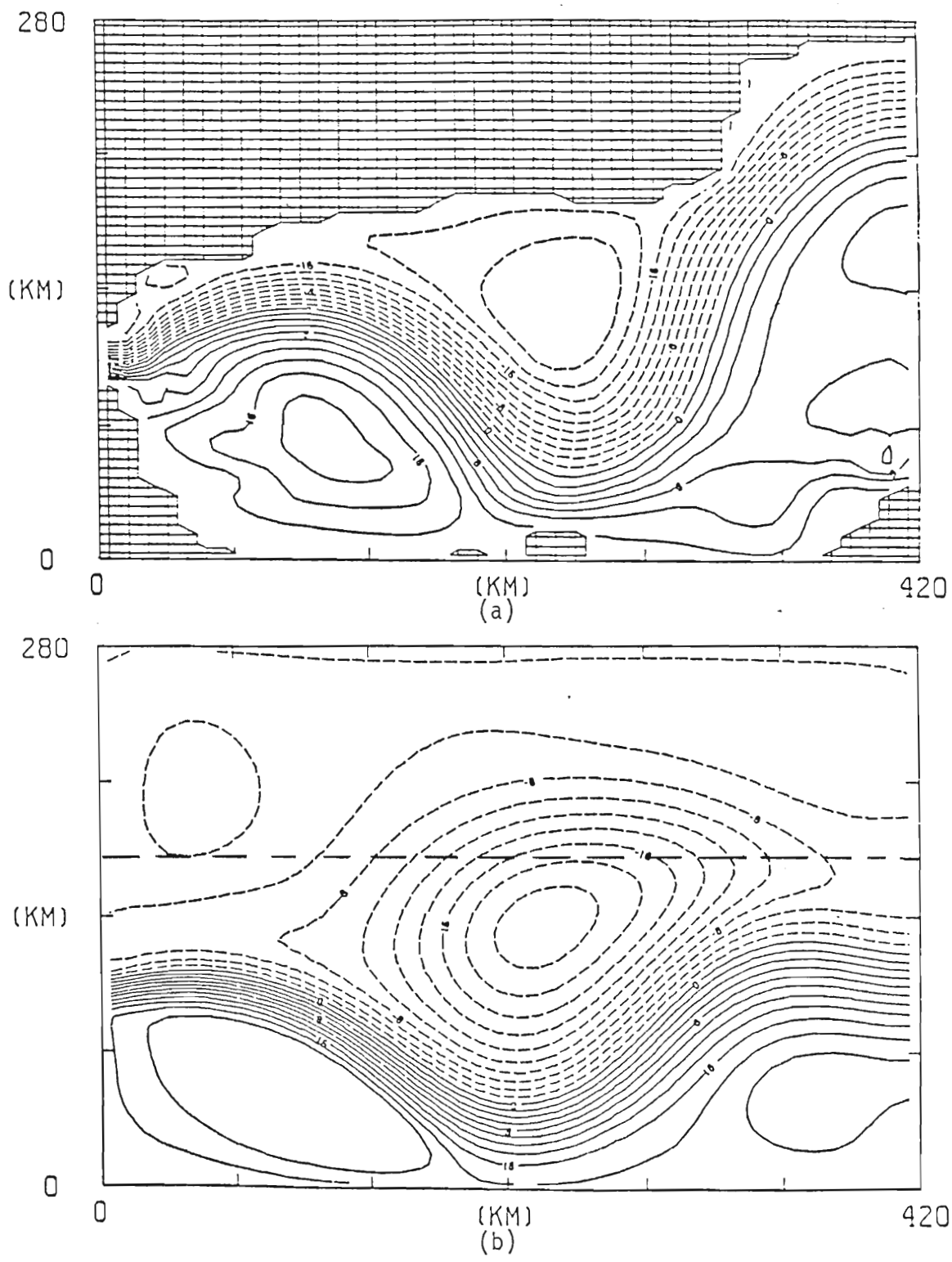

Fig. 34. Solutions for two cases with "standard" inflow forcing a) topography and geometry and b)flat bottom no geometry. Inflow and outflow boundaries are identical..

Observational insight into the circulation of both upper and lower layers has been gained by studying the movement of floats at various depths in the Alboran sea. Studies of floats in the surface layers have been made by Gascard and Richez (1984). Three surface floats were launched along $5^{o}10'W$ longitude. The two northernmost floats took cyclonic paths to the north and west Fig. 35a. This region along the Spanish coast has been well documented as a region of colder surface water temperatures (Laniox, 1974; Cano, 1977; Copin-Montegur et al., 1981 and Parrilla and Kinder, 1984). It has been suggested that this is a possible region of upwelling (Stevenson, 1977; Gallagher et al., 1981) due to predominance of eastward winds in this area. Other authors have indicated the existence of a cyclonic eddy in this region (Cano, 1978). This type of cyclonic circulation north of the incoming jet is observed in the model. The cyclonic circulation was shown to be confined to the northwestern corner of the basin in both the reduced gravity and two-layer cases with the inflow angled north of east (Figs. 8a and b). Measuring from the standard reduced gravity case, Fig. 8b, the size of the gyre is 25 km in radius or approximately one internal radius of deformation. This is in agreement with the observations of Gascard and Richez (1982). The third float, the southernmost float, Fig. 34b, turns north and east and follows the circulation of the gyre. It then makes two cyclonic paths around the island-ridge system back into the gyre and leaves the western Alboran sea by cutting across the

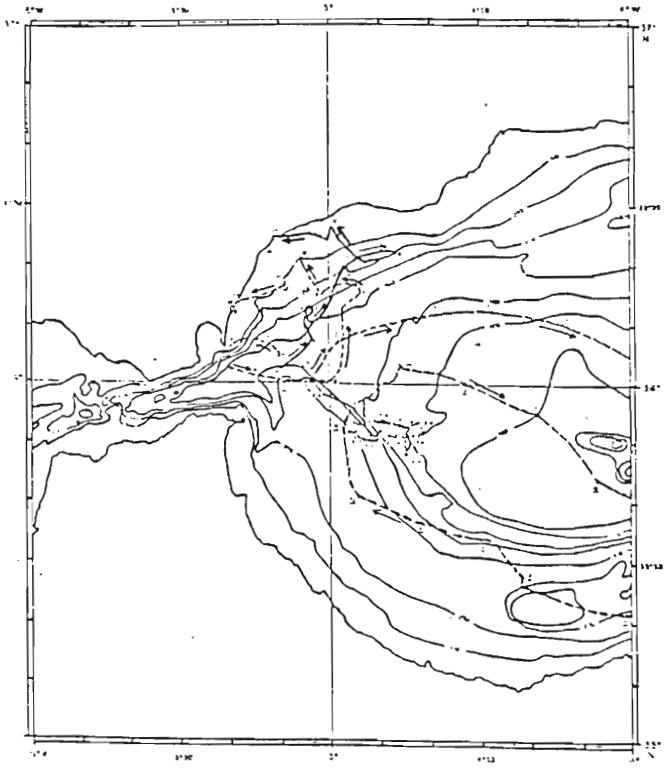

(a)

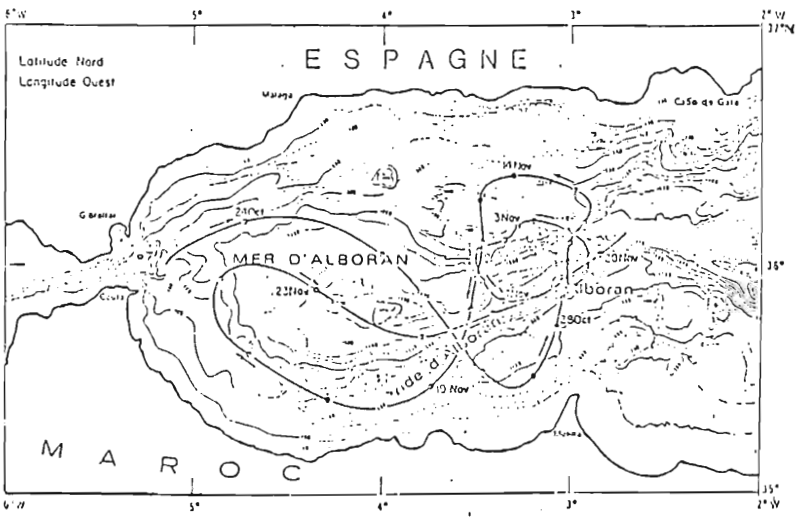

(b)

Fig. 35. a) Drifter paths taken by surface drifters in the western Alboran Sea, from Gascard and Richez, 1984. b) Extension of the path taken by the southern most drifter.

island-ridge system.

Similar Lagrangian trajectories were calculated from the resulting circulation of the numerical model. Drifters may be placed at any horizontal location in the basin, in either the upper or lower layer. They drift based on the currents generated by the model. Figure 36 shows the paths taken by six such drifters placed in the upper layer of a two layer, full topography and angled inflow case (standard case). The drifters are placed in position at day 360 of model integration and continue moving in time until day 720 is reached or until they leave the basin. Three of the drifters entering at the strait are caught in the fast moving inflow. They are carried south of the island-ridge and then turn to exit from the northern part of the basin. Two additional drifters, 4 and 5, originating farther south then the first three drifters are trapped in the gyre. Both drifters eventually curve towards Cape Tres Forcas where number 5 runs aground at the cape while drifter 4 turns westward towards the gyre and slows. Both drifters 4 and 6 become trapped at a stagnation point slightly west of the cape. It is important to note that none of these drifters follow the cyclonic paths near the Alboran Island that are taken by Gascard's drifters. This type of complicated motion is probably attributed to the island-ridge topography in the upper 200 m which cannot be accounted for by the two layer model.

Model drifters can similiarly be placed in the model's lower layer

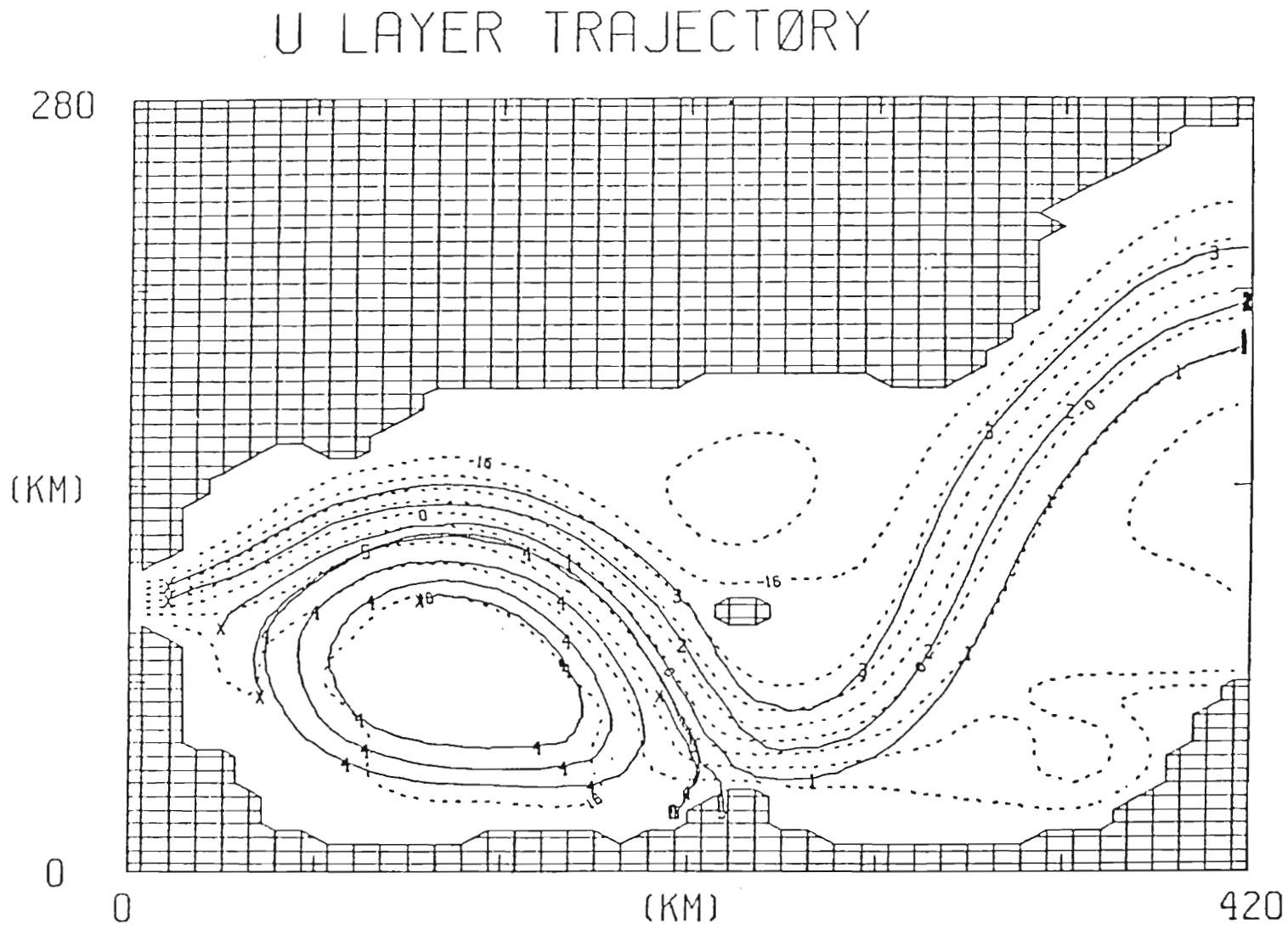

Fig. 36. Six model drifter tracks released in the upper layer of the "standard" two-layer plus topography case Fig. 25. Dashed contours are PA contours in 4 m intervals. The drifter number is written out every 10 days in its new location.

flow. Figure 37 shows 6 drifters placed in the lower layer of the standard case solution. Dashed contours in this case represent the contours of bottom topography. Drifter 1 placed at the center of the eastern boundary barely moves, indicative of the very small velocities in that region. Drifter 2 moves westward until it reaches the island, veers to the south and continues very slowly westward across the ridge. Drifter three, originally placed close to the southern shelf, moves relatively quickly westward across the basin and out through the strait. Drifter 6, also in the southern shelf region, follows a similiar path. Drifter 4 appears caught in a weak anticyclonic gyre while drifter 5 travels very slowly westward. An interesting comparison can be made between these drifters and those in the lower layer of a flat bottom case Fig. 38. In contrast to the drifters of the topography case, drifters in the southern half of the flat bottom case move very slowly. Drifters placed in the northern half of the basin move slowly and steady westward until they exit at the strait. This type of movement agrees with the observed circulation of the Levantine Intermediate water.

Figure 39 shows some additional drifter paths for the lower layer of the topography case. The drifter at the far eastern boundary shows the path taken by the flow as it enters the basin and is forced south by the steep topographic contours. Drifter 3, placed just north of the island, travels slowly around the western side of the island until it

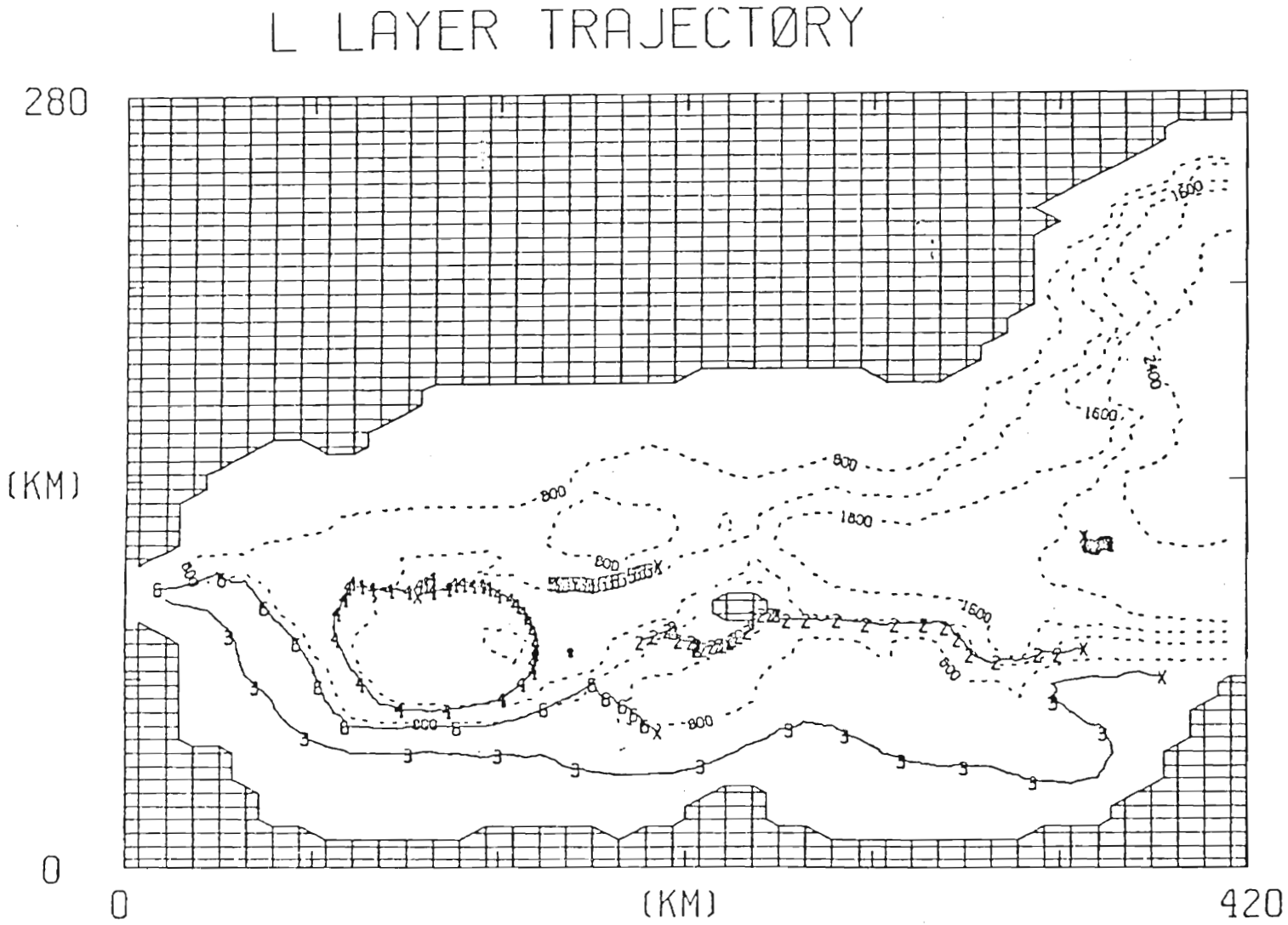

Fig. 37. Six model drifters released in the lower layer of the standard case. Dashed contours are bottom topography in 400 m intervals. The drifter number is written every 10 days in its new location.

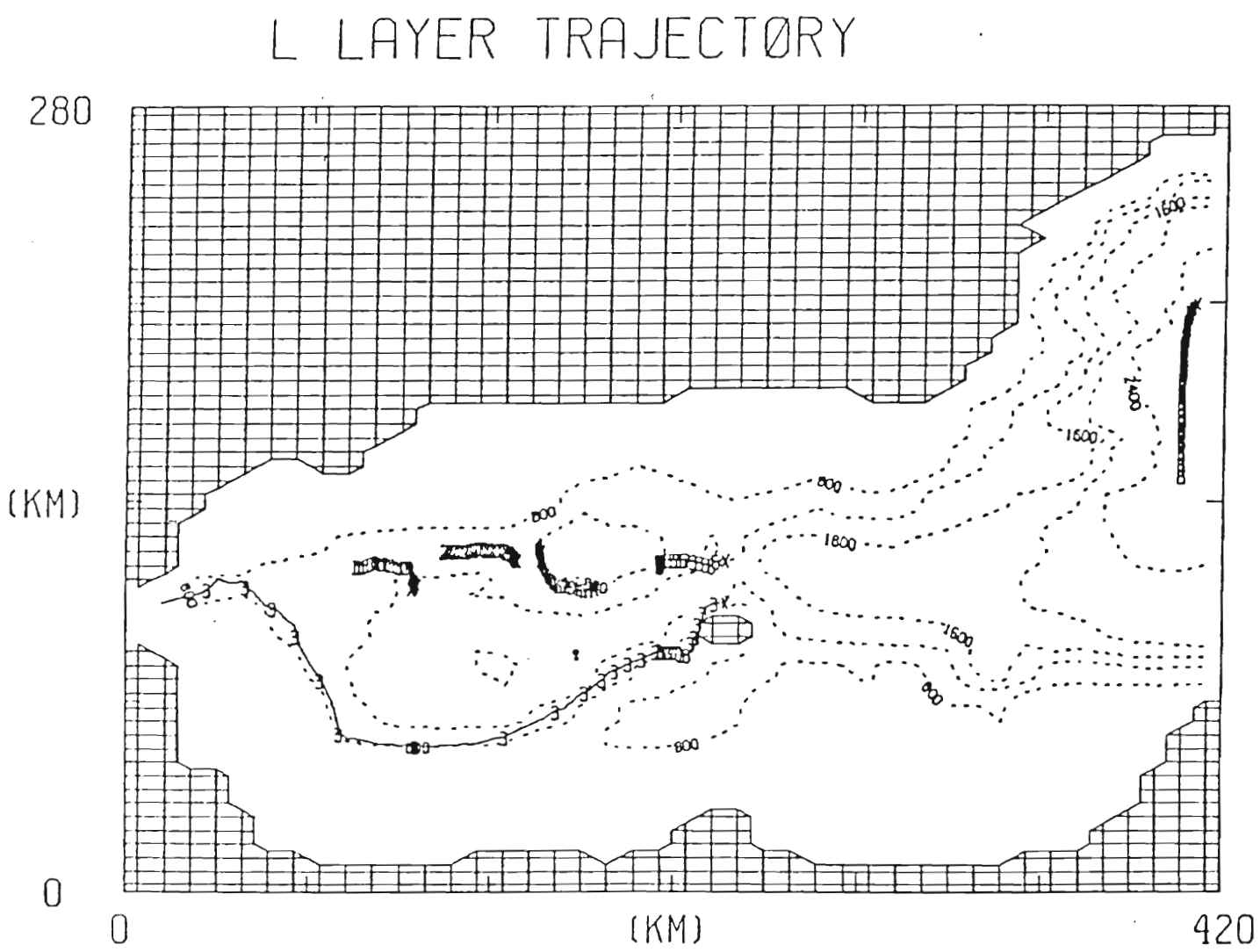

Fig. 39. Six additional drifter track released in the lower layer of the standard case, Fig. 25. Drifter numbers are written every 10 days.

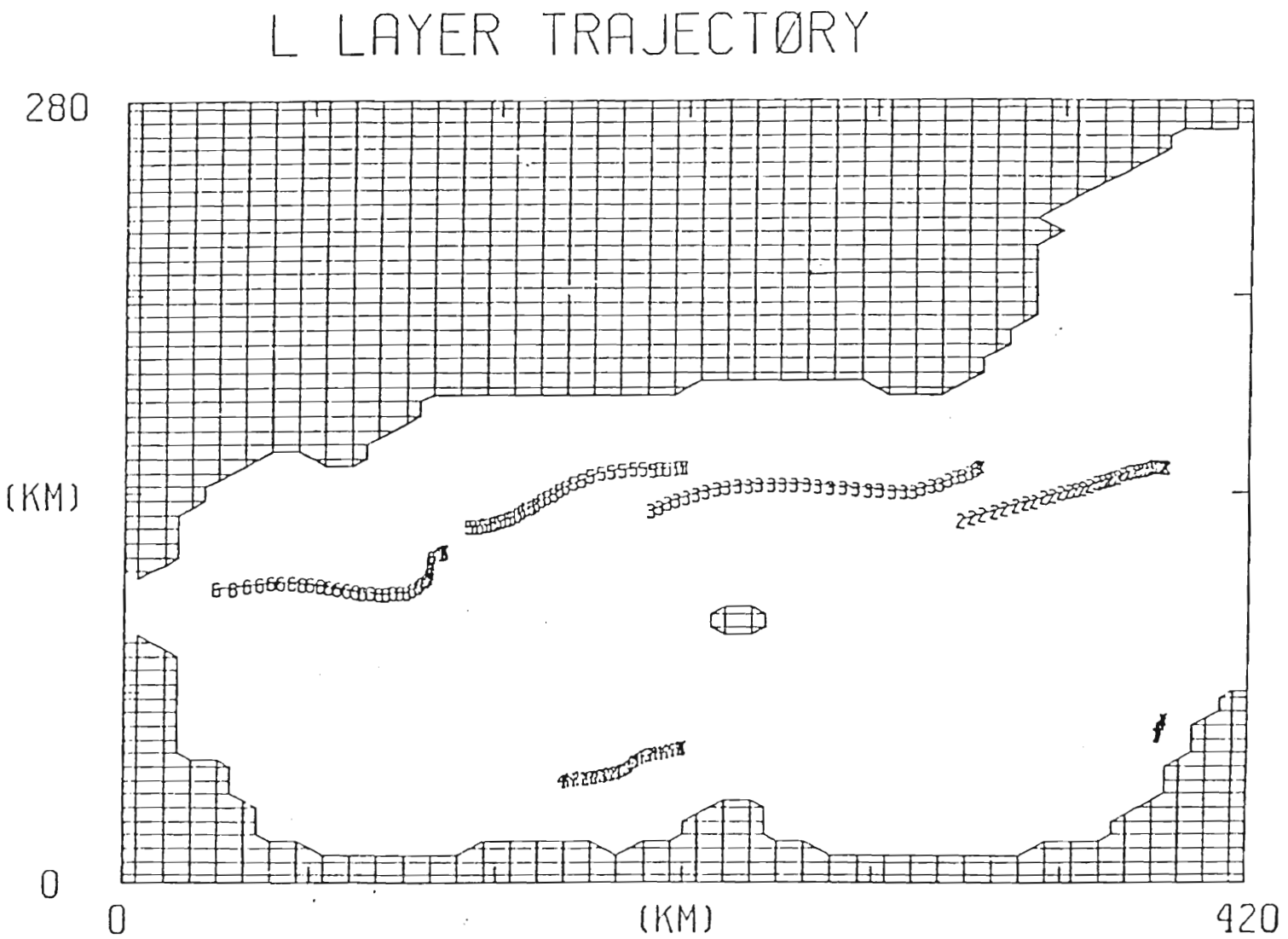

Fig. 38. Six model drifters released in the lower layer of the standard case with a flat bottom, Fig. 30a. Drifter numbers are written every 10 days.

becomes caught in the faster moving westward flow and follows the topographic contours out of the basin. The remaining four drifters, located just south and west of the island, move slowly toward the strait. Unlike drifter 4 (Fig. 37), these drifters display cyclonic type motion. The circulation displayed by these four drifters is in general agreement with drifters (1,2,4,6) placed in similar locations by Pistek (1984), Fig. 40. The somewhat eratic behavior displayed by Pistek's remaining drifters, moving in small counterclockwise circles or moving back and forth along the ridge, can not be explained by these steady state model solutions. This type of motion may be due to temporal variability in the lower layer flow or bottom frictional effects not included in the model.

f. The importance of the time varability of the Atlantic water inflow

Knowing the detailed characteristics of the inflowing Atlantic water has been important in defining the Alboran Sea circulation, in particular the gyre. The effect of angling the inflow was shown to help determine the horizontal dimensions of the gyre. It was also seen that increasing the transport shifted the Alboran gyre east. Experiments were also performed to determine the effect of drastically reducing the velocity (i.e. transport). Starting from the day 360 standard two-layer solution, the angled velocity was changed sinusoidally from 30 cm/sec to 1 cm/sec to 30 cm/sec over a period of

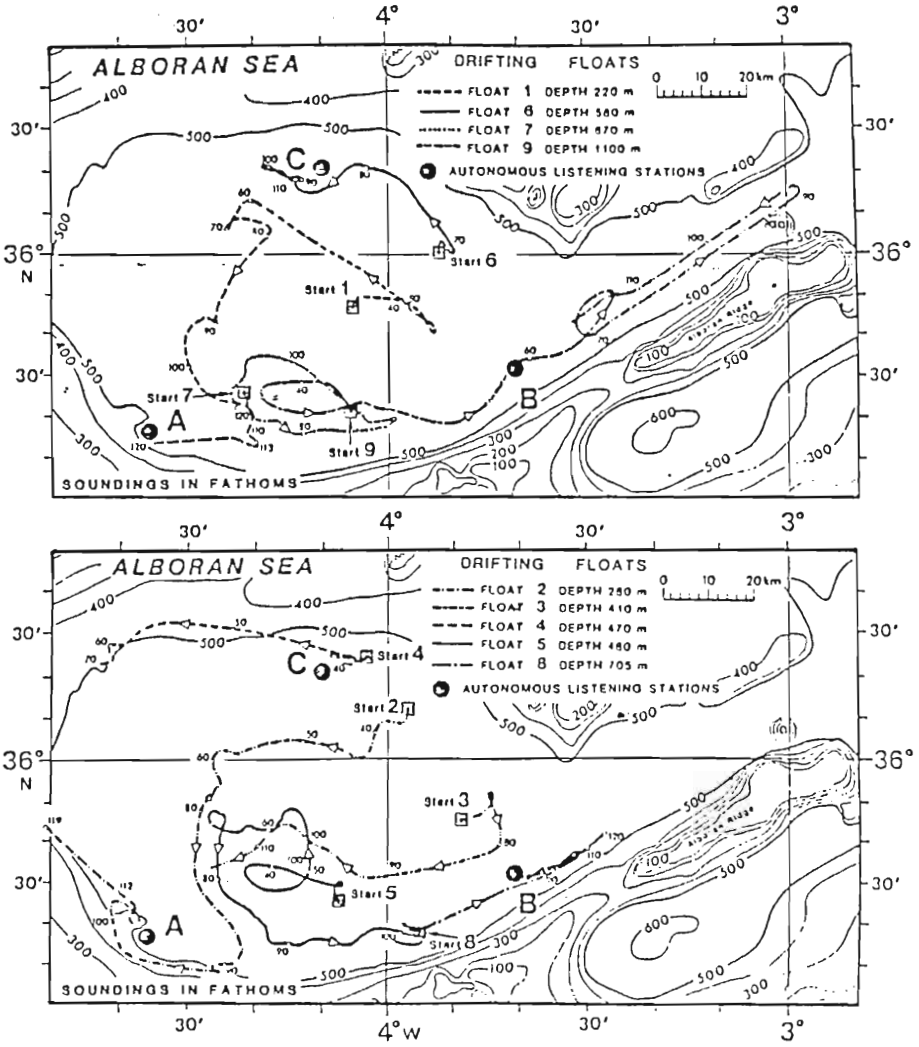

Fig. 40. Observed drifter tracks located at 220 m and below from Pistek, 1984.

180 days. Velocity then remained constant at 30 cm/sec for an additional 180 days. Solutions for this oscillating velocity are shown in Figs. 41a-j. As velocity decreases Figs. 41a-d, the gyre becomes less intense and its center shifts toward the west. The small cyclonic gyre north of the Alboran Island feels the same effect and shifts to the west as well. This results in the rather unique configuration of days 440-500; two oppositely rotating gyres exist west of Alboran Island. A two gyre configuration has been observed in the satellite infrared imagery Figs. 41e-h, however the direction of rotation of the second gyre has not been determined. As the velocity increases, the centers of these gyres move eastward and return to the configuration of the day 360 solution.

Results similar to this were also observed by Chao, 1982. When Kuroshio transports were reduced, the wavelength of the current meanders decreased, shifting the centers of the gyres associated with these meanders in an upstream direction. Similar observations were made by Cheney and Doblar (1982) for the Alboran Sea (Fig. 42). In cases where wind and pressure effects should minimize inflow, the center of the gyre was at its westernmost location, while in the reverse case, the center of the gyre was at its easternmost location. Parrilla and Kinder (1984) provide additional documentation of the variability of both the Alboran gyre and the cyclonic gyre north of the island.

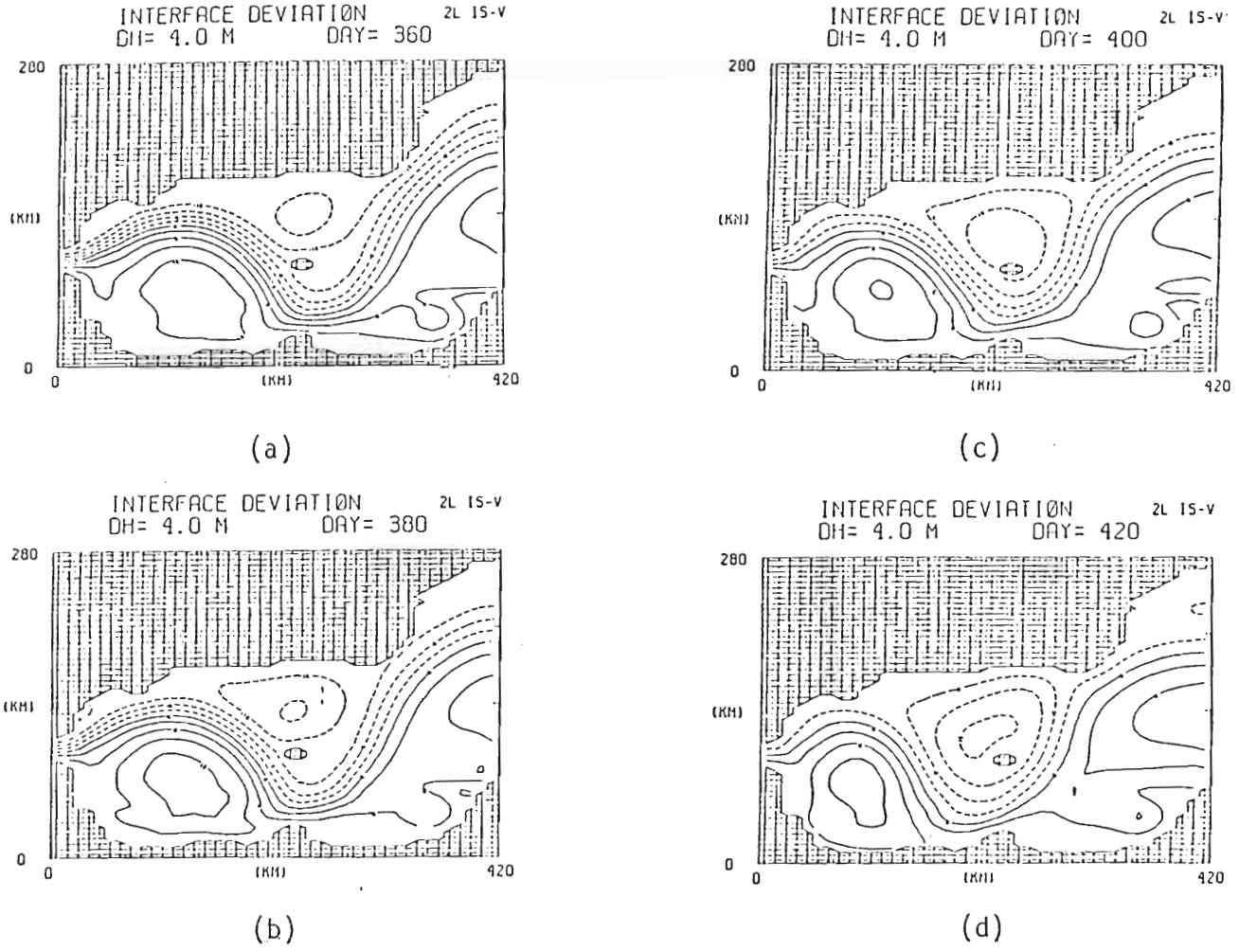

Fig. 41. PA of the two-layer case with 21^{o} angled north of east inflow. Starting from day 360 solutions, Fig. 25, velocity changes from 30-1-30 cm/sec over a period of 180 days; a) day 360, b) day 380, c) day 400 and d) day 420.

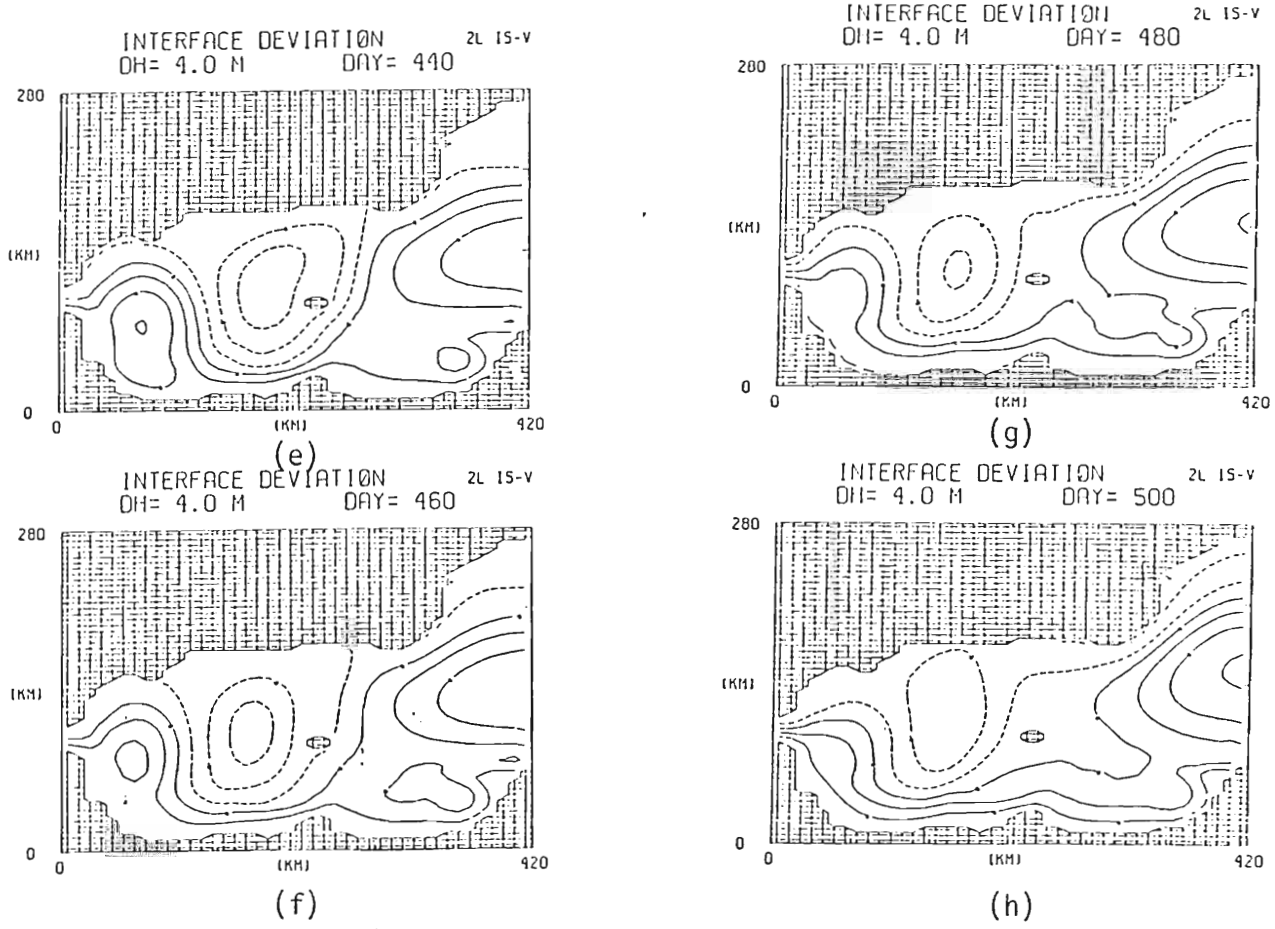

Fig. 41. PA of two-layer case with 21^{o} angled north of east inflow; e) day 440, f) day 460, g) day 480 and h) day 500.

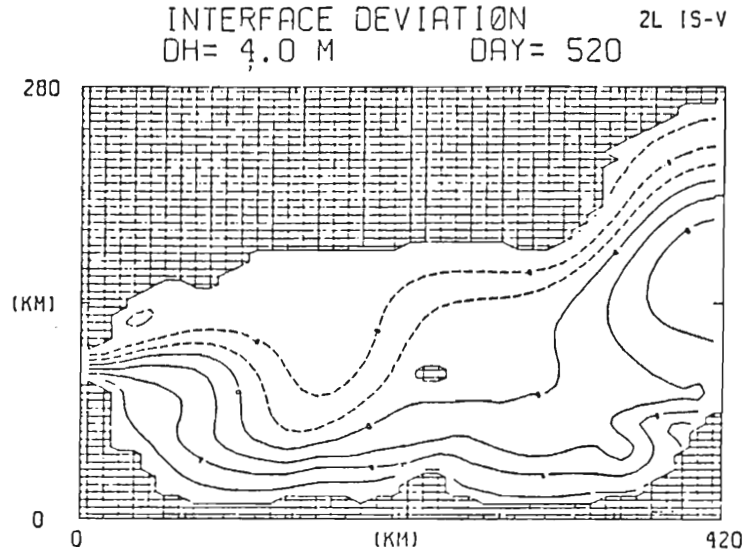

(i)

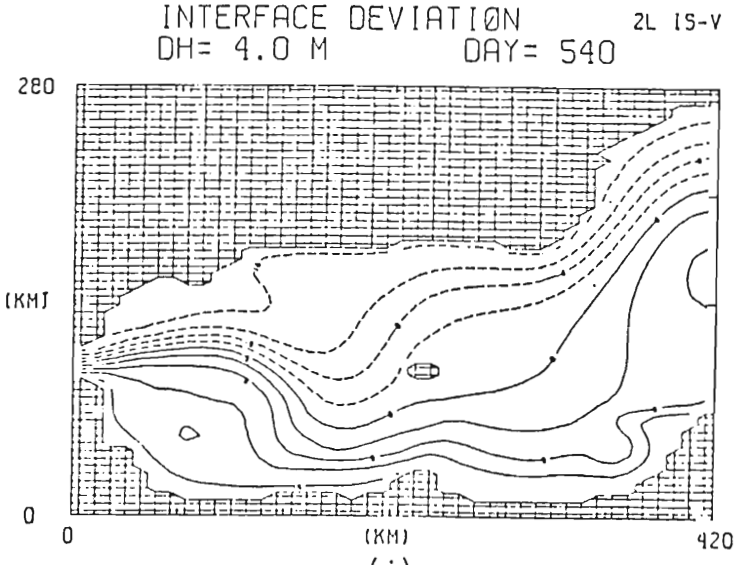

(j)

Fig. 41. PA of two-layer case with 21° angled north of east inflow. i) day 520, and j) day 540.

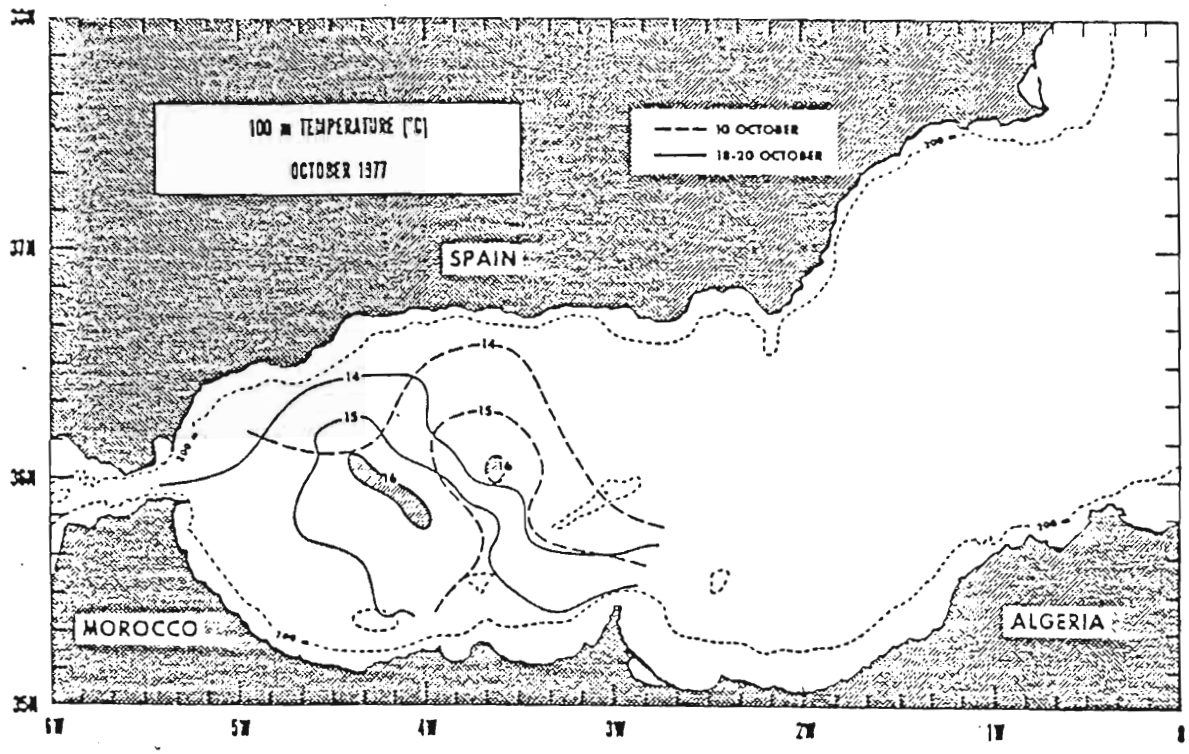

Fig. 42. 100 m temperature contours from Cheney and Doblar (1982) for October in the Alboran sea. Analysis are separated by 8-10 days.

As the velocity decreases in this experiment, a change appears in the configuration of the height contours at the Strait of Gibraltar port. The contours no longer smoothly curve north, they are instead oriented east-west and then abruptly ($\simeq$ 20 km into the basin) turn towards the northeast. A 21^{o} angle is maintained even when the velocity is decreased. Thus, when the u-component of the inflow is reduced to 1 cm/sec, the v-component is reduced to 0.43 cm/sec. With the northward component so small, the height contours barely curve northward. There is however, a delayed effect on the anticyclonic circulation of the gyre. Circulation within the gyre does not decrease or increase as quickly as the inflow. Thus, approximately 20 km into the basin, the anticyclonic circulation of the gyre, containing a much larger northward component, meets the inflowing water and the contours curve abruptly northward (day 450). As the inflow increases again, so does the northward component and the contours again curve northward at the Strait of Gibraltar port. As this happens, the anticyclonic circulation all but disappears, eventually reforming as the inflow continues to increase. This indicates a temporal delay occuring between the time in which the Strait of Gibraltar flow again increases and when the gyre exhibits the effects of the increased flow. For the particular grid interval Reynolds number used in this case (a small value for A = 85 $m^2 sec^{-1}$ was used resulting in a grid interval Reynolds number of

$$.3 \text{ m sec}^{-1} \times (10^4) / 85 \text{ m}^2\text{sec}^{-1} = 35),$$

the temporal delay is approximately 40 days.

A number of tests were performed in which the velocity was increased and decreased from an initial velocity value of 30 cm/sec sinusoidally varying the periods (60,120,40 days) over which the change takes place. The results of this test show that the configuration of the gyre is most drastically changed when the velocity values change over a longer period of time, Figs. 43a-e. Over shorter time scales, Figs. 44a-f, changes such as the appearance of the two gyre configuration and the almost complete disappearance of the gyre do not develop. The gyre instead seems to oscillate back and forth about an axis through its center. The gyre tilts to the west when the velocity decreases and to the east when it increases. These changes are less intense over shorter periods of time because the clockwise circulation developed in the gyre takes a finite amount of time to decay. Thus very short oscillations in the inflow, on the order of a few days, may appear only as small perturbations to the normal gyre configuration.

The change that takes place in the gyre dimensions as a result of the change in magnitude of the velocity can also be seen in the drifter tracks of Fig. 45. Drifters are placed in the same locations as they are in Fig. 36. The drifters paths begin at day 360 just as the oscillation (decrease) in velocity takes place. On comparison of the two figures, 36 and 45, the most noticeable difference takes place in

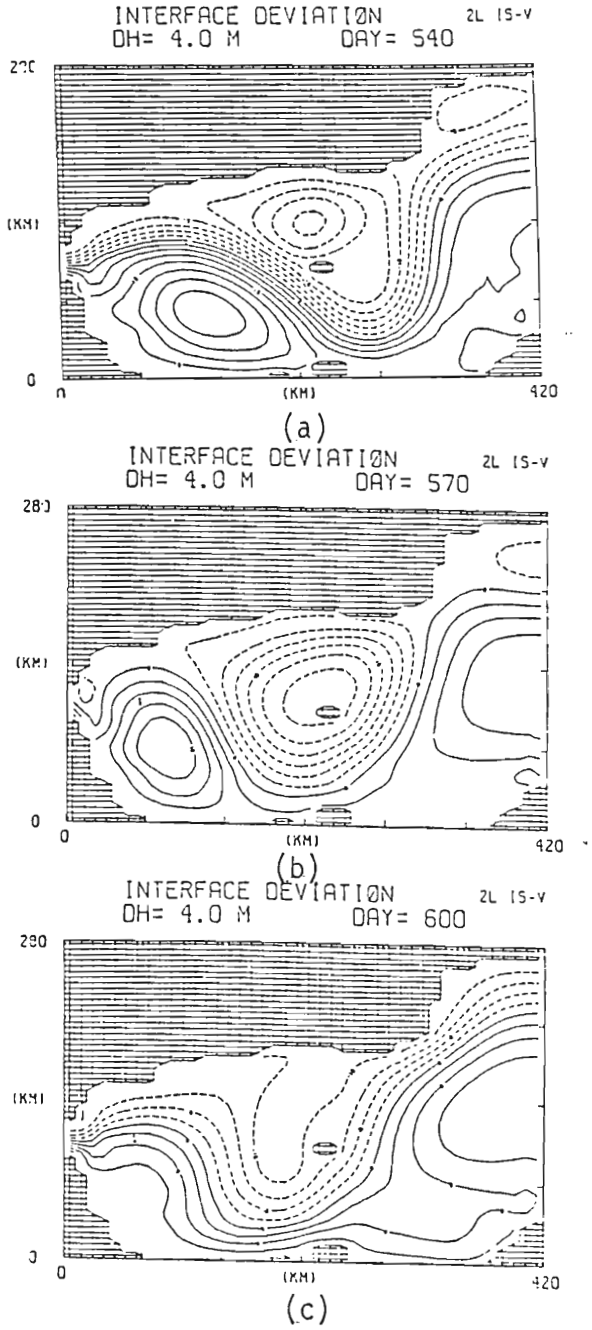

Fig. 43. Two-layer solutions with constant .2 cm/sec lower layer flow but upper layer flow osicllated about 30 cm/sec with an amplitude of 30 and a period of 120 days; a) day 540, b) day 570 and c) day 600.

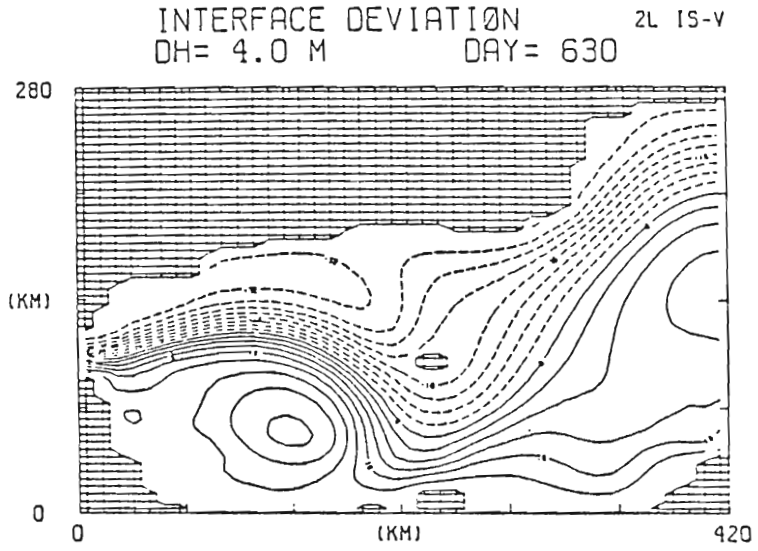

(d)

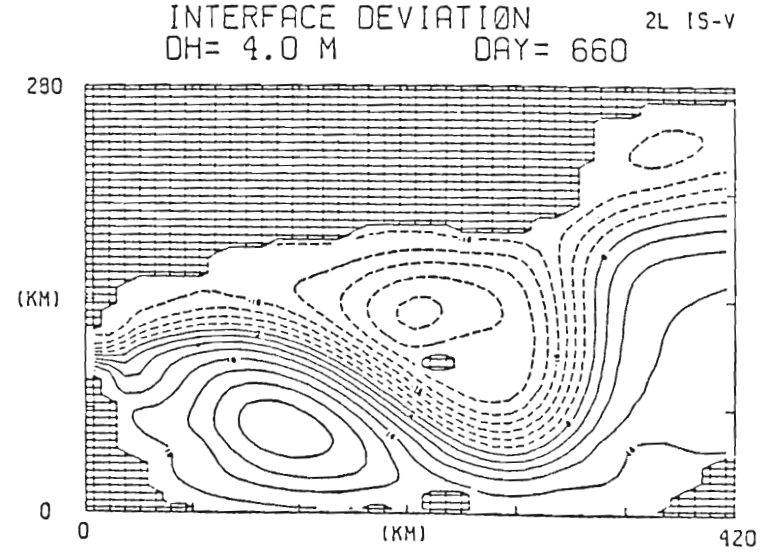

(e)

Fig. 43. Solutions of oscillating upper layer flow with a period of 120 days. d) day 630 and e) day 660.

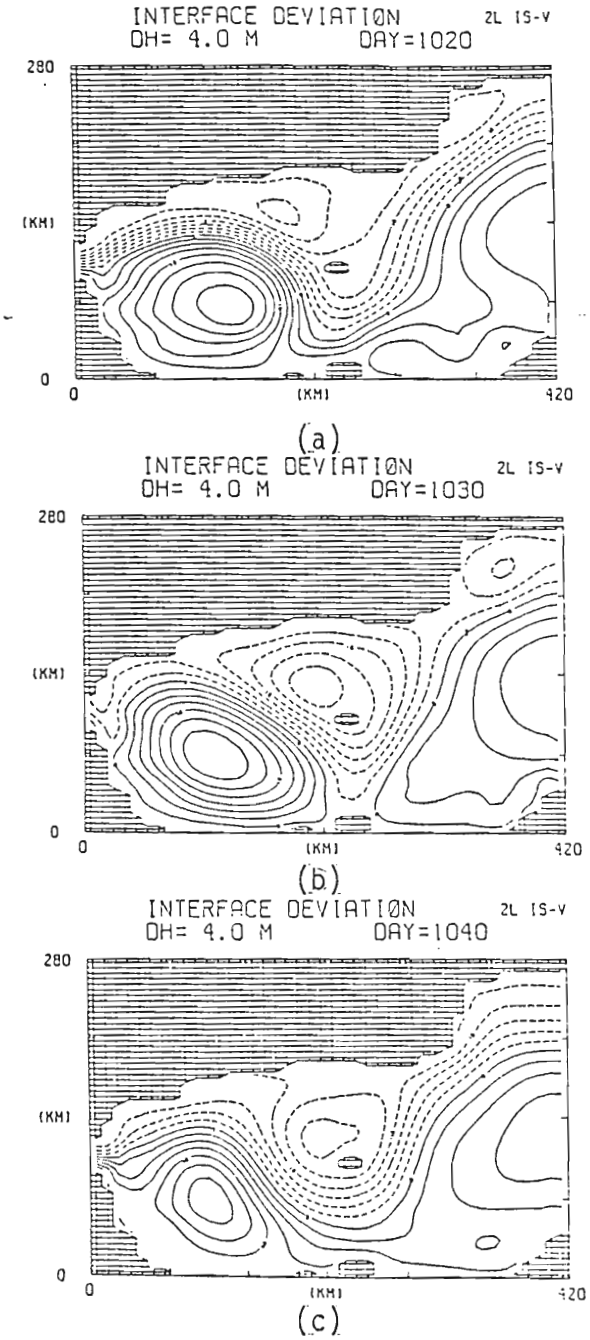

Fig. 44. Solutions similar to the case presented in Fig. 43 except the period of oscillation is 40 days; a) day 1020, b) day 1030 and c) day 1040.

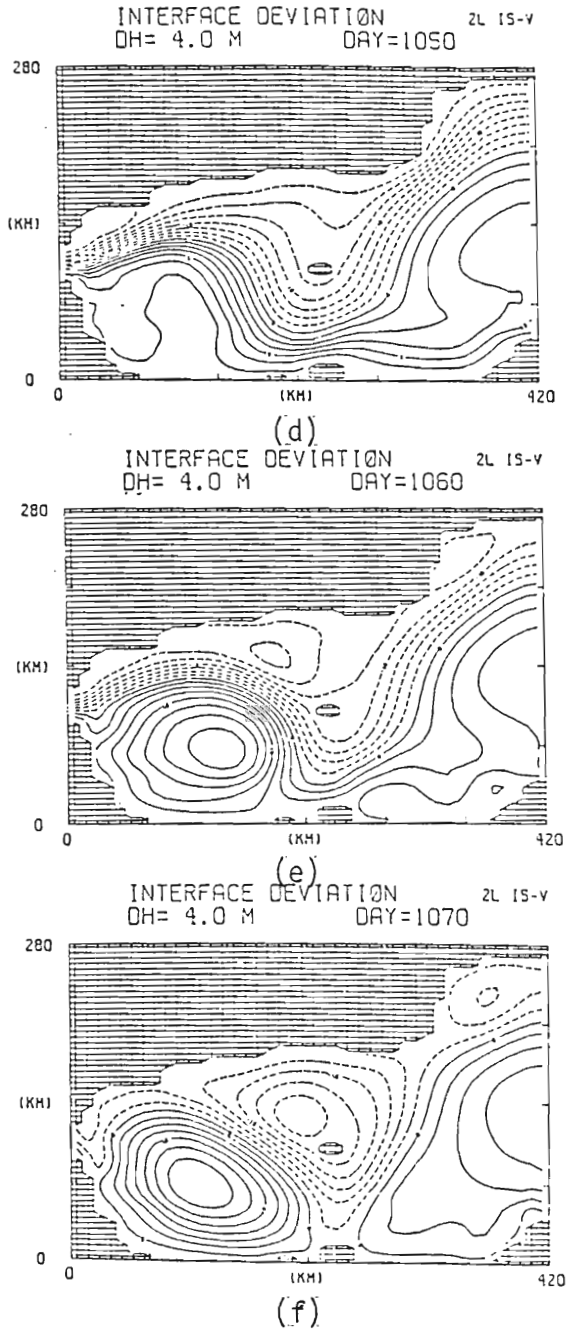

Fig. 44. Solutions of 40 day oscillating case; d)day 1050, c) day 1060 and e) day 1070.

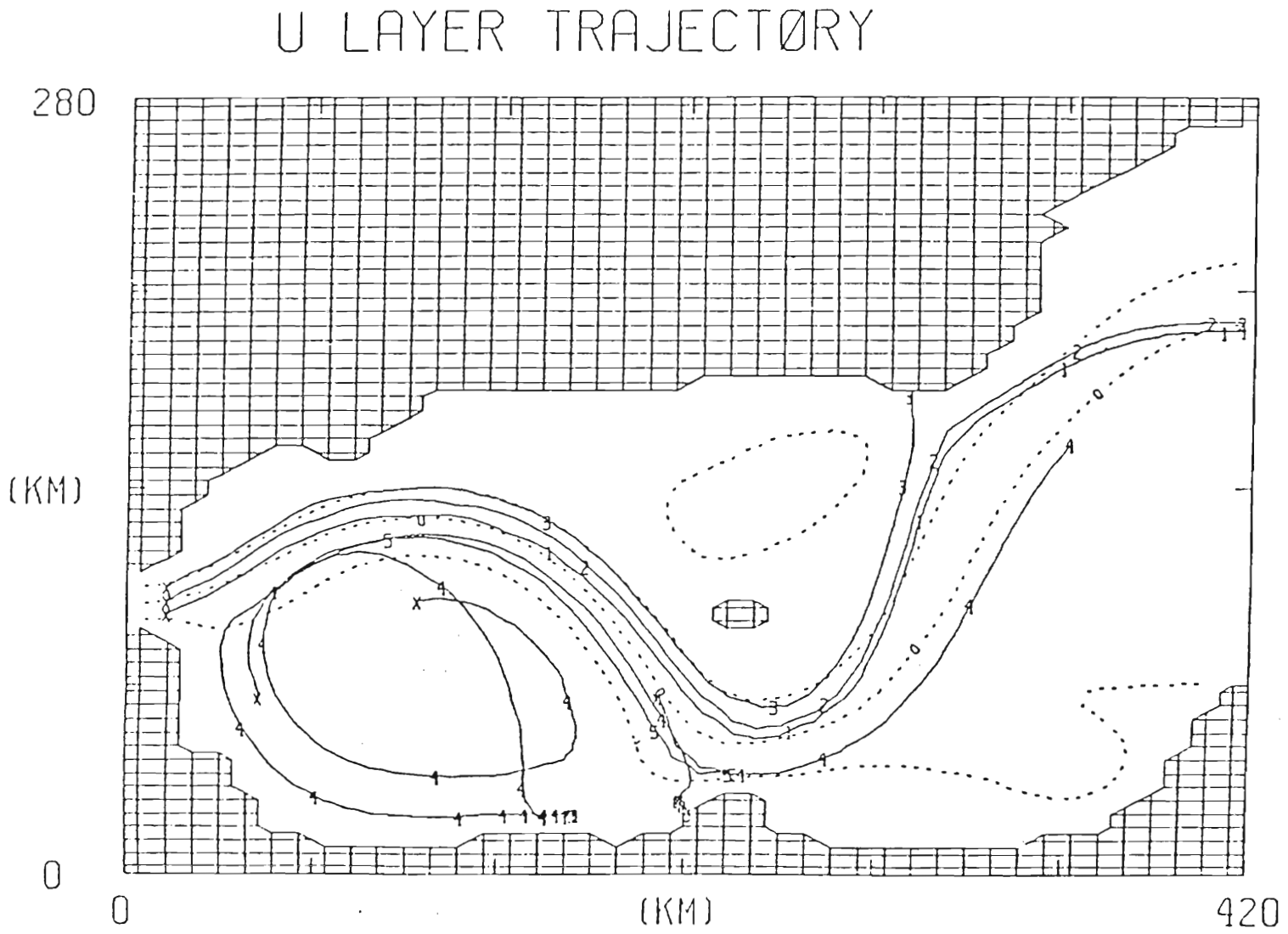

Fig. 45. Six model drifter tracks for the case of decreasing then increasing velocity presented in Figs. 34 and 35. The drifter number is written every ten days.

the path taken by drifter #4, the drifters located in the gyre. These drifters originally follow the same paths until the decrease in velocity is felt and the drifter, Fig. 45, slows in its eastward movement. This decrease in velocity is so dramatic that the drifter slows almost to a halt at the southern boundary. The inflow velocity then increases, the gyre circulation increases, and the drifter is once again caught in the anticyclonic circulation and is eventually steered into the jet.

5. SUMMARY AND CONCLUSION

Both hydrographic observations and satellite infrared imagery indicate that the circulation of the upper 200 m of the Alboran Sea is dominated by a permanent anticyclonic gyre. Observations have also shown that the configuration of the gyre is highly variable, ranging from a very small gyre confined to the southwestern part of the Alboran Sea, to a gyre filling the entire western half of the basin. This circulation appears to be driven by the Atlantic water entering through the Strait of Gibraltar. This water is less saline and usually cooler then the water of Mediterranean origin, thus it appears distinctly different in satellite infrared imagery. Intuitively, one would expect the water entering the Alboran Sea to turn south and be confined to the Moroccan coast, while it in fact is observed off the southern coast of Spain.

A number of theories have been suggested to explain this phenomenon. Nonlinear, semi-implicit, reduced gravity numerical model experiments have been used to demonstrate mechanisms by which the inflow can turn north and, characteristic features of the inflow which determine the variability of the gyre. In addition, realistic geometry and topography, as well as a slowly moving westward lower layer flow, are added to the model to determine what effect if any they have on the circulation of the upper 200 m. These experiments also shed some

insight on the observed circulation of the Levantine Intermediate Water and the Mediterranean Deep Water.

Reduced gravity model results show the importance of the Coriolis force turning the incoming flow to the right. This model also shows two methods by which the incoming flow may turn towards the north. The first is the simple geometric forcing of the flow northward. The geometry of the Alboran Sea-Strait of Gibraltar system indicates that flow should be channeled into the Alboran Sea in a 21^{o} north of east direction. It was also shown that if large enough negative relative vorticity is induced by the upstream channel (Strait of Gibraltar), the flow will turn north, in agreement with theory (Nof, 1978).

If the large anticyclonic Alboran gyre was simply formed by the existence of a restoring force on a β-plane, Rossby wave theory alone should define the meandering current which forms the boundary of the gyre. However, the narrow width of the basin alters the path defined by the effects of the restoring force, limiting the amplitude of the wave and shortening its wavelength.

The reduced gravity solutions show that the size of the gyre is not determined by topographic or geometric effects but rather by the complicated interaction between the boundaries, the restoring force and the magnitude of the incoming mass transport. Variations in the mass transport vary the wavelength of the meander. Small mass transport values shift the gyre westward decreasing the wavelength. Large mass

transports shift the gyre eastward increasing the wavelength.

When topography, geometry and a slowly moving westward layer are added, the basic configuration of the gyre found in the reduced gravity cases remains the same. Results show that the path taken by the lower layer follows contours of f/h. Flow is turned southward by the topography as it enters the basin. As a result, the majority of the flow is confined to the southern shelf. If the topography is removed, the flow, affected by rotation, turns north and is mainly confined to the northern half of the basin. These two different results look very similar to the paths of the Mediterranean Deep Water and the Levantine Intermediated Water. These results indicate that the Deep Water circulation is due to topographic steering. The Levantine Intermediate water which does not interact as strongly with the topography is dominated by rotational effects.

Although the basic configuration of the gyre in the two-layer case is the same as that of the reduced gravity case, some differences do appear in the southern half of the basin. The effects of the relatively large currents along the southern shelf are visible in the pynocline anomaly contours. In the shelf region, these contours are more curved and irregular. The lower layer circulation generally raises the pycnocline in the northern half of the basin while it decreases it in the southern half. As a result, the anticyclonic gyre of the two-layer case is not as deep as the gyre of the reduced gravity

case.

Results show that the Alboran island-ridge system does not have a dominating effect on the dimensions of the gyre. The combination of the ridge and cape however, serve to channel the southward moving flow and deflect it abruptly northward off of the cape.

Model drifters were placed in both the upper and lower layer of the two-layer model. These paths taken by these drifters are in good agreement with the drifter tracks of Gascard and Richez (1984) and Pistek et al., (1984).

In conclusion, the basic dynamics defining the Alboran gyre may be accounted for by the reduced gravity model. This model shows that the meandering current is a standing Rossby wave with a highly distorted conservation of vorticity trajectory. This distortion is mainly a result of the interaction of the inflowing Atlantic water with the side wall boundaries. The flow trajectory is also changed by varying the mass transport. The main effect of the westward moving lower layer with topography and geometry is to slightly distort the appearance of the circulation in the southern half of the basin. This is due to the relatively high currents channeled along the southern shelf by the topography.

APPENDIX A

WIND DRIVEN CIRCULATION

Both the reduced gravity and the two-layer models, strictly driven by flow from the Strait of Gibraltar have been able to simulate very closely the observed surface circulation of the Alboran sea. It has been documented that average inflow through the strait is affected by meteorological forcing (Lacombe, 1961). The most important meteorological force appears to be atmospheric pressure not wind stress (Crepon, 1965; Garrett, 1983). High pressure over the Mediterranean depresses the surface forcing water out through the strait. Low pressure over the Mediterranean allows the surface to rise and Atlantic water inflow increases. If wind stress and atmospheric pressure act together, the effect on inflow is even greater, possibily varying the inflow by a factor of two (Lacombe and Tchernia, 1971). Atmospheric pressure forcing has not been included in this model however, its observed effect of altering the transport through the strait has been examined and discussed in section 4.

The main thrust of this work did not originally include examining the effects of wind stress on the circulation of the Alboran sea. However, as a result of the appearance of a good data set of climatological wind stresses (May, 1982) for the Mediterranean sea, a

number of reduced gravity numerical model experiments were performed to examine the effects of climatological wind stress forcing. Climatological winds do not include short term effects such as frontal passage. The effect of simulated frontal passage could be examined. However changes on the time scale of 1-3 days may be too short for the numerical model to adequately respond. This study will then concentrate on the effects of climatological wind stress forcing only.

The type of model used to examine the effects of wind forcing was an explicit version of the reduced gravity model (Preller and Heburn, 1985). A slight deviation from the basic parameters (Table 1) is used when investigating the effects of climatological wind forcing alone on the Alboran sea. The study was done in conjunction with a study of the entire western Mediterranean (Heburn, 1985). Solutions were obtained for the entire western Mediterranean on a 7.5 km x 5 km grid. These wind forced solutions for the Alboran Sea subsection of the western Mediterranean were more realistic than solutions from an Alboran Sea only model. One reason for this difference lies in the limiting effect of the integral constraint on mass. This constraint dictates that the amount of mass entering through the Strait of Gibraltar must leave at the eastern boundary. In the case of wind forcing alone, no transport enters the strait therefore no transport leaves the basin at the eastern boundary unless an equal amount returns through the eastern boundary. This could create an unrealistic recirculation at the

eastern boundary. However, in a model which includes the entire western Mediterranean, the eastern Alboran Sea boundary is left open to both inflow and outflow with no restrictions. The integral constraint is instead placed on the Strait of Sicily and should have a very small effect on the Alboran sea. The second reason for using this larger domain is to include the possibile effect of wind forced flow from east of the Alboran Sea. The first domain referred to as the "small" sea is a basin of similar dimensions to the standard two layer case, Fig. 46. The second domain, referred to as the "large" sea, is the Alboran sea subsection of the western Mediterranean sea including the westernmost part of the Balearic basin, Fig. 47.

In both cases, the model domains are closed and forced only by winds. The wind forcing is derived from climatological wind stresses obtained from twenty years (1950-1970) of ship observations in the Mediterranean (May, 1982). Individual stresses were estimated from ship observations of wind speed and direction using a quadratic aerodynamic drag law with a drag coefficient dependent on the wind speed and stability. Monthly averages of the wind stresses were then calculated by averaging the individual wind stress estimates from each month on a one degree latitude by one degree longitude grid. These monthly averages were bilinearly interpolated to the model grid . Wind forcing in the model is cyclic with a period of one year.

The wind stress forcing, interpolated from the $1^{o} \times 1^{o}$ grid

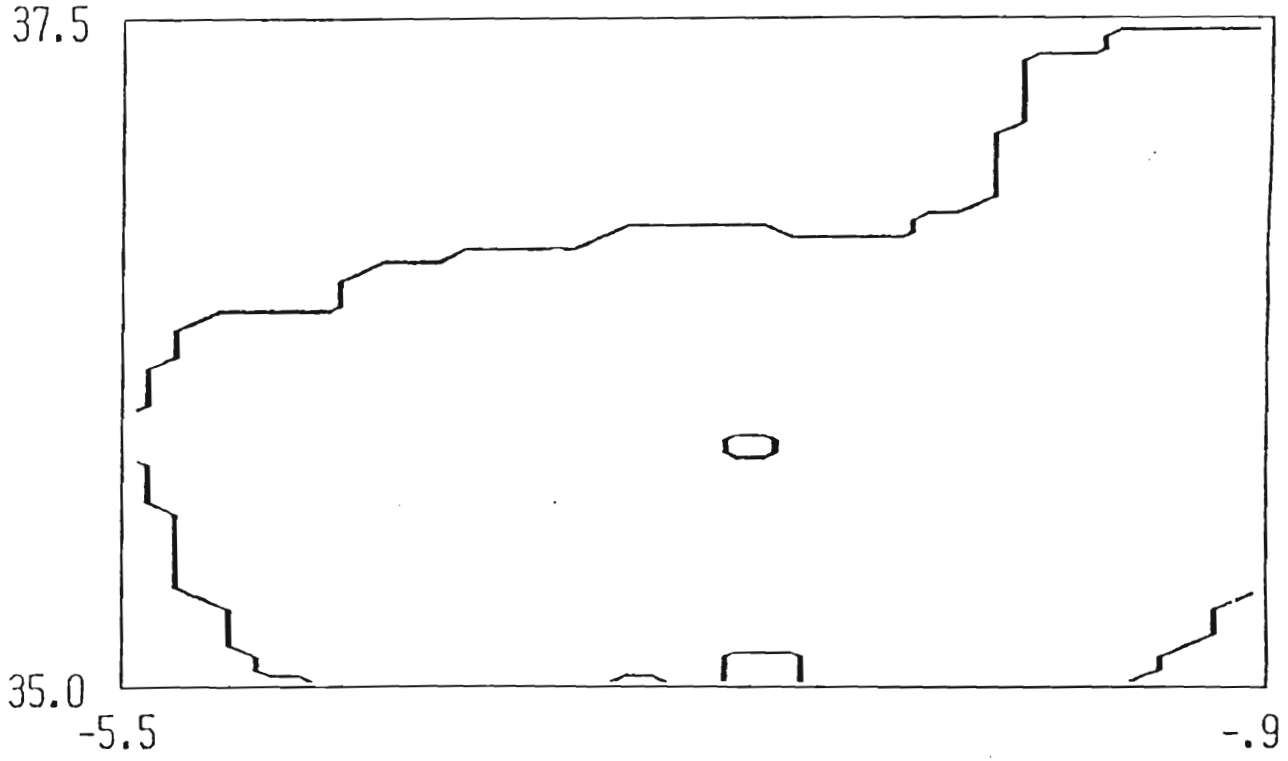

Fig. 46. Geometry of the explicit reduced gravity Alboran Sea model.

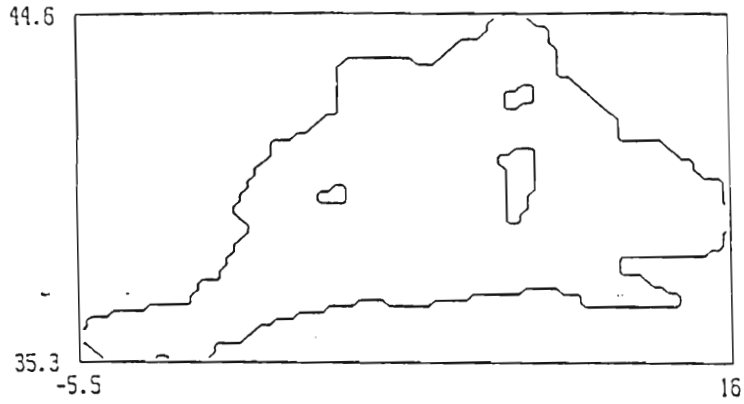

(a)

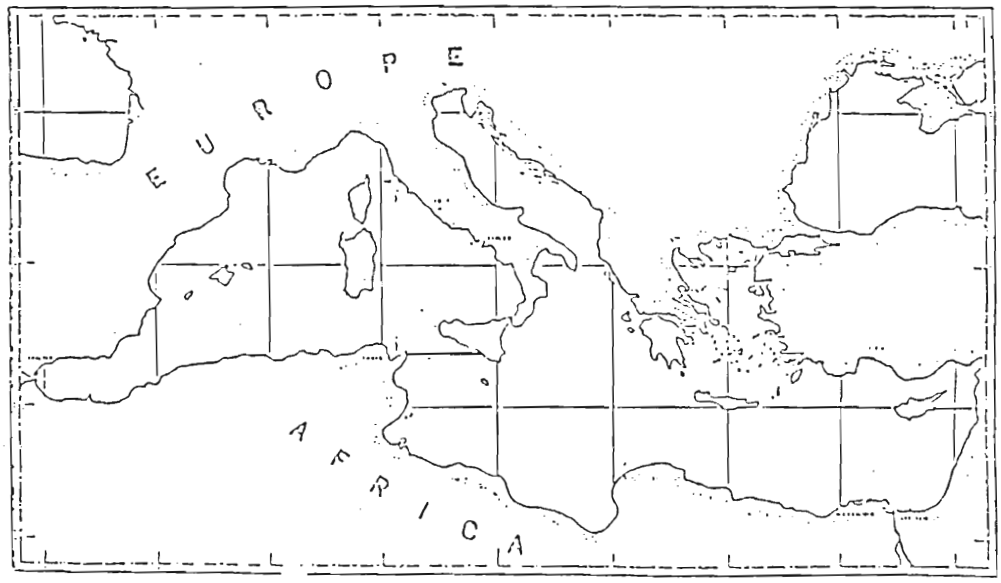

(b)

Fig. 47. The geometry of a) a reduced gravity western Mediterranean model compared to a b) map of the entire Mediterranean.

of the original data set to the model grid, is shown for the "small" sea case in Figs. 48-50. In general, the wind stress has a strong westward component in the winter with a area of divergence located near the strait. By summer a second area of divergence exists in the center of the basin near Alboran Island. The westward component weakens and a south westward stress appears to dominate the eastern half of the Alboran Sea.

The "small" sea solutions, Figs. 51a-d, show that the climatological winds reinforce the anticyclonic flow of the gyre. This wind induced anticyclonic circulation appears to be weakest in winter and strongest in summer extending east of the Alboran Island in many cases.

The wind stress forcing used for the entire western Mediterranean basin is shown in Figs. 52-54. Results for the "large" sea over the same time period shown in Fig. 51, indicate a very different effect from the wind, Figs. 55a-d. In winter, the time of weak anticyclonic circulation in the "small" sea, the "large" sea results show cyclonic circulation in the region of the gyre. This cyclonic circulation is induced by the large overall cyclonic flow at the Alboran Sea-Balearic Sea boundary. Three months later this cyclonic circulation still exists but is weakened. By July, the circulation has reversed and become anticyclonic. By October, the anticyclonic circulation has become stronger and then weakens to a cyclonic flow once again in the

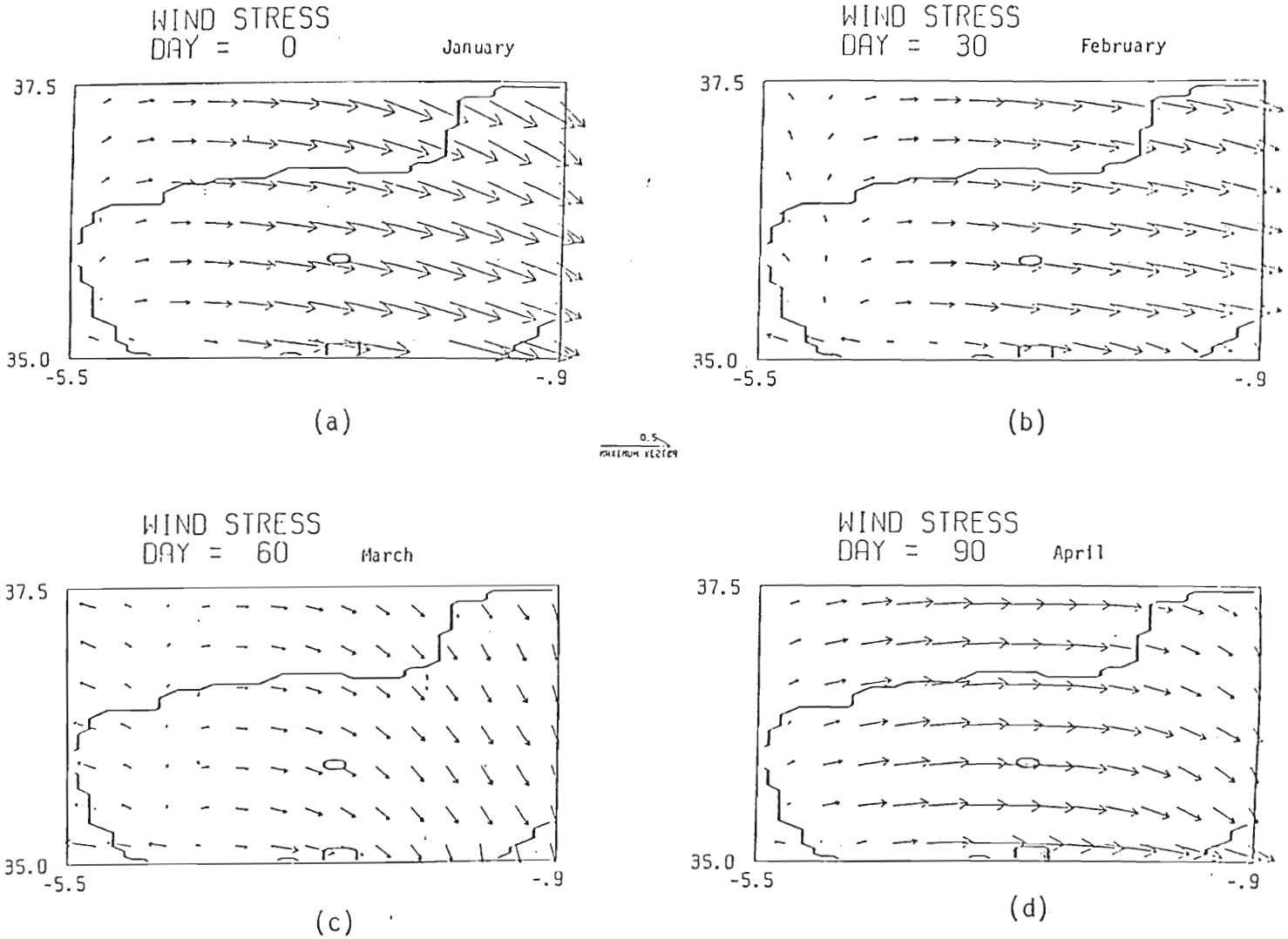

Fig. 48. Monthly mean climatological winds for the Alboran Sea (small sea) interpolated from $1^{o} \times 1^{o}$ gridded data for the entire Mediterranean from May (1982); a) January, b) February, c) March and d) April.

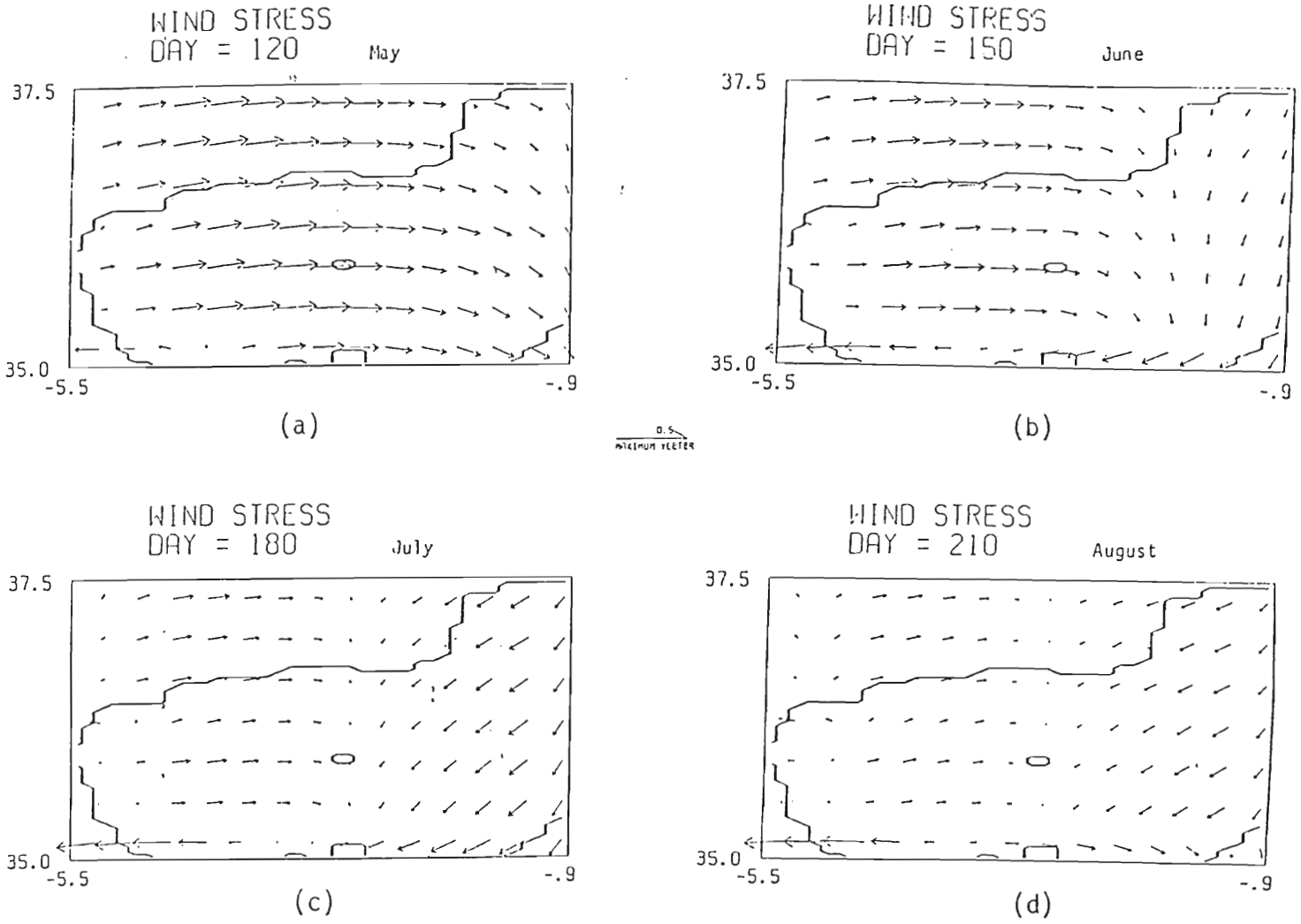

Fig. 49. Monthly mean climatological winds for a)May, b) June, c) July and d) August.

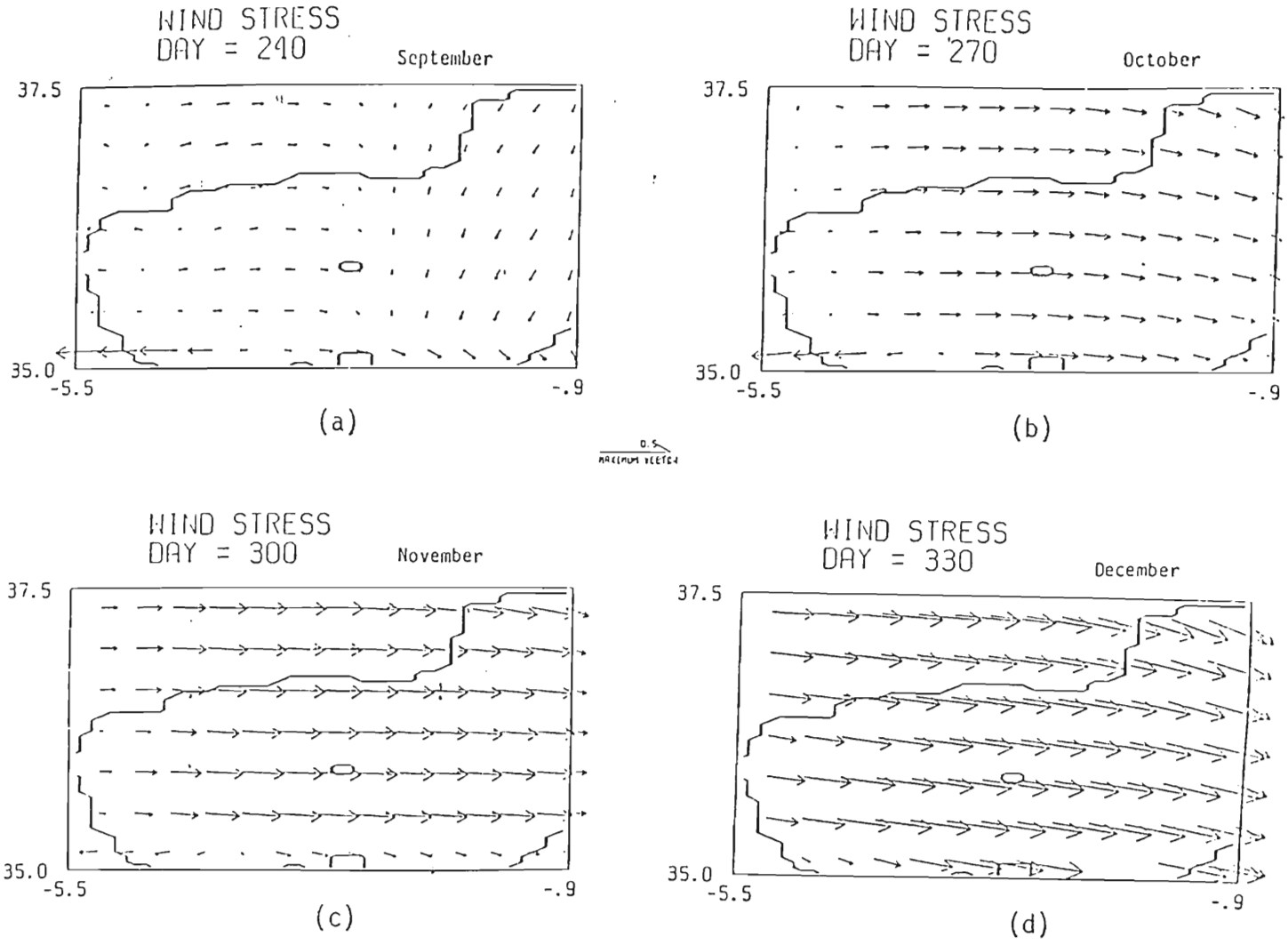

Fig. 50. Monthly mean climatological winds for a)September, b) October, c) November and d) December.

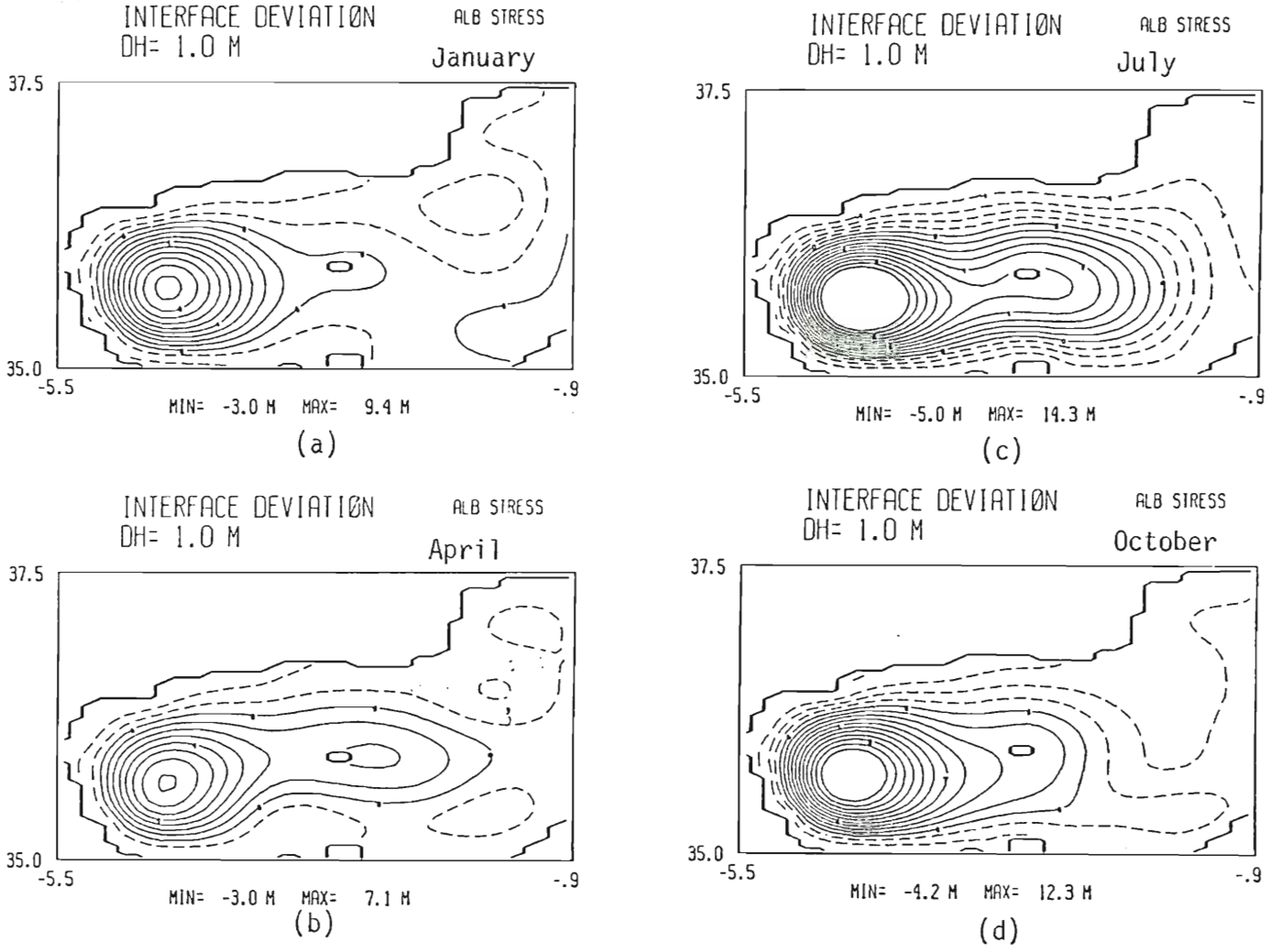

Fig. 51. PA of the "small" sea solution during the third year of integration. Solutions are shown every 90 days with a contour interval of 1 m; a) day 720, b) day 810, c) day 900 and d) day 990.

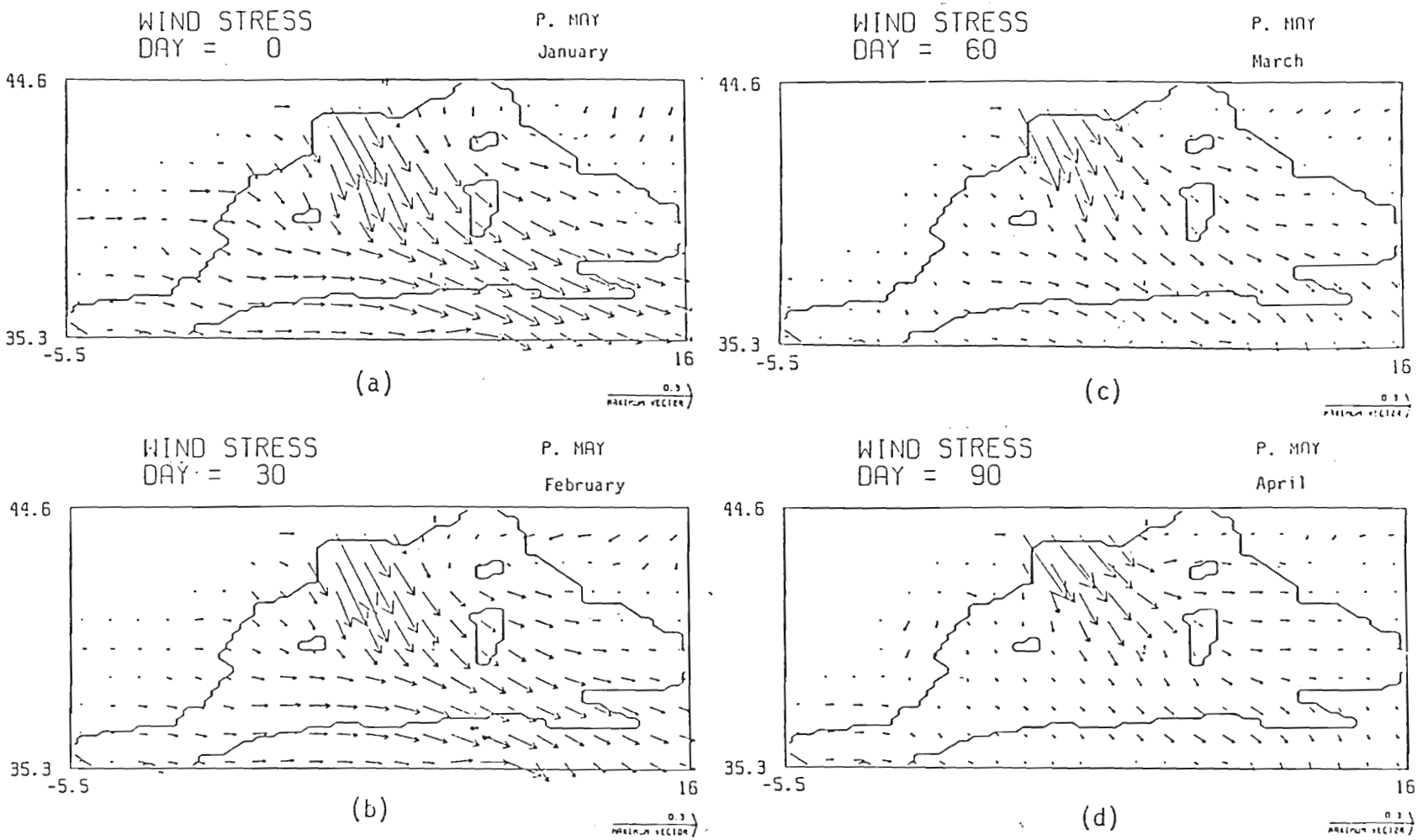

Fig. 52. Monthly mean winds from May, 1982 for the entire Mediterranean a) January, b) February, c) March and d) April.

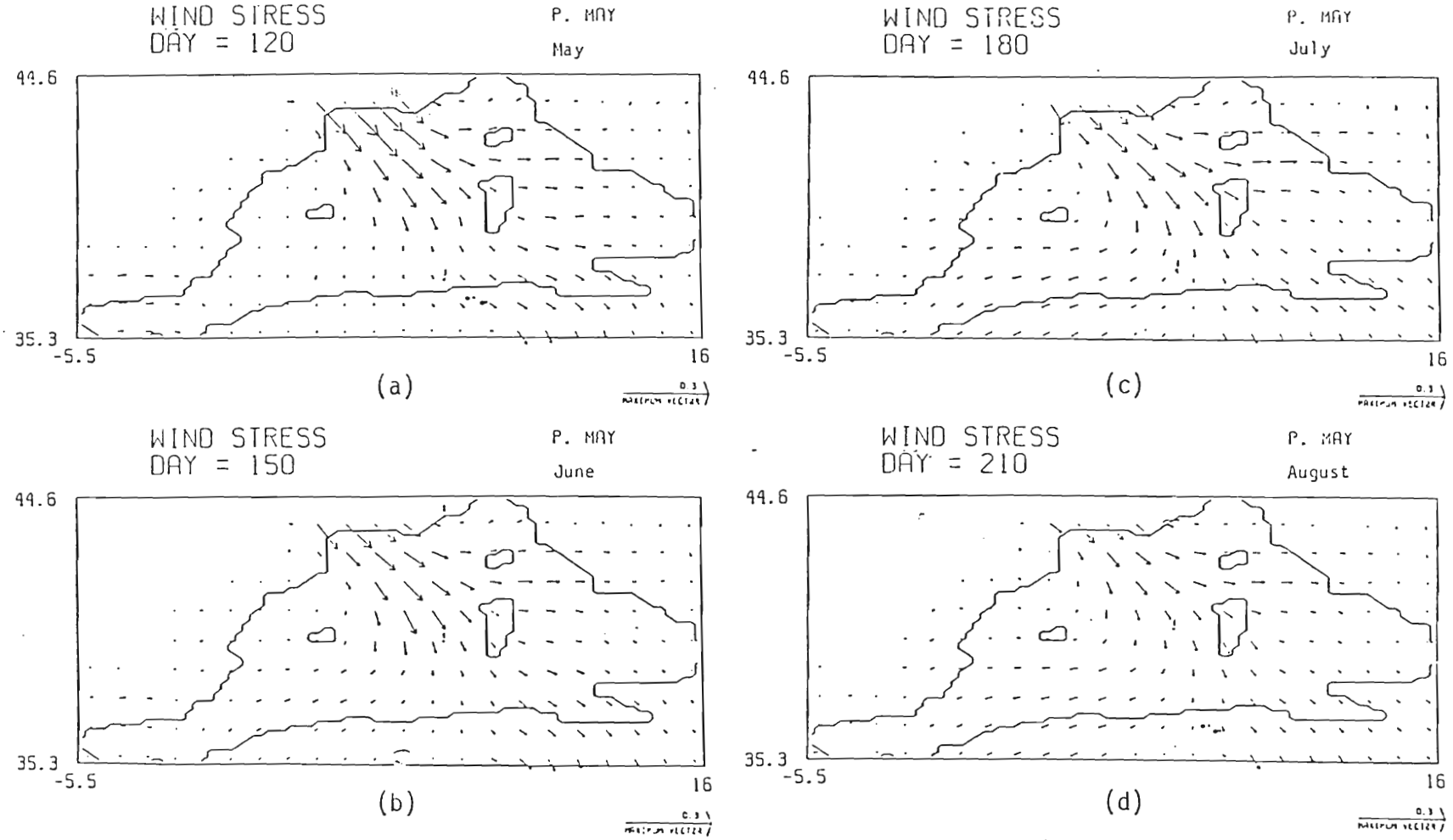

Fig. 53. Monthly mean winds for a) May, b) June, c) July and d) August.

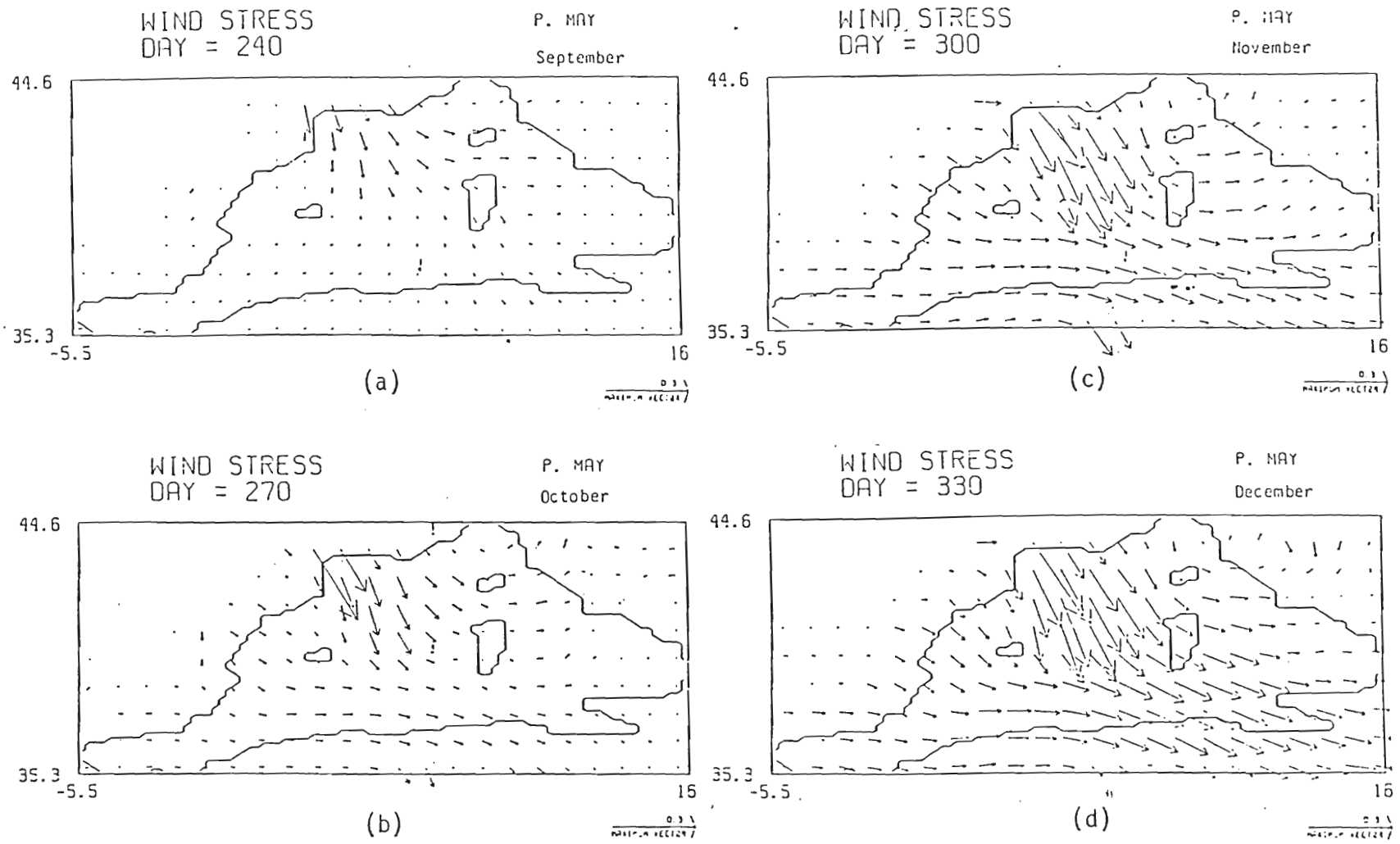

Fig. 54. Monthly mean winds for a) September, b) October, c) November and d) December.

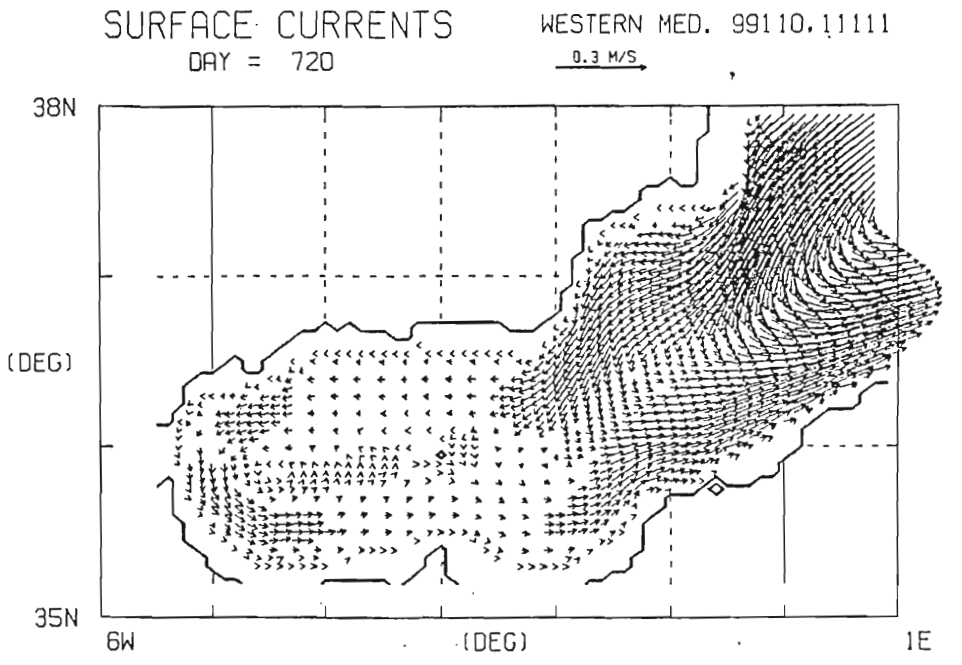

(a)

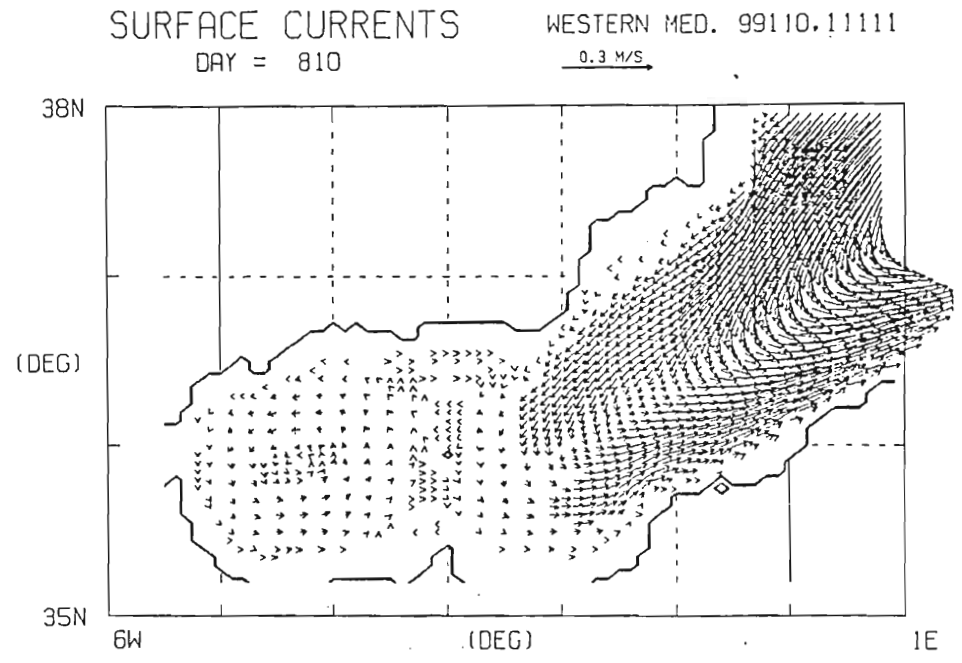

(b)

Fig. 55. Vector solutions of the "large" sea case a) day 720 and b) day 810. Maximum vector is 10 cm/sec.

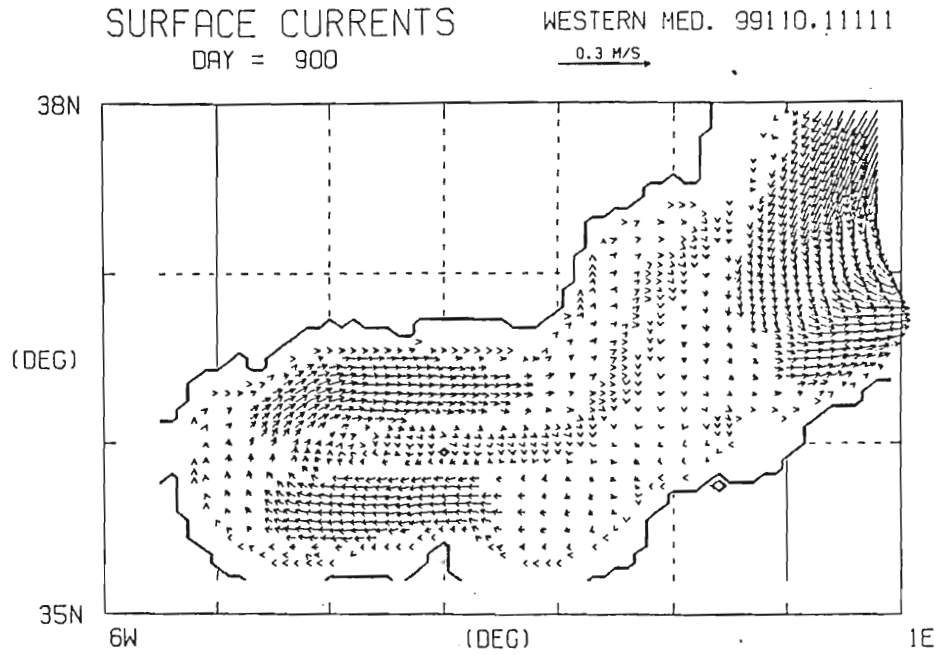

(c)

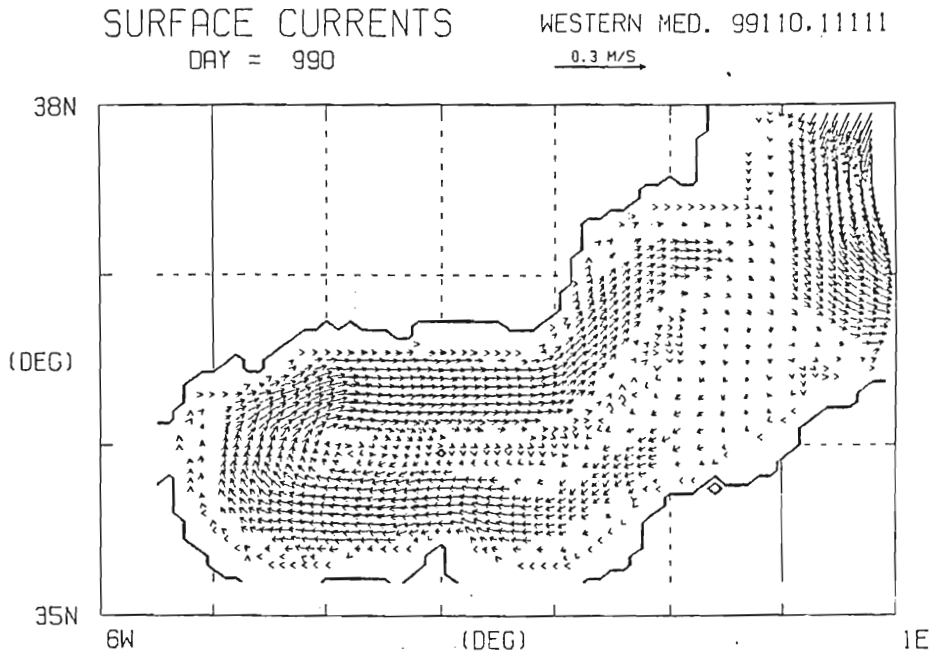

(d)

Fig. 55. Vector solutions of the "large" sea case c)day 900 and d) day 990. Maximum vector is 10 cm/sec.

winter.

Why do these solutions differ? The answer lies in the effects of the wind driven flow from the Balearic Sea. The "large" sea solutions appear to be a superposition of the "small" sea solutions plus the strong cyclonic flow from the Balearic. The "small" sea exhibits weak anticyclonic circulation in the winter. If the strong winter cyclonic circulation from the Balearic is added to this weak anticyclonic circulation, a weak cyclonic circulation results. In summer, however, the cyclonic circulation in the Balearic weakens and the anticyclonic circulation of the "small" sea case strengthens. The result is anticyclonic circulation in the gyre region. The cyclonic circulation from the Balearic increases again in the winter and a weak cyclonic gyre results in the location of the Alboran gyre.

How does this wind driven circulation affect the system when inflow from the strait is included? In the small sea case, the wind always adds, to a greater or lesser degree, to the anticyclonic circulation. Figures 56a-d shows the results of the large sea case including 40 cm/sec due east inflow forcing. In all cases the anticyclonic gyre exists. The wind forcing weakens it in the winter and strengthens it in the summer. The effect of the wind stress is not strong enough to reverse the gyre because the currents it induces are too weak to overcome the circulation established by the inflow. Currents induced by the wind are approximately 3-5 cm/sec while the

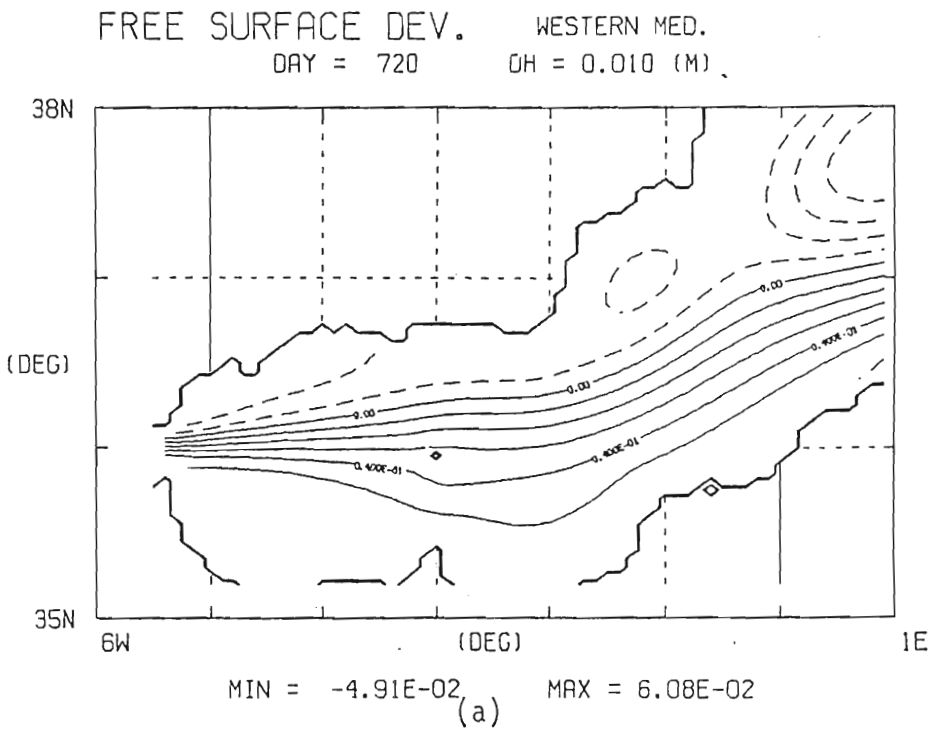

Fig. 56. Free surface contour solutions of the "large" sea case with a constant 40 cm/sec inflow due east. a) day 720, b) day 810. Contour interval is 1 cm.

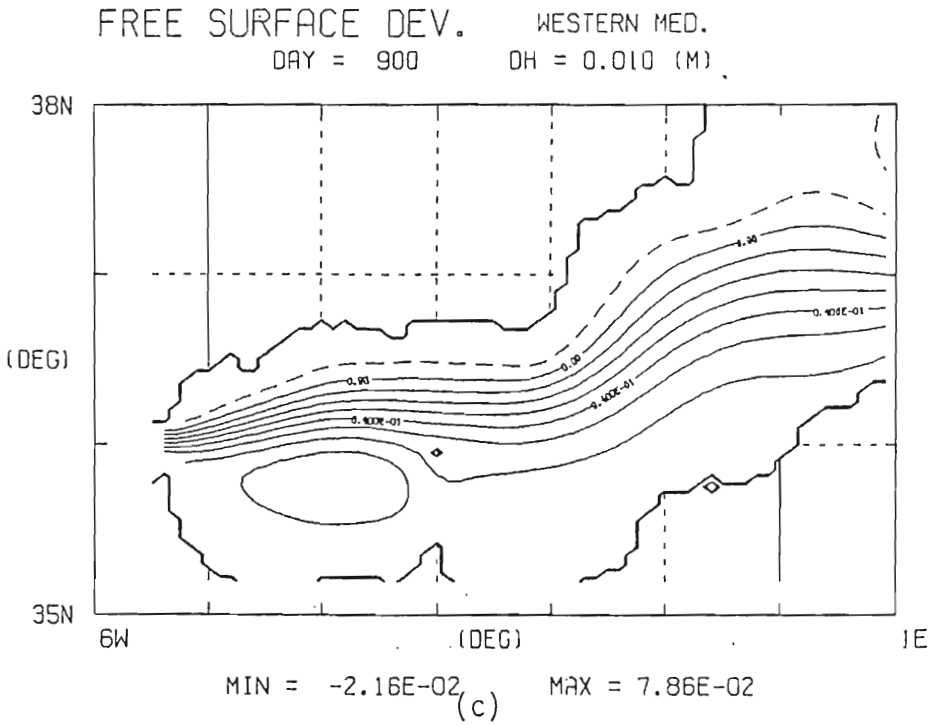

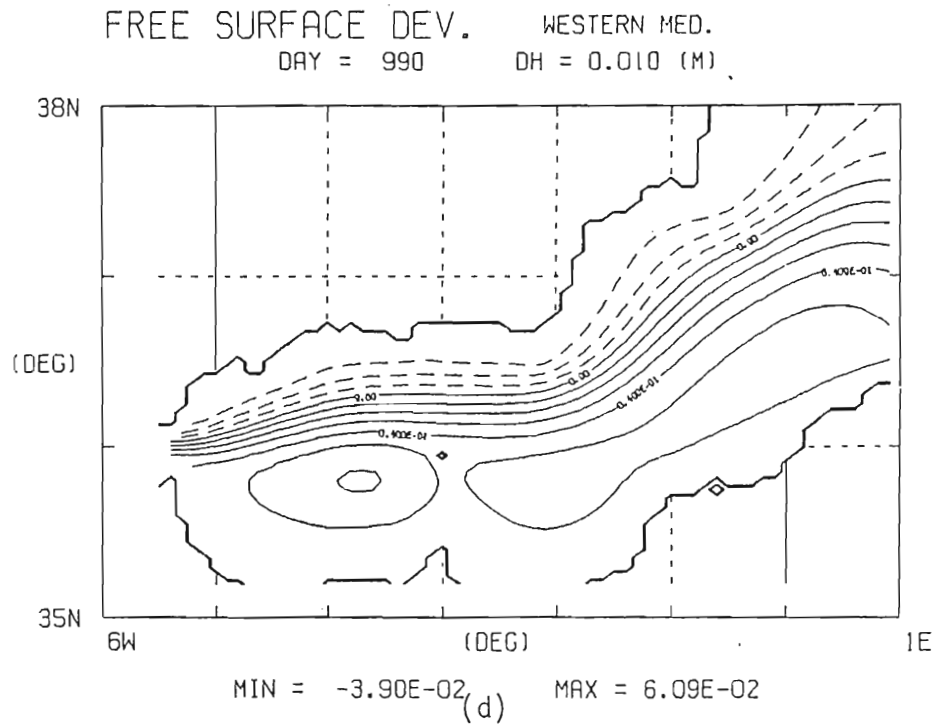

Fig. 56. Free surface contour solutions of the "large" sea case with a constant 40 cm/sec inflow due east. c) day 900 and d) day 910. Contour interval is 1 cm.

inflow velocities are approximately 30 - 40 cm/sec. If the inflow was weak, less then 3 cm/sec, over extended periods of time, the climatological wind forced currents could destroy the anticyclonic gyre, possibly reversing its flow. However, on a climatological scale, such weak inflow is not an accurate estimate for flow through the strait. Measurements have shown that on smaller time scales, tidal influences can be strong enough to reduce the inflow to very small values (Gascard and Richez, 1984). If such a situation existed when the wind stress forcing contributed a cyclonic component to the cirulation, it might be speculated that the gyre could disappear or even reverse. However, the model results indicate (section 4) that the variability due to inflow oscillation of very short duration is too small to affect the overall appearance of the gyre. Thus on a climatological scale, with normal inflow conditions, the effects of wind forcing are far less important then those of inflow forcing.

REFERENCES

Batchelor, G. K., 1970. An Introduction to Fluid Dynamics. Cambridge University Press, Cambridge, pp. 615.

Bethoux, J. P., 1979. Budgets of the Mediterranean Sea. Their dependence on the local climate and on characteristics of the Atlantic waters. Oceanol. Acta., 2, 2: 137-163.

Bucca, P. J., and T. H Kinder, 1984. An example of meteorological effects on the Alboran Sea gyre. J. Geophys. Res., 89: 751-757.

Burkov, V.A., Krivosheya, V. G., Ovchinnikov, I. M. and Savin, M. T., 1979. Eddies in the current system of the western Mediterranean Basin. Oceanology, 19: 9-13.

Bryden, H. L., and Stommel, H. M., 1982. Origin of the Mediterranean outflow. J. Mar. Res., 40: 55-71. Cano, N. (Lucaya), 1977. Resultados de la campana "Alboran 73". Boletin del Instituto Espanol Tomo I, Enero.

Cano, N. , 1978. Hidrologia del Mar de Alboran en primaveraverano. Boletin del Instituto Espanol de Oceanografia No. 248: 51-66.

Chao, S. Y., 1982. The Bimodality of the Kuroshio. Ocean Modelling, 42: 1-4.

Cheney, R. E., 1977. Recent observations of the Alboran Sea. NAVOCEANO Technical Note 370-73-77, pp. 24.

Cheney, R. E., 1978. Recent observations of the Alboran Sea frontal system. J. Geophys. Res., 83: 4593-4597.

Cheney, R. E., and R. A. Doblar, 1982. Structure and variablity of the Alboran Sea frontal system. J. Geophys. Res.,87: 585-594.

Copin-Montegut, G., B. Coste, J.-C. Gascard, J. Gostan, P. Le Corre, H.J. Minas, T. T. Packard and A. Poisson, 1982. Nutrient regeneration and circulation patterns in the Strait of Gibraltar and in the Western Mediterranean Sea. Abstract is EOS 63 (3): 109.

Crepon, M., 1965. Influence de la pression atmospherique sur le niveau moyen de la Mediterranee occidentale et sur le flux a travers le Detroit de Gibraltar. Presentation d'observations. Cahiers Oceanographiques 17(1): 15-32.

Gallagher, J. J., Fecher, M. and Gorman, J., 1981. Project HUELVA oceanographic/acoustic investigation of the western Alboran Sea. NUSC Technical Report 6023, pp. 106.

Garrett, C.J.R., 1983. Variable sea level and strait flows in the Mediterranean: a theoretical study of the response to meteorological forcing. Oceanological Acta, Vol. 6, No. 1: 79-87.

Gascard, J. C., 1978. Mediterranean deep water formation. Baroclinic instability and oceanic eddies. Oceanologica Acta 1, 3: 315-330.

Gascard, J. C. and Richez, C., 1984. Water masses and circulation in the western Alboran Sea and in the Strait of Gibraltar. Submitted to Deep Sea Res.

Grammeltvedt. A., 1969. A survey of finite difference schemes for the the primitive equations for a barotropic fluid. Mon. Wea. Rev., 97: 384-404.

Grousson, F. and Faroux, J. 1963. Measure de courants de surface en Mer d'Alboran. Cah. Oceanogr., 15: 716-721.

Haltiner, G. J. and F. L. Martin, 1957. Dynamical and Physical Meteorology. McGraw Hill Book Company, Inc., New York, pp 470.

Heburn, G. W., 1985. Effects of wind versas hydraulic forcing on the dynamics of the western Mediterranean Sea. In: H. Perkins (Editor), NORDA Papers Presented at the XXIXth Congress and Plenary Session of the International Commission for the Scientific Exploration of the Mediterranean Sea. NORDA Technical Note in press.

Heburn, G. W., Kinder, T. H., Allender, J. H. and H. E. Hurlburt, 1982. A numerical model of eddy generation in the southeastern Caribbean Sea. In: J. C. J. Nihoul (Editor), Hydrodynamics of Semi-enclosed Seas. Elsevier, Amsterdam, 299-327.

Holland, W. R. and Lin, L. B., 1975. On the generation of mesoscale eddies and their contribution to the oceanic general circulation. I. A preliminary numerical experiment. J. Phys. Oceanogr., 5: 642-657.

Hurlburt, H. E., and Thompson, J. D., 1980. A numerical study of Loop Current intrusions and eddy shedding. J. Phys. Oceanogr., 10: 1611-1651.

Katz, E. J., 1972. The Levantine intermediate water between the Strait

of Sicily and the Strait of Gibraltar. Deep Sea Res., 19: 507-520.

Kinder, T. H., 1984. Current meter measurements in the northwestern Alboran Sea. In: G. Parrilla (Editor) Donde Va? Meeting Report, Fuengirola, October, 1983. Instituto Espanol de Oceanografica.

Kinder, T. H. and Parrilla, G., 1984. Hydrographic structure in the western Alboran Sea, June 1982. In: G. Parrilla (Editor) Donde Va? Meeting Report, Fuengirola, October, 1983. Instituto Espanol de Oceanografica.

Kinder, T. H. and G. Parrilla, 1984b. Shallow hydrographic structure in the western Alboran Sea, October, 1982. In: G. Parrilla (Editor) Donde Va? Meeting Report, Fuengirola, October, 1983. Instituto Espanol de Oceanografica.

Lacombe, H., 1961. Contribution A L'Etude du Regime du Detroit de Gibraltar. Cah. Oceanogr., XIII: 74-107.

Lacombe, H., 1971. Le Detroit de Gibraltar. Note et Memoires de Service Geologique du Maroc., No. 222 bis, 111-146.

Lacombe, H., 1982. Regime of the Strait of Gibraltar and of its east and west approaches. In : J. C. J. Nihoul (Editor), Hydrodynamics of semi-enclosed seas. Elsevier, Amsterdam, 13-73.

Lacombe, H. and Tchernia, Paul, 1972. Caracters hydrologiques et circulation eaux en Mediterranee. In: D. J. Stanley (Editor), The Mediterranean Sea: A Natural Sedimentation Laboratory. Dowden, Hutchinson, and Ross, Inc., Stroudsburg, Pennsylvania, 25-36.

Lanoix, F., 1974. Project Alboran Etude Hydrologique Dynamique de la Mer d'Alboran. Tech. report 66, N. Atl. Treaty Org. Brussels, pp. 39.

LaViolette, P. E., 1983. The advection of cyclic submesoscale thermal features in the Alboran gyre. IAPSO Programme and Abstracts, pp. 78.

May, P. W., 1982. Climatological flux estimates in the Mediterranean sea: Part I. Winds and wind stress. Naval Ocean Reasearch and Development Activity, NSTL Station, Ms. NORDA Technical Report 54: pp. 56.

May, P. W. and D. L. Porter, 1975. Geostrophic calculations for the Alboran Sea EOS 56(6): 377. (Abstract).

Messinger, F. and A. Arakawa, 1976. Numerical Methods used in atmospheric models. GARP publication series no. 17. World Meteorological Organization. Geneva, Switzerland. Chapter 4, pp. 45.

Nof, D., 1978. On geostrophic adjustment in sea straits and estuaries: theory and laboratory experiments. Part II: Two-layer system. J. Phys. Oceanogr., 8: 861-872.

Ovchinnikov, I. M., 1966. Circulation in the surface and intermediate layers of the Mediterranean. Oceanology, 6: 48-59.

Parrilla, G. and Kinder, T. H., 1984. The physical oceanography of the Alboran Sea. IN: H. Charnock (Editor) Proceeding of NATO Advanced Research workshop, La Spezia.

Peluchon, G. and Donguy, J. R., 1962. Travaux Oceanographiques d "l'Origny" dans le Detroit de Gibraltar. Compaign internationale - 15 mpi, 15 Juin 1961. Zemi partie. Hydrologie en Mer d'Albroan. Cah. Oceanogr., 14: 573-578.

Perkins, H. and Saunders, K. D., 1984. Sections of Current, Salinity and temperature in the northwestern Alboran Sea, October, 1982. In: G. Parrilla (Editor) Donde Va? Meeting Report, Fuengirola, October, 1983. Instituto Espanol de Oceanografica.

Petit, M., Klaus, V., Gelchi, R., Fusey, F., Thery, J. J. and Bouly, P., 1978. Etude d'un tourbillon coeanique d'echelle moyenne en mer d'Alboran par emploi coinjoint techniques spatiales et oceanographiques. C. R. Acad. Sci. 287: 215-218.

Pistek, P., de Strobel, F., and C. Montanari, 1984. Deep sea circulation in the Alboran sea. J. Geophys. Res. (In press).

Porter, D. L., 1976. The anticyclonic gyre of the Alboran Sea. Independent research report from M.I.T.-WHOI joint program, Woods Hole, MA, pp. 29.

Preller, R. H., 1983. Numerical modeling of circulation in the Alboran Sea. IAPSO Programme and Abstracts, 77-78.

Preller, R. H. and Hurlburt, H. E., 1982. A reduced gravity numerical model of circulation in the Alboran Sea. In: J. C. J. Nihoul (Editor), Hydrodynamics of Semi-enclosed Seas. Elsevier, Amsterdam, 75-89.

Preller, R. H. and Heburn, G. W., 1985. A simple numerical model of

circulation in the western Mediterranean. Submitted to Oceanologica Acta.

Rossby,C. G., 1939. Relatin between variations in the intensity of the zonal circulation of the atmoshpere and the displacements of the semi-permanent centers of action. J. Marine. Res., 2, 38-55.

Stevenson, R. W., 1977. Heulva Front and Malaga, Spain eddy chains as defined by satellite and oceanographic data. Deut. Hydrogr. A., 30, 2: 51-53.

Stommel, H., Bryden, H. and Magelsdorf, P., 1973. Does some of the Mediterranean outflow come from great depth? Pure and Appl. Geophysics., 105: 879-889.

Vanwyckhouse, R. J., 1973. Synthetic Bathymetric Profiling System (SYNBAPS). Naval Oceanographic Office, Washington, D.C. Technical Report 233, pp. 138.

Vanwyckhouse, R. J., 1979. SYNBAPS, Volume I - Data sources and data preparation. Naval Ocean Research and Development Activity, NSTL Station, Ms. NORDA Technical Note 35.

Wannamaker, B., 1979. The Alboran Sea gyre: Ship satellite and historical data. SACLANT ASW Research Centre Report SR-30, La Spezia, Italy, pp. 27.

Whitehead, J. A. and Miller, A. R., 1979. Laboratory simulation of the gyre in the Alboran Sea. J. Geophys. Res. 84: 3733-3742.